“ Towards monitoring nitric oxide mediated cGMP metabolism in mouse retinal neurons using a FRET-based genetically encoded sensor ”

Von der Fakultät für Mathematik, Informatik und Naturwissenschaften der RWTH Aachen University zur Erlangung des akademischen Grades eines Doktors der Naturwissenschaften genehmigte Dissertation

vorgelegt von

Master of Science

Zhijian Zhao

aus Shanghai, P.R.China

Berichter: Universitätsprofessor Dr. rer. nat. Frank Müller

Universitätsprofessor Dr. rer. nat. Marc Spehr

Tag der mündlichen Prüfung: 03.02.2015

Diese Dissertation ist auf den Internetseiten der Hochschulbibliothek online verfügbar.

ABSTRACT

Cyclic guanosine monophosphate (cGMP) is a second messenger that plays an important role in many cell types of the retina. It is involved in a variety of intracellular signaling processes mostly by activating protein kinases or by binding to ion channels. In photoreceptors, cGMP is crucially involved in visual signal transduction. In many neurons of the inner retina, cGMP is synthesized by soluble guanylate cyclases (sGC) upon activation by nitric oxide (NO). So far, there is no common view of the contribution of cGMP to retinal adaptation or to the modulation of signaling processes in other retinal cell types, although many attempts to investigate those processes have been made in the past.

Using stimulation of the retina with the nitric oxide donor SNAP followed by immunohistochemistry with an antibody against cGMP, I could demonstrate cGMP synthesis controlled by NO in a variety of cell types of the intact mouse retina. However, this method does not enable to resolve the dynamics of this process. I, therefore, aimed at the expression of the FRET-based genetically encoded cGMP sensor Cygnet-2.1 in retinal cultures and in the intact retina to monitor the production of cGMP in real time using imaging techniques.

In control experiments I expressed Cygnet-2.1 functionally using the lipofectamine transfection in FlpTS GC-A cells (derived from HEK-293 cells) that served as model system. In these cells the synthesis and degradation of intracellular cGMP could be monitored upon activation of membrane-bound guanylate cyclases with atrial natriuretic peptide (ANP). The next aim was to establish Cygnet-2.1 expression in retinal cells. To this end, retinal cultures were established and seven different AAV serotypes encoding GFP were screened for their transduction efficiency in this *in vitro* model. AAV2 was selected as the most promising vector based on its wide range of transduction patterns among the retinal cell types and the high transduction efficiency. In the next step, AAV-mediated transduction was established *in vivo.* AAVs were delivered via ocular injection to newborn mice. Again, AAV2 was determined as the most promising candidate for transduction of retinal neurons. Finally, Cygnet-2.1 sensors were expressed in dissociated retinal cultures by using lipofectamine transfection and AAV-mediated transduction. Using lipofectamine transfection,

changes in Cygnet-2.1 fluorescence revealed a fast increase in the internal cGMP concentration upon NO stimulation in cultured retinal neurons that were immunoreactive for sGC. Upon AAV2-mediated transduction, no change in the Cygnet-2.1 fluorescence could be detected in retinal cells upon stimulation with NO donors or in the FlpTS GC-A cells upon stimulation with ANP. Most likely, AAV-mediated transduction did not yield functional Cygnet-2.1 sensors. Nevertheless, the proof of principle experiments clearly demonstrated that it is possible to investigate cGMP metabolism in the retina under physiological conditions using Cygnet-2.1. In future, the established methods in this thesis can drive the investigation of cGMP modulation *in vivo* and *in vitro* by means of optogenetic approaches and, thereby, foster our understanding of retinal adaptation and signal modulation.

ZUSAMMENFASSUNG

Zyklisches Guanosinmonophosphat (cGMP) ist ein sekundärer Botenstoff, der in vielen retinalen Zelltypen eine wichtige Rolle spielt. cGMP ist an einer Reihe verschiedener intrazellulärer Signalverarbeitungsprozesse beteiligt indem es Proteinkinasen aktiviert oder an Ionenkanäle bindet. In den Photorezeptoren ist cGMP entscheidend an der visuellen Signalweiterleitung beteiligt. Viele Neurone der inneren Retina synthetisieren cGMP mit Hilfe einer durch Stickoxid (NO) aktivierten löslichen Guanylatzyklase (sGC). Trotz zahlreicher Untersuchungen ist bisher nicht vollkommen geklärt, wie cGMP zum Prozess der retinalen Adaptation beiträgt oder die Signalverarbeitung in den unterschiedlichen retinalen Zelltypen moduliert.

Nach Stimulation der Retina mit dem NO-Donor SNAP und anschließender Immunhistochemie mit einem Antikörper gegen cGMP konnte ich zeigen, dass NO die Synthese von cGMP in einer Reihe unterschiedlicher Zelltypen bewirkt. Die Methode ermöglicht es aber nicht, die Dynamik der cGMP Synthese im retinalen Netzwerk zu untersuchen. Das Ziel der Arbeit war es deshalb, den genetisch codierten FRET basierten cGMP Sensor Cygnet-2.1 in retinalen Zellkulturen und in der intakten Retina zu exprimieren. Diese Methode ermöglicht es mittels Imagingtechnik die Synthese von cGMP in Echtzeit zu verfolgen.

Zunächst exprimierte ich Cygnet-2.1 in FlpTS GC-A-Zellen, die als Modellsystem dienten (abgeleitet aus HEK293-Zellen). Hier konnte ich die Synthese und den Abbau von intrazellulärem cGMP nach Aktivierung von membranständigen Guanylatzyklasen durch das atriale natiuretische Peptid (ANP) verfolgen. In einem nächsten Schritt sollte Cygnet-2.1 in retinalen Zellen exprimiert werden. Hierzu habe ich retinale Kulturen etabliert und anschließend in diesem in vitro Modellsystem die Transduktionseffizienz von sieben verschiedenen GFP exprimierenden AAV Serotypen überprüft. AAV2 war hier der vielversprechendste Vektor, da er in allen retinalen Zellklassen zu einer starken Expression führte. In einem nächsten Schritt habe ich die AAV-gestützte Transduktion in vivo etabliert. Die AAVs wurden hierzu in die Augen neugeborener Mäuse injiziert. Auch in diesem Fall schien AAV2 der erfolgversprechendste Vektor zu sein.

Im Anschluss habe ich Cygnet-2.1 in retinalen Dissoziatkulturen sowohl mittels Lipofectamintransfektion als auch mit Hilfe der AAV vermittelten Transduktion exprimiert. Nach Transfektion mit Lipofectamin und Stimulation mit NO Donoren konnte durch Änderungen der Cygnet-2.1 Fluoreszenz ein schneller Anstieg der internen cGMP Konzentration in retinalen Neuronen, die lösliche GC exprimierten, nachgewiesen werden. Nach AAV vermittelter Transducktion waren dagegen keine Änderungen in der Cygnet-2.1 Fluoreszenz in retinalen Zellen nach Stimulation mit NO Donoren oder in FlpTS GC-A-Zellen nach Zugabe von ANP erkennbar. Die Vermutung liegt nahe, dass die AAV vermittelte Transduktion zu nicht-funktionellen Cygnet-2.1 Sensoren führte. Nichtsdestoweniger konnten die Machbarkeitsstudien dieser Arbeit deutlich zeigen, dass grundsätzlich die Möglichkeit besteht, den Metabolismus von retinalem cGMP unter physiologischen Bedingungen mit Hilfe von Cygnet-2.1 zu untersuchen.

Die hier etablierten Methoden können in Zukunft weiterführende, optogenetische Untersuchungen zur Modulation von cGMP sowohl in vitro als auch in vivo ermöglichen und so unser Verständnis der retinalen Adaptation und Modulation voranbringen.

CONTENT

ABSTRACT ····· **I**

ZUSAMMENFASSUNG ····· **III**

CONTENT ····· **V**

ABBREVIATIONS ····· **IX**

1. INTRODUCTION ····· **1**

1.1 Retina and phototransduction ····· **1**

1.2 Bipolar cells and Amacrine cells ····· **4**

1.3 Cyclic guanosine monophosphate (cGMP) and the NO-cGMP pathway in the retina ····· **7**

1.4 Genetically encoded FRET-based cGMP sensors ····· **10**

1.4.1 Förster resonance energy transfer ····· 11

1.4.2 The cGMP biosensor Cygnet-2.1 ····· 12

1.5 FlpTS GC-A cell line and its signalling pathway ····· **13**

1.6 Adeno-associated viruses (AAV) ····· **14**

1.7 Motivation ····· **15**

2. MATERIALS AND METHODS ····· **17**

2.1 Materials ····· **17**

2.2 Cygnet-2.1 calibration in a cell model ····· **17**

2.2.1 Cell line ····· 17

2.2.2 Transient transfection of FlpTS GC-A cells ····· 18

2.2.3 Setup of the measuring chamber ····· 18

2.2.4 Calcium-imaging ····· 19

2.2.5 FRET-based cGMP-imaging ····· 22

2.3 Retinal culture ····· 24

2.3.1 Animals ····· 24

2.3.2 Organotypic retinal whole-mount culture ····· 24

2.3.3 Dissociated retinal cell culture ····· 26

2.3.4 Organotypic retinal slice cultures ····· 28

2.3.5 Native retina preparation and immunohistochemistry ····· 28

2.3.6 Confocal laser scanning microscopy ····· 29

2.4 Adeno-associated viruses mediated transduction ····· 30

2.4.1 AAV mediated transduction of organotypic retinal whole-mount cultures · 30

2.4.2 AAV mediated transduction of dissociated retinal cell cultures ····· 31

2.4.3 AAV mediated transduction of FlpTS GC-A cells ····· 31

2.5 Ocular injection *in vivo* ····· 31

2.5.1 Micro-injection system ····· 31

2.5.2 Operation for ocular injection ····· 32

2.5.3 Immunohistochemistry ····· 34

2.6 NO induced cGMP-immunoreactivity (cGMP-IR) in dissociated retinal cultures ····· 34

2.7 cGMP-imaging of dissociated retinal cultures upon transient transfection ·· ····· 35

2.8 Antibodies ····· 35

3. RESULTS ····· 38

3.1 Characterization of Cygnet-2.1 in the model system FlpTS GC-A ····· 38

3.1.1 Calcium-imaging in FlpTS GC-A cells ····· 38

3.1.2 FRET-based cGMP-imaging in FlpTS GC-A cells ····· 41

3.1.3 In the presence of the cGMP-specific PDE5a Cygnet-2.1 displays rapidly reversible signals in FlpTS GC-A cells ····· 47

3.1.4 Selectivity of Cygnet-2.1 ····· 49

3.2 Retinal culture ····· 52

3.2.1 Organotypic retinal whole-mount culture ····· 52

3.2.2 Dissociated retinal cell culture ····· 74

3.2.3 Organotypic retinal slice culture ····· 83

3.3 AAV-mediated transduction *in vitro* ····· 88

3.3.1 AAV-mediated transduction in dissociated retinal cell cultures ····· 88

3.3.2 AAV transduction in organotypic retinal whole-mount cultures ····· 105

3.4 AAV-mediated transduction *in vivo* ····· 108

3.4.1 Expression of GFP in the retina using AAV-mediated transduction *in vivo* ····· 108

3.4.2 AAV2 targeted neurons in the INL involved in NO-cGMP pathway. ····· 115

3.5 AAV2-mediated expression of Cygnet-2.1 in dissociated retinal cultures ····· 119

3.5.1 Expression of the viral form of Cygnet-2.1 sensor ····· 119

3.5.2 cGMP-imaging of dissociated retinal cultures using Cygnet-2.1 ····· 121

3.5.3 Transduction with AAV2-Cygnet-2.1 leads to non-functional sensor ····· 125

4. DISCUSSION ····· 129

4.1 Sensitivity and selectivity of Cygnet-2.1 ····· 130

4.2 Development, degeneration and remodelling of retinal culture ····· 132

4.2.1 Organotypic retinal whole-mount culture ····· 133

4.2.2 Dissociated retinal cell culture ····· 134

4.3 AAV-mediated transduction ····· 135

4.3.1 AAV-mediated transduction *in vitro* ····· 136

4.3.2 AAV-mediated transduction *in vivo* ····· 137

4.4 Cygnet-2.1 expression upon AAV-mediated transduction ····· 141

4.5 Outlook ····· 143

5. REFERENCES ·····144

ACKNOWLEDGMENT·····156

CURRICULUM VITAE ·····157

ABBREVIATIONS

5'-GMP	5'- guanosine monophosphate
AAV	adeno-associated viruses
AC	amacrine cell
ANP	atrial natriuretic peptide
AOTF	acousto-optical tunable filter
BC	bipolar cell
bNOS	brain nitric oxide synthase
BNP	brain natriuretic peptide
βAR	β-adrenergic receptor
CaBP	calcium binding protein / calbindin
CaBP5	calcium binding protein 5
CAG	cytomegalovirus-actin-globin hybrid (promoter)
cAMP	cyclic adenosine monophosphate
CBA	chicken β-actin (promoter)
cDNA	complementary DNA
CFP	cyan fluorescent protein
cGMP	cyclic guanosine monophosphate
CMF-Hank's	Calcium-Magnesium-free Hank's Balanced Salt Solution
CMV	cytomegalovirus (promoter)
CNG	cyclic nucleotide-gated
CNGA2	cyclic nucleotide-gated channel subunit A2
CNS	central nervous system
DIC	differential interference contrast
DNA	deoxyribonucleic acid
dsDNA	double-stranded DNA
DMEM	Dulbecco's Modified Eagle Medium
EMCCD	electron multiplying charge-coupled-device

e.g.	exempli gratia (for example)
ES	extracellular solution
et al.	et alii (and so on)
etc.	et cetera (and so forth)
FCS	fetal calf serum
FRET	Förster resonance energy transfer
GABA	γ-aminobutyric acid
GABAergic	γ-aminobutyric acidergic
GAD	glutamic acid decarboxylase
GAD65	glutamic acid decarboxylase isoform 65
GAD67	glutamic acid decarboxylase isoform 67
GC	ganglion cell
GC-A / pGC-A	particulate guanylate cyclase-A
GCL	ganglion cell layer
GFAP	glial fibrillary acidic protein
GFP	green fluorescent protein
GlyT1	glycine transporter 1
G-Protein	guanine nucleotide binding protein
GS	glutamine synthetase
GTP	guanosine triphosphate
Hank's	Hank´s Balanced Salt Solution
HC	horizontal cell
HEK	human embryonic kidney (cell)
HEPES	4-(2-hydroxyethyl)-1-piperazineethanesulfonic acid
IBMX	3-isobutyl-1-methylxanthine
ID	inner diameter
i.e.	id est (that is)
INL	inner nuclear layer
IPL	inner plexiform layer

IS	inner segments
ITR	inverted terminal repeats
K_D	dissociation constant
MC	Müller cell
mDMEM	modified DMEM medium
mITR	mutated ITR
NA	noradrenaline
NFL	nerve fiber layer
nNOS	neuronal nitric oxide synthase
NO	nitric oxide
NOS	nitric oxide synthase
OS	outer segments
ONL	outer nuclear layer
OPL	outer plexiform layer
P	postnatal day
p.a.	pro analysi (purity grade)
PB	0.1 M phosphate buffer
PDE	phosphodiesterase
PDE5a	phosphodiesterase type 5A
PDL	poly-D-lysine
pGC	particulate guanylate cyclase
PKARIIβ	protein kinase A, regulatory subunit IIβ
PKCα	protein kinase C, α isoform
PKG	cGMP-dependent protein kinase or protein kinase G
rAAV	recombinant AAV
ROI	region of interest
scAAV	self-complementary AAV
sGC	soluble guanylate cyclase
SNAP	S-nitroso-N-acetylpenicillamine

SNP	sodium nitroprusside dihydrate
ssDNA	single-stranded DNA
Syt2	synaptic vesicle associated protein synaptotagmin-2
TH	tyrosine hydroxylase
TRPM1	transient receptor potential cation channel subfamily M member 1
YFP	yellow fluorescent protein
vp	viral particles
-IR	-immunoreactivity
Φ	diameter

Abbreviations of units

bp	base pair(s)
kb	kilobase(s)
mg, ng	milligram, nanogram
ml, µl	milliliter, microliter
M, mM, µM, nM	molar, millimolar, micromolar, nanomolar
mm, µm, nm	millimeter, micrometer, nanometer
mOsm	milliosmole
°C	degree Celsius
%	per cent

1. INTRODUCTION

The mammalian retina is a light sensitive tissue lining the inner surface in the posterior portion of the eye. During embryonic development, the retina and the optic nerve originate from the developing brain, therefore, the retina is considered as part of the central nervous system (CNS). There are several features that make the mammalian retina particularly attractive for scientific research. Most importantly, unlike the rest of the CNS, the retina is unusually suitable to be studied intact *in vitro*. Although its thickness is just about several hundred μm (no more than 200 μm in mouse), the retina remains intact when being separated from surrounding tissues except that the optic nerve has to be cut. The retina can be kept alive for several hours when incubated in oxygenized physiological solutions. *In vitro*, physiological investigations like imaging or patch clamp can be performed. Therefore, the retina is a very suitable model of the central nervous system for neurophysiological or neurochemical studies.

Mice are the most commonly used vertebrate species due to their suitable size, low cost and quick reproduction rate. They are considered to be a good experimental model. Most importantly, taking the advantages of genetic technology, gene modification in mice is possible; therefore, mice or their organs can be genetically modified. Most commonly used techniques encompass knock-out or knock-in of genes or expression of reporter genes or cellular markers.

All in all, the mouse retina is an ideal model of the mammalian CNS in the research fields of neurobiology and neurophysiology.

1.1 Retina and phototransduction

Intuitively one could expect that the front surface of the retina harbors the light sensing cells, the photoreceptors; however, in the vertebrate retina these cells are

located at the opposite side. This means that light has to pass through the entire retina with its different layers of neurons before it reaches the outer segments of photoreceptors where visual pigments are found (Figure 1.1). There are two kinds of photoreceptors in the retina: rods and cones. In humans, rod density decreases close to the fovea, whereas cone density peaks in the fovea (Osterberg, 1935; Curcio et al., 1990). Rods are very sensitive to light and are capable of detecting single photons. They are specialized for scotopic vision. Cones are less sensitive, but faster due to their short response time to stimuli (Kandel et al., 2000). The cone system provides us with good resolution and the perception of color. In humans, there are three types of cones with different opsins, having absorption maxima at different wavelengths (Jameson et al., 2001; Purves et al., 2001). Hence, cones are responsible for photopic and color vision. The photoreceptor cell bodies form the outer nuclear layer (ONL).

In the absence of light, both rods and cones are depolarized and release glutamate as transmitter at their synapses. A key second messenger molecule that maintains the cells in their depolarized state is cyclic guanosine monophosphate (cGMP). (As cGMP is of special interest in this thesis, detailed information will be given in Chapter 1.3.) A high concentration of cGMP in the photoreceptor outer segment keeps cGMP-gated ion channels open and causes an inward current carried mainly by sodium ions that leads to depolarization of the cell. Upon illumination, photons are captured by opsins in the outer segments of photoreceptors and the opsins become activated. The activated opsins unlock the activity of phosphodiesterases (PDEs) via G-proteins. As a consequence, PDEs can hydrolyze cGMP, thereby reducing its intracellular concentration. The decrease of the cGMP level causes the closing of cGMP-gated ion channels, which leads to the hyperpolarization of the photoreceptors. Subsequently, glutamate release ceases (reviewed by Müller and Kaupp, 1998). The changes in neurotransmitter release are registered by bipolar cells and horizontal cells in the first synaptic layer, the outer plexiform layer (OPL). Bipolar cells relay the information to the inner plexiform layer (IPL) where they are connected to retinal ganglion cells (GCs) and amacrine cells (ACs). The ganglion cells are the retinal

output neurons that transmit the visual signals to the brain through the optic nerve.

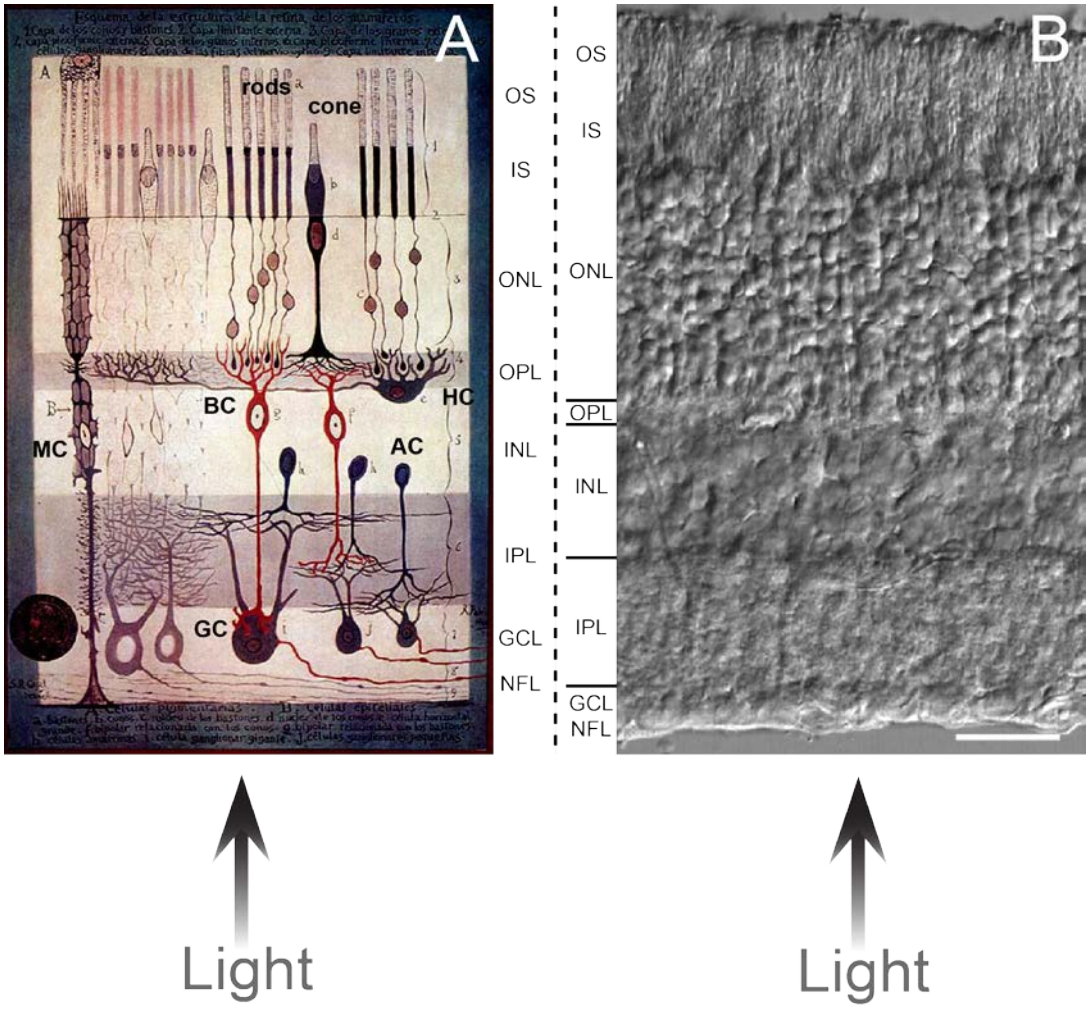

Figure 1.1: Cellular organization of the retina.

A: Schematic drawing of a vertical section through the mammalian retina ca. 1900 by Santiago Ramon y Cajal. The scheme is based on observations of cells impregnated by the Golgi method. In the picture, the cell types are marked: rods and cone; HC, horizontal cell; BC, bipolar cell; AC, amacrine cell; GC, ganglion cell; MC, Müller cell. The following layers are shown: OS, outer segments; IS, inner segments; ONL, outer nuclear layer; OPL, outer plexiform layer; INL, inner nuclear layer; IPL, inner plexiform layer; GCL, ganglion cell layer; NFL, nerve fiber layer. Arrows represent the direction of light passing through the retina.

B: Differential Interference Contrast (DIC) image of a vertical section through the mouse retina. Scale bar = 20 µm.

The transmission of visual information from photoreceptors to ganglion cells is not just a relay race. At every synaptic connection, the information is further processed. Basically, there are two pathways after the first synaptic relay in the OPL: the ON- and the OFF-pathway. While all photoreceptors are hyperpolarized during

illumination, two groups of bipolar cells behave in opposite ways. Their response is determined by two different glutamate receptors at their dendrites. OFF-bipolar cells have ionotropic glutamate receptors and, therefore, follow the behavior of photoreceptors. They are depolarized in the dark, but hyperpolarized upon illumination when glutamate release from photoreceptors ceases. ON-bipolar cells are depolarized or activated during illumination. In the light, cation channels in ON-bipolar cells, most likely the TRPM1 channels (Morgans et al., 2009), are open leading to a depolarizing ion flux. In the dark, glutamate acting at metabotropic glutamate receptors at the ON-bipolar cell dendritic tips leads to the activation of G-Proteins followed by the closing of the cation channels and, hence, hyperpolarization of the cell (Slaughter and Miller, 1981; Nawy and Jahr, 1990, 1991; Yamashita and Wässle, 1991). The ON/OFF dichotomy is preserved in the subsequent stages of the visual system. The processing of visual signals is affected by extending processes from horizontal cells in the OPL and from amacrine cells in the IPL. These connections are called lateral pathways. Horizontal cells extend long lateral processes and collect signals from distant photoreceptors. They modulate the output signals from photoreceptors via lateral inhibition and are, therefore, important for the generation of antagonistic receptive fields. In the IPL, light responses are strongly modulated by amacrine cells providing feedback inhibitory input to bipolar cells, or lateral inhibitory input to other amacrine cells and ganglion cells. To this end, there are various types of amacrine cells with different functions. In the end, a ganglion cell may transmit visual information which is quite complex, but best described by the properties of the cells receptive field.

1.2 Bipolar cells and Amacrine cells

Bipolar cells and amacrine cells are the main retinal neurons involved in the nitric oxide (NO)-cGMP pathway, which will be introduced in Chapter 1.3. Thus, more information about these two retinal cell classes will be provided in the following.

Bipolar cells received their name from the fact that two processes arise from their soma. They work as bridges connecting the two plexiform layers. Usually, bipolar cell bodies are located in the outer half of the INL. Their dendrites synapse with photoreceptors and horizontal cells in the OPL to collect the visual information. The information is relayed via their axon and passed on to ganglion cells at the bipolar cell axon terminal. Bipolar cells propagate signals via graded potentials instead of action potentials. The axons of different bipolar cells branch at different levels of the IPL (described by Cajal, 1892) where processes of different types of amacrine cells and ganglion cells ramify. ON-bipolar cells terminate in the inner half part of the IPL close to the GCL, while OFF-bipolar cells terminate in the outer half. Within the ON- or OFF-sublayers, axons of different bipolar cell types terminate at different levels, suggesting that they contact different postsynaptic partners (Boycott and Wässle, 1991). Based on this morphological criteria, in the mammalian retina bipolar cells are subdivided into 9 ~ 12 different types (reviewed by Masland, 2001). In mouse retina, 11 types of cone bipolar cells and 1 type of rod bipolar cell have been classified (Ghosh et al., 2004; Wässle et al., 2009). Each type of bipolar cell shows a characteristic cell number per unit area as well as characteristic sets of neurotransmitter receptors and signaling proteins. Figure 1.2 shows a schematic diagram of bipolar cells of the mouse retina. The IPL is subdivided into 5 sublaminae. The level of stratification of bipolar cell axon terminals in the IPL is the major criterion for bipolar cell classification. Furthermore, specific immunomarkers and transgenic mouse lines that express markers in certain bipolar cell types can be used to identify bipolar cells. Until now, classification of bipolar cells is most likely complete (Wässle et al., 2009). It greatly helps to functionally understand the bipolar cells and their role within the circuitry of the retina.

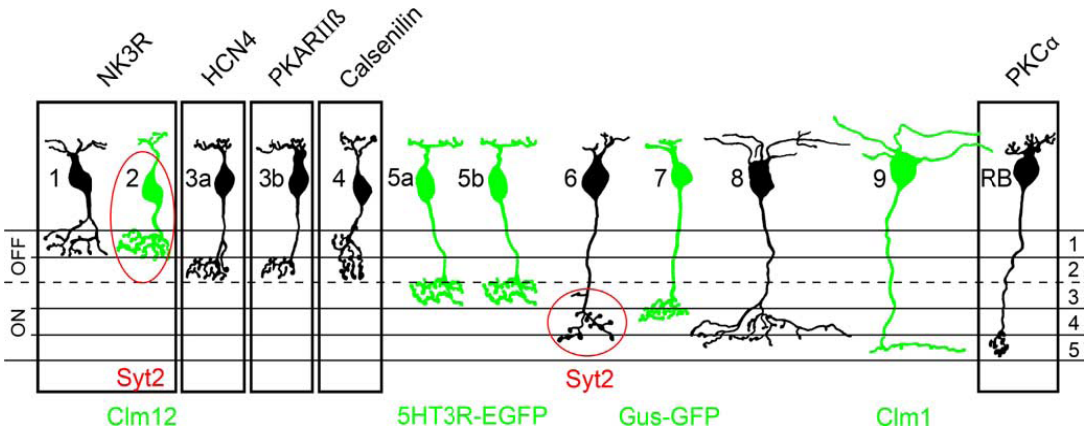

Figure 1.2: Schematic diagram of bipolar cells in the mouse retina. *(taken from Wässle et al., 2009)*

A total of 11 cone bipolar cells and 1 rod bipolar cell can be distinguished by immunohistochemical staining (outlines; markers given above cell type) or by GFP/Clomeleon expression in transgenic mouse lines (green cells). The level of stratification of bipolar cell axon terminals in the IPL is the major criterion for classification.

Amacrine cells interact with bipolar cells and ganglion cells in the IPL and appear to be the most diverse class of retinal interneurons. In the mouse retina, their somata are localized to the two innermost cell layers of the INL, but are also found as “displaced amacrine cells” in the GCL. In the INL, they make up 41% of all cells (Jeon et al., 1998). In mammals about 20 to 30 different types of amacrine cell have been discovered (Vaney, 1990; Wässle and Boycott, 1991; MacNeil and Masland, 1998; Menger et al., 1998) which are thought to have distinct dedicated functions like adaptation, shaping output signals from bipolar cells, controlling of ganglion cell responses, etc. The different amacrine cells differ considerably in their pre- and postsynaptic partners as well as their neurotransmitters and molecular components. The major subdivision is into γ-aminobutyric acidergic (GABAergic) amacrine cells and glycinergic amacrine cells with each representing 40% ~ 50% of the whole amacrine cell population in the mouse retina (Pourcho and Goebel, 1985; Marc, 1988; Nguyen-Legros et al., 1997; Pow and Hendrickson, 1999; Lin and Masland, 2006). In addition, other neuroactive substances are also found in specific amacrine cell types, like: tyrosine hydroxylase in dopaminergic amacrine cells, choline acetyl transferase in cholinergic amacrine cells, and nitric oxide synthase (NOS) in NO-releasing

amacrine cells.

1.3 Cyclic guanosine monophosphate (cGMP) and the NO-cGMP pathway in the retina

Since the fundamental plan of the retina has been introduced in detail, the essential background about the key molecule in this project “cGMP” will be provided in this chapter. cGMP is a cyclic nucleotide composed of a sugar residue, a nitrogenous base and a phosphate forming a cyclic bond (Figure. 1.3).

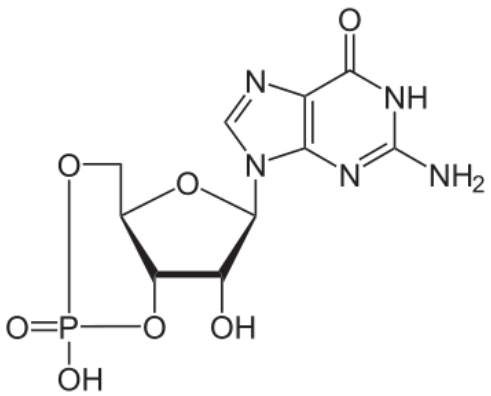

Figure 1.3:
Molecular structure of cyclic guanosine monophosphate (cGMP).

cGMP is derived from guanosine triphosphate (GTP) in an enzymatic reaction catalyzed by guanylate cyclases. It was in the 1960s, together with cyclic adenosine monophosphate (cAMP), that cGMP was found as a natural compound (for review see Beavo and Brunton, 2002). Since then, cAMP was paid much attention and its important role as second messenger in relaying signals from receptors on the cell surface to the cell interior has been elucidated. Earl W. Sutherland won a Nobel Prize for his contributions to the formulation of the second-messenger concept in 1971. Consequently, cGMP was rewarded little attention, although it was considered a second messenger quite early in 1970. The biological function of cGMP had remained a mystery until two key discoveries were made in the 1980s. First, atrial natriuretic peptide (ANP), a peptide synthesized in the heart, was found to stimulate cGMP synthesis by binding to a transmembrane receptor named particulate guanylate cyclase (pGC). Second, a substance known to dilate blood vessels - the elusive endothelium-derived relaxing factor - was identified as nitric oxide, which stimulates

soluble guanylate cyclase (sGC) in smooth muscle cells to synthesize cGMP, thereby causing vasorelaxation (Feil and Kemp-Harper, 2006). For the discovery of the NO-cGMP pathway in the cardiovascular system, Robert F. Furchgott, Louis J. Ignarro and Ferid Murad were awarded the Nobel Prize in 1998. After that, interest in cGMP metabolism grew. Later on, other mysteries of cGMP metabolism and signal transduction were revealed. So far, it has been quite clear that there are two possible processes controlled by cGMP (reviewed by Scott, 1991): 1) cGMP acts as a second messenger most notably to activate cGMP-dependent protein kinase or protein kinase G (PKG) which in turn phosphorylates several downstream targets responsible for diverse functions of cGMP such as regulation of vascular tone, gastrointestinal function, neuronal activity, and many others (for review Hofmann et al., 2006). 2) cGMP also can bind to certain ion channels known as cGMP-gated channels leading to channel opening and causing a sodium inward current. This channel type was initially identified in rod photoreceptors (Kaupp et al., 1989). Inactivation of cGMP is possible as it is degraded to 5'-GMP by PDEs (Beavo and Reifsnyder, 1990). PDEs can be inhibited by a number of substances including the nonselective PDE inhibitor 3-isobutyl-1-methylxanthine (IBMX). Interestingly, the various functions of cGMP are all found in visual transduction where cGMP-gated channels, PDEs and PKG are all involved (Maelicke, 1990).

Therefore, the retina turns out to be a particularly suitable tissue for the investigation of cGMP metabolism and function. Moreover, advances in the field of cGMP metabolism in the retina can help to understand its respective function in the other parts of the CNS.

Nitric oxide synthase (NOS), the enzyme catalyzing the generation of nitric oxide from L-arginine, exists in three major isoforms: neuronal, endothelial and immunologic NOS (reviewed by Goldstein et al., 1996). In immunohistochemical studies neuronal NOS (nNOS), also termed brain NOS (bNOS), was detected by specific antibodies in mammalian retinal neurons. It was revealed that certain types of amacrine cells in the rat, mouse, cat, guinea pig, and rabbit retina were consistently

labelled for nNOS (Kim et al., 1999); furthermore, some bipolar cells of the rat and guinea pig, some photoreceptors of the rabbit, and some Müller cells of the cat showed NOS immunoreactivity, as well (Kim et al., 1999). These results suggest that nitric oxide acts as a signaling molecule in retinal physiology. Since nitric oxide is a gaseous molecule with very short half-life, the spatial distribution of nitric oxide and its relationship to neuronal activity is difficult to resolve. However, detection of cGMP via specific antibodies in sections of retinae treated with nitric oxide-releasing chemicals gave insight into the NO-cGMP pathway in the retina. Blute and his coworkers examined turtle retina and found an increase of cGMP immunoreactivity in the inner retina (Blute et al., 1998). Similar results were observed in bovine retina (Gotzes et al., 1998), rat retina (Johansson et al., 2000), the goldfish retina (Baldridge and Fischer, 2001), and salamander retina (Blom et al., 2009). By using a specific antibody against sGC, Ding and Weinberg found that the nitric oxide receptor sGC was expressed in many neurons of the rat inner retina (Ding and Weinberg, 2007).

During my previous studies, using an antibody against cGMP I have studied the modulation of cGMP synthesis in the mouse retina (Zhao, 2010). I found that cGMP levels in the inner part of the retina can be strongly modulated by NO (Figure 1.4). Mainly bipolar cells and amacrine cells were involved. The bipolar cells immunoreactive for cGMP were identified as type 3a, 3b, 5, and 7 bipolar cells. Therefore, the NO-cGMP pathway has been demonstrated in the mouse inner retina (Zhao, 2010; Blom et al., 2012).

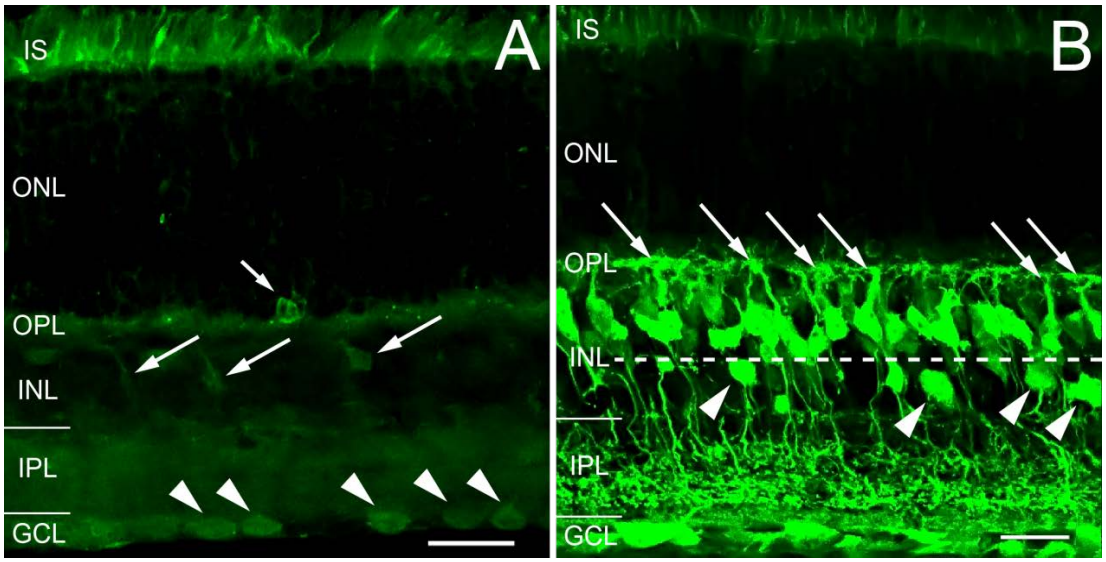

Figure 1.4: Increase of cGMP-immunoreactivity (cGMP-IR) in the mouse inner retina by exogenous NO. *(taken from Zhao, 2010)*

A: A vertical section of a mouse retina after incubation in the PDE inhibitor IBMX. Moderate cGMP-IR was found in the IS, weak label in the OPL and the IPL. Short arrow marks a soma of a photoreceptor with strong cGMP-IR. Three bipolar cells (marked by long arrows) in the INL were weakly positive. In the GCL, some cells (arrow heads) were also found to show cGMP-IR.

B: A vertical section of the second retina from the same mouse incubated in the presence of the NO-donor SNAP and IBMX. The staining pattern in the outer retina was the same as in A. Strong cGMP-IR was found in the inner retina. The dendrites of bipolar cells were seen to ramify in the OPL (arrows). The dashed line separates the outer part and the inner part of the INL. Several amacrine cells (arrow heads) also showed cGMP-IR. The entire IPL (borders marked by horizontal lines) displayed very strong staining patterned in several bands. Enhanced cGMP-IR was also observed in the GCL.

Scale bar = 20 µm.

1.4 Genetically encoded FRET-based cGMP sensors

Immunochemistry with antibodies against cGMP offers a valuable tool to study cGMP metabolism in an intact tissue. However, as cGMP immunohistochemistry is only possible after the tissue has been fixed, the results are “snapshots” and the method is limited mostly in neglecting the dynamic of metabolism processes. Therefore, it is necessary to use additional approaches that allow the investigation of cGMP with high temporal and spatial resolution. During the recent decades, several genetically encoded biosensors have been generated. They can be introduced and expressed in

cells in living organisms and tissues. Typically these sensors are designed in a stereotypical way: two fluorescent proteins are fused to a binding protein that interacts with the cellular compound that is to be detected. In the case of a cGMP sensor, the cGMP binding domain was chosen from cGMP interacting proteins such as PKG (Honda et al., 2001; Honda et al., 2005; Russwurm et al., 2007) or PDE2/PDE5 (Nikolaev et al., 2006; Niino et al., 2009). The working principle of all these sensors is based on the Förster resonance energy transfer (FRET).

1.4.1 Förster resonance energy transfer

FRET is a non-radiative energy transfer between an excited donor and an acceptor fluorophore, which leads to specific fluorescence emission of the acceptor without its direct excitation (Förster, 1948). When a donor fluorophore is excited to a higher-energy state by incident light within its absorption spectrum, it will normally decay to the ground state by emitting a photon within a characteristic emission spectrum. If another fluorophore (the acceptor) exists in proximity (≤ 10 nm) to the donor and has an absorption spectrum that overlaps with the emission spectrum of the donor, the energy of the donor can be transferred to the acceptor causing the acceptor to emit fluorescence. Figure 1.5 shows the absorption and emission spectra of cyan fluorescent protein (CFP) and yellow fluorescent protein (YFP), which form the FRET pair in most FRET-based sensors.

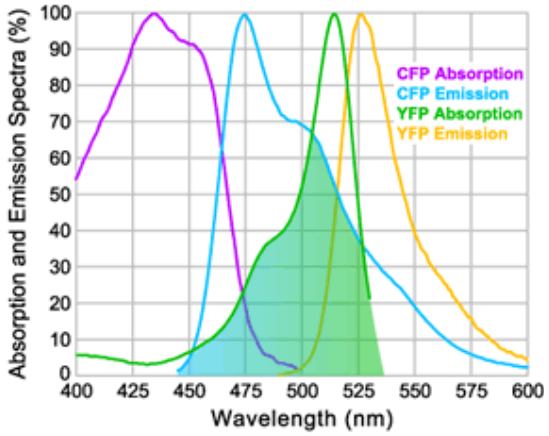

Figure 1.5:
CFP (donor) and YFP (acceptor) absorption and emission spectra.
Overlap between CFP emission and YFP absorption (shaded region) leads to efficient FRET interaction.
(http://www.semrock.com/Data/Sites/1/semrockimages/technote_images/graph_fret_cfpyfpoverlap.gif)

1.4.2 The cGMP biosensor Cygnet-2.1

In this project, a biosensor named Cygnet-2.1 (Honda et al., 2001; Honda et al., 2005) was employed for real-time cGMP imaging. Cygnet-2.1 is a genetically encoded FRET-based cGMP sensitive protein. This biosensor is composed of three parts (Figure 1.6): a cGMP binding site cloned from PKG flanked by the two fluorescent proteins CFP and YFP. CFP is the donor, whereas YFP is the acceptor. When the sensor is free of cGMP, energy can be transferred from CFP to YFP due to FRET. Upon the binding of cGMP, a conformational change in the sensor is induced. Therefore, the distance between donor CFP and acceptor YFP is increased, reducing the FRET efficiency between the two fluorescent proteins. To read out cGMP binding, emission intensities of the donor and the acceptor upon donor excitation are detected, and the FRET signal is depicted as a ratio of donor and acceptor fluorescence. The incidence of FRET is inversely related to the cGMP concentration.

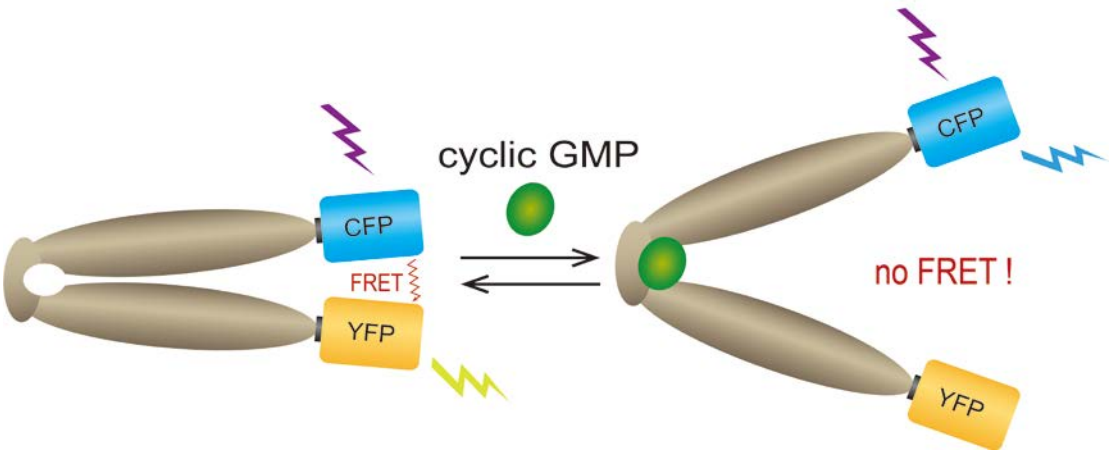

Figure 1.6: Mechanism of the cGMP sensor Cygnet-2.1.
Cygnet-2.1 contains a cGMP binding site (brown) and the two fluorescent proteins CFP and YFP. Upon the binding of cGMP, a conformational change is induced that reduces FRET efficiency between the two fluorescent proteins.

1.5 FlpTS GC-A cell line and its signalling pathway

The FlpTS GC-A cell line can be used as a model system to test Cygnet-2.1. This cell line was derived from HEK-293 cells. A cGMP signaling pathway was designed (Figure 1.7) by co-expressing appropriate signaling proteins: the membrane-bound receptor guanylate cyclase-A (GC-A) and a cyclic nucleotide-gated (CNG) ion channel. The GC-A can be activated by application of atrial natriuretic peptide (ANP). Binding of ANP induces a conformational change in the receptor that causes receptor dimerization and activation (Wilson and Chinkers, 1995; Yang and Garbers, 1997; Labrecque et al., 1999) and conversion of GTP into cGMP by the GC-A, raising the intracellular cGMP concentration. As a consequence, the elevation of intracellular cGMP causes CNG channels to open. This channel is permeable to calcium; hence the activation of the CNG channel can easily be monitored using calcium imaging techniques.

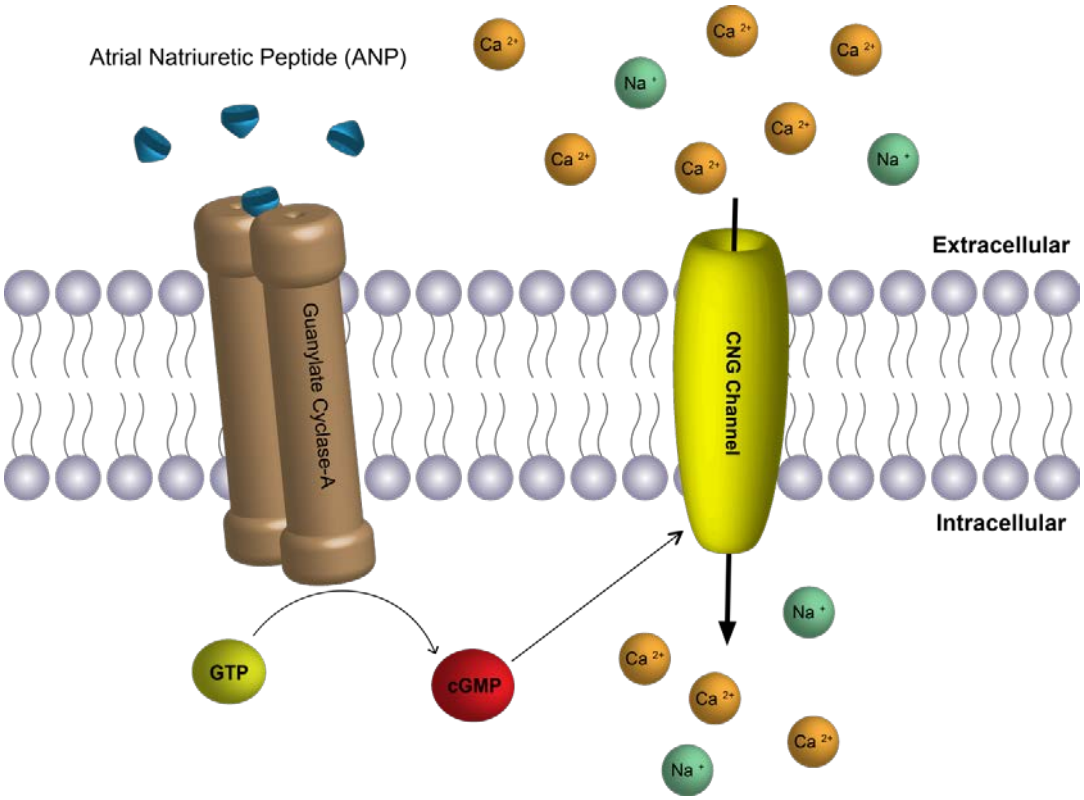

Figure 1.7: Signaling pathway in the FlpTS GC-A cell line.
Upon the binding of ANP, guanylate cyclase-A is activated and synthesizes cGMP from GTP. cGMP activates cGMP-gated channels, allowing for the entry of calcium into the cell.

1.6 Adeno-associated viruses (AAV)

To introduce the sensor protein into individual cells or living organisms *in vivo*, recombinant AAVs can be used as a gene ferry.

Adeno-associated viruses were discovered and isolated in 1960's. They were initially described as adenovirus-associated small DNA-containing particles behaving like defective viruses (Atchison et al., 1965, 1966). They are one of the smallest virus types with a non-enveloped capsid of approximately 22 nm diameter (Hoggan et al., 1966). AAVs display very low immunogenicity (Chirmule et al., 1999) and they induce no clearly defined cytotoxic response (Ponnazhagan et al., 1997). Most importantly, AAVs are considered to be non-pathogenic for humans (Monahan and Samulski, 2000). So far, 14 different serotypes of AAVs have been described. Serotypes differ from each other by the protein composition of their capsid. Different serotypes seem to infect certain cell types with a higher efficiency than others. This preferential targeting is probably mediated by receptor-mediated endocytosis of the AAVs.

A wild-type AAV has a linear single-stranded DNA (ssDNA) genome of approximately 4.7 kilobases (kb), containing only two genes: a "rep" gene and a "cap" gene (Figure 1.8 A). The "rep" gene encodes replication proteins; and the "cap" gene encodes capsid structural proteins. At each end of the ssDNA, there is a 145 nucleotide-long double-stranded complementary DNA (cDNA) as inverted terminal repeats (ITR), which is important for the replication of the viral plasmid and works as the signal sequence for packing virus DNA into the capsid (Lusby et al., 1980; Berns et al., 1988; Zhou and Muzyczka, 1998).

The virus does not encode a polymerase and therefore relies on host cell polymerases for genome replication. The 3'-end of the viral genome at the end of one ITR serves as a primer to start synthesis of the second DNA strand. The double-stranded DNA (dsDNA) is necessary for transcription and thus expression of viral proteins (Brister

and Muzyczka, 2000).

Recombinant AAV (rAAV) is produced by removing the viral genes and replacing them with the gene of interest (transgene) (Figure 1.8 B). The viral vectors used in this thesis are self-complementary AAVs (scAAVs) (Figure 1.8 C). Each scAAV genome contains a mutated ITR (mITR) in the middle connecting two ssDNAs that are complementary to each other, and two wild-type ITRs at the ends. Thus, the DNA is already double stranded so that it can be directly used for transcription and final translation without a duplication step in between making expression faster. The important trade-off for this efficiency is the loss of half the coding capacity of the vector (McCarty et al., 2001).

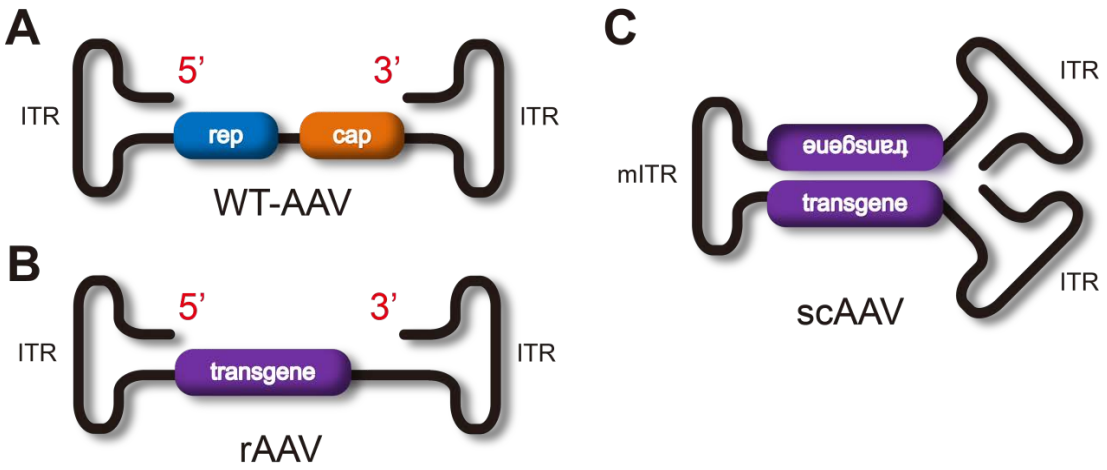

Figure 1.8: Schematic drawing of AAVs genome.

A: Wild type AAV genome with ssDNA containing a "rep" gene and a "cap" gene with ITRs at each end.

B: Conventional rAAV genome with ssDNA containing the transgene with ITRs at each end.

C: scAAV genome has two complementary transgenes connected by mITR in the middle and wild-type ITRs at each end.

1.7 Motivation

In my master thesis, I focused on the second messenger cGMP in the mouse retina and its regulation by nitric oxide in the inner retina. Using a specific antibody against cGMP, I visualized cGMP-immunoreactivity (cGMP-IR) in the mouse retina and found strongly increased cGMP-IR among many bipolar cells and amacrine cells

upon the stimulation with exogenous NO. Genetically encoded cGMP sensor proteins are suitable to study the spatiotemporal dynamics of cGMP signaling in living cells. This should lead to a better understanding of the NO-cGMP pathway and its role in adaptation or modulation of retinal signaling.

The aim of my thesis is to express the genetically encoded cGMP sensor Cygnet-2.1 in retinal cells. To this end, appropriate techniques have to be established. First, imaging techniques have to be optimized and proof of principle experiments have to be performed using Cygnet-2.1 to detect changes in intracellular cGMP in an appropriate model system. Second, different serotypes of AAVs have to be tested for transduction efficiency on retinal cells. As this can be achieved much more easily *in vitro* than *in vivo*, as an intermediate step, retinal cell cultures have to be established and characterized. Finally, a safe method has to be established for the intraocular injection of AAVs in order to transduce neurons in the intact retina *in vivo*.

2. MATERIALS AND METHODS

2.1 Materials

Chemicals and reagents with purity grade pro analysi (p.a.) were purchased from AppliChem (Darmstadt, Germany), Biozym (Hessisch Oldendorf, Germany), Enzo (Lörrach, Germany), GE Healthcare (Freiburg, Germany), Merck (Darmstadt, Germany), MWG-Biotech (Ebersberg, Germany), Qiagen (Hilden, Germany), Sigma (Deisenhofen, Germany) and Sigma-Aldrich (Munich, Germany). Materials for cell line culture and primary cell and tissue culture were ordered from GIBCO (Invitrogen, Germany). All solutions were prepared with bi-distilled water. Solutions were sterilized by filtration or autoclaving for 20 minutes at 121°C, when necessary.

2.2 Cygnet-2.1 calibration in a cell model

2.2.1 Cell line

HEK-293 cells are a cell line generated by transformation of human embryonic kidney cell cultures with sheared adenovirus 5 DNA (Graham et al., 1977). The FlpTS GC-A cell line was modified from HEK-293 cells by stably expressing the cyclic nucleotide-gated channel subunit A2 (CNGA2) and the particulate guanylate cyclase A (pGC-A). This cell line was kindly provided by Prof. Arnd Baumann's lab (ICS-4). In this project, all FlpTS GC-A cells were seeded on PDL-coated coverslips (Φ 13 mm) and kept in culture medium DH10 at 37°C, 5% CO_2 and 95% humidity.

DH10
Dulbecco's Modified Eagle Medium (DMEM; high Glucose, Invitrogen)
10 % fetal calf serum (FCS; Gibco/BRL)
1 % Glutamax (Gibco/BRL)
1 % penicillin-streptomycin (Gibco/BRL)
1 % non-essential amino acids (Gibco/BRL)

2.2.2 Transient transfection of FlpTS GC-A cells

Cells for imaging were transiently transfected with the following plasmids either alone or in combination: Cygnet-2.1 (Plasmid 19737, AddGene) and cGMP-specific phosphodiesterase type 5A (PDE5a; Clone ID: 8991949, Thermo Scientific). Both DNAs were introduced into cells via Lipofectamine® 2000 Reagent (Invitrogen).

For Lipofectamine-transfection, FlpTS GC-A cells were cultured on coverslips (2×10^4 cells/coverslip) in multi-well plates. The culture medium DH10 was replaced by OPTI-MEM (Invitrogen) (500 µl/well) at least 30 minutes before transfection. The transfection assay is described in Table 2.1.

Table 2.1: Transfection assay for a 13 mm coverslip.

Single-transfection		Double-transfection	
DNA in H_2O	500 ng	DNA (Cygnet-2.1) in H_2O	500 ng
Lipofectamine® 2000	1 µl	DNA (PDE5a) in H_2O	500 ng
OPTI-MEM	100 µl	Lipofectamine® 2000	1.5 µl
		OPTI-MEM	100 µl

The assay was mixed gently and incubated for 30 minutes at room temperature. Then the DNA-Lipofectamine® 2000 complexes were directly pipetted onto the cells followed by incubation at 37°C, 5% CO_2 and 95% humidity for 3 hours. Thereafter the medium was entirely exchanged by fresh DH10 (500 µl/well).

After 24 hours, the cells could be used for experiments.

2.2.3 Setup of the measuring chamber

All imaging was performed in a Plexiglas chamber with a volume of about 400 µl (constructed by the workshop of ICS-4) mounted on the microscope stage (Figure 2.1). This chamber was sealed with a glass coverslip at the bottom and a transparent lid on top. A multichannel perfusion system was connected to the chamber through plastic tubes (Neolab, Heidelberg). The perfusion system was driven by gravity and excess solution in the chamber was aspirated by a roller pump (Meredos GmbH, Germany).

The flow rate was adjusted between 3 and 4 ml/min.

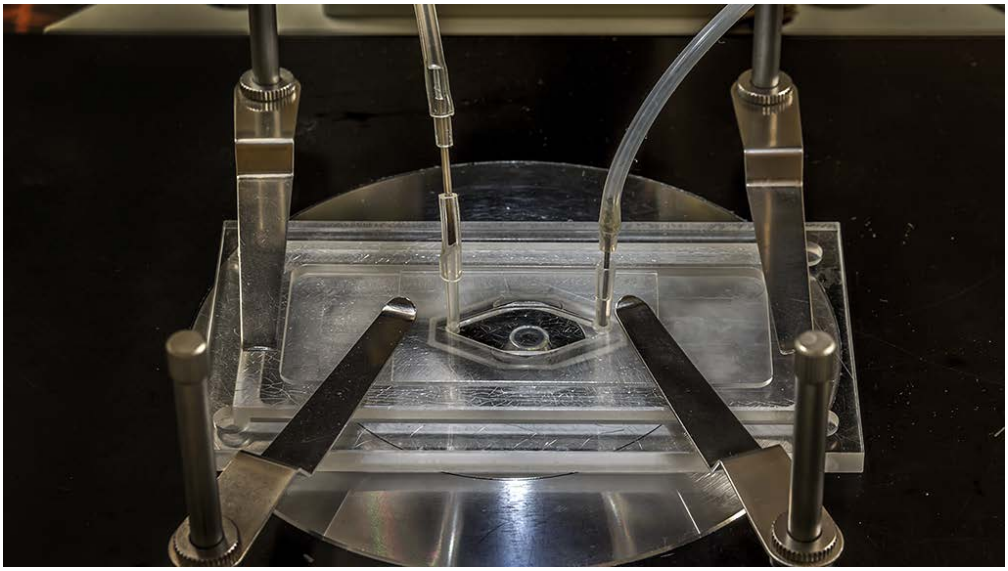

Figure 2.1: Measuring chamber with feed and drain of the perfusion system.
The feed is installed on the right side, from which solution flowed into the chamber. From the left side, the drain constantly removed the excess of bath solution. The coverslip with the cells was placed in the center of the chamber.

2.2.4 Calcium-imaging

2.2.4.1 Setup for Calcium-imaging

The setup (Figure 2.2) was mainly composed of a Laser source used for wide field illumination, an acousto-optical tunable filter (AOTF), an inverted microscope, and an electron multiplying charge-coupled-device camera (EMCCD-camera).

For calcium imaging, Fluo-4-AM (Invitrogen), a fluorescent synthetic Ca^{2+} indicator was used in this project. The excitation and emission maxima of the Ca^{2+}–bound form are 494 nm and 506 nm, respectively. All optical elements fitted to that fluorescence spectrum.

A laser beam with a wavelength of 447 nm was generated by a diode laser (MDL III 447, 500 mW, CNI Laser). It passed through an AOTF (AA.AOTF.nC-T 1001, AA Opto-Electronic), which diffracted the laser beam and controlled the exposure time in

the millisecond range. From the AOTF, the laser beam was guided by a flexible glass fiber to an inverted microscope.

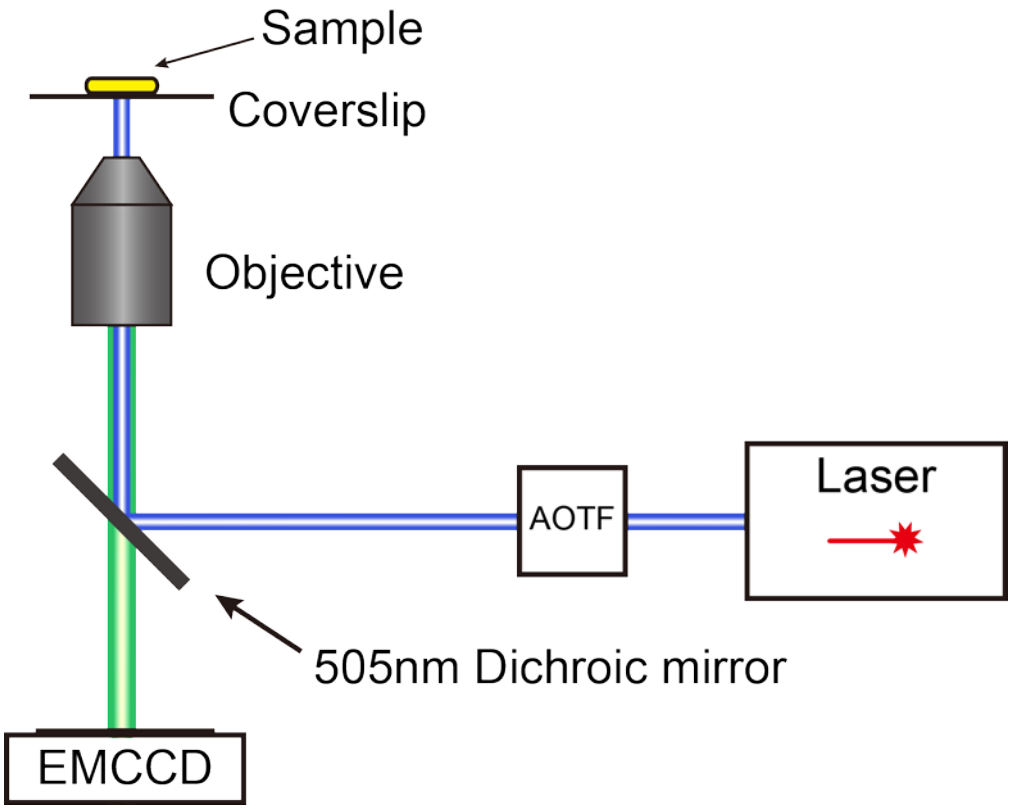

Figure 2.2: Setup for calcium imaging.

Inside the inverted microscope (Model IX70, Olympus), the laser beam was reflected by a 505 nm dichroic mirror (505DRLPXR XF2031, Omega Optics) to a 40x objective (LCAch Ph2, NA 0.55, Olympus) or a 60x objective (UPlanApo/IR, NA 1.2, Olympus), either of which focused the beam onto the sample. The emitted fluorescence light from the sample was transmitted through the objective and the dichroic mirror and finally projected onto the chip of the EMCCD-camera (iXON DU-897D-CSO, Andor Technology). The entire setup was controlled by a personal computer running the operation system MCtrl v0.7 programmed by Dr. Johnny Hendriks (ICS-4).

2.2.4.2 Measurements and data evaluation

A coverslip with adherent cells was carefully transferred into a 15 mm well containing 500 µl loading solution (3 µM Fluo-4-AM in ES). In this membrane permeable form, the calcium indicator can enter the cell. Once inside the cell, the acetoxymethyl group is cleaved by non-specific esterases, thereby generating free Fluo-4 in the cytosol. After 30 ~ 45 minutes of loading in the dark, the coverslip with cells was carefully placed into the center of the measuring chamber. During the measurement, extracellular solution (ES) or ES containing desired agents was continuously applied using a perfusion system. Fluo-4 was excited by the 447 nm laser light. Recording of pictures was acquired at 1 or 2 Hz and images were stored as stacks of TIF files.

The original data were processed using ImageJ (Abramoff et al., 2004; Schneider et al., 2012). The fluorescence intensity within a region of interest (ROI) was determined after subtracting the background intensity. Then the data were further progressed according to the formula:

$$(F_t - F_0) / F_0$$

F_0 is the base line intensity in the ROI; F_t is the intensity in the ROI at the time t in the recording.

All diagrams were produced using Origin 8.0 (OriginLab).

Extracellular solution (ES)

120 mM	NaCl
5 mM	KCl
2 mM	$CaCl_2$
2 mM	$MgCl_2$
10 mM	HEPES
10 mM	Glucose

* Adjusted to pH=7.4 (with NaOH)
* Adjusted to an osmolarity of 300 mOsm (with Glucose, 1mM ≈1 mOsm)

2.2.5 FRET-based cGMP-imaging

2.2.5.1 Setup for FRET measurement

FRET-based imaging was performed on the same setup (Figure 2.3) as calcium imaging, except that a beam splitter was employed.

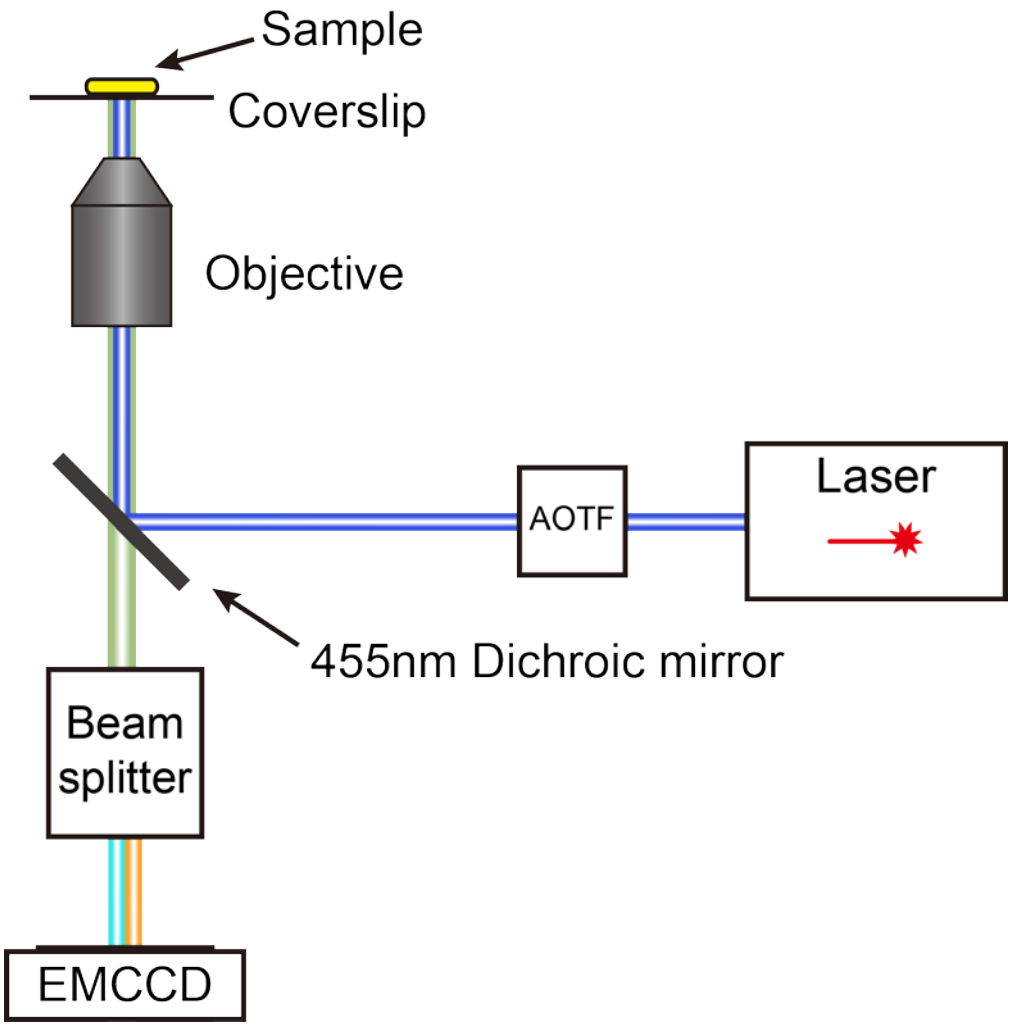

Figure 2.3: Setup for FRET measurement.

During FRET imaging, two fluorescent proteins CFP and YFP were used. For CFP, maximal absorption is at 434 nm and maximal emission is at 477 nm. For YFP, maximal absorption is at 513 nm and maximal emission is at 527 nm. All the optical elements were adjusted to match the two fluorescence spectra.

The laser beam of 447 nm wavelength was used to excite CFP. Inside the inverted microscope, the laser beam was reflected by a 455 nm dichroic mirror (455DRLP XF2034, Omega Optics). The emitted fluorescence light from the sample was transmitted through the objective and the dichroic mirror into a beam splitter (Optosplit II, Cairn Research). Within the beam splitter a dichroic mirror (505 nm DRLP XF2010, Omega Optics) was used to separate CFP emission from YFP emission by reflecting light below 505 nm (CFP emission) and transmitting light above 505 nm (YFP emission). The CFP component was passed through a 465 to 500 nm band-pass filter (AF30 Emitter XF3075, Omega Optics) and the YFP component through a 520 to 555 nm band-pass filter (AF26 Emitter XF3097, Omega Optics). At the output of the beam splitter the two fluorescent images were projected side by side onto the chip of the EMCCD-camera.

2.2.5.2 Measurements and data evaluation

A coverslip with adherent cells expressing Cygnet-2.1 was carefully transferred into the center of the measuring chamber. During measurement, ES or ES containing desired agents was continuously applied via the perfusion system. Images were captured at 1 or 2 Hz and recorded as stacks of TIF files.

The original data were initially processed with a series of programs designed by Dr. Luru Dai (ICS-4) in the environment of Matlab (The MathWorks). Within the programs, the fluorescence signals of a defined ROI in both CFP and YFP channels were determined after subtracting the background intensity and a ratio was calculated as CFP signal/YFP signal. Afterwards, the ratio (CFP/YFP) was further processed by the following formula in Excel (Microsoft):

$$(R_t - R_0) / R_0$$

R_0 is the base line ratio; R_t is the ratio measured at time t in the recording.

All diagrams were produced via Origin 8.0.

2.3 Retinal culture

2.3.1 Animals

Wild type mice (C57BL/6; Charles River, Germany) were bred in a local colony. Animals aged between postnatal day 2 and 8 (P2 to P8) were used. All procedures were approved by the local animal care committee of the Forschungszentrum Jülich (Tierschutzbeauftragte) and were in accordance with the law of animal experimentation issued by the German Government (Tierschutzgesetz). Ocular injections were performed according to LANUV NRW, Aktenzeichen 84-02.04.2011.A331.

2.3.2 Organotypic retinal whole-mount culture

2.3.2.1 Primary culture

C57BL/6 mice at P8 were deeply anaesthetized with isoflurane and quickly decapitated. The eyes were quickly enucleated and collected in Hank´s Balanced Salt Solution (Hank's; Sigma-Aldrich). The front part of the eye (cornea, lens, and vitreous) was discarded and the retina carefully isolated from the pigment epithelium. The intact retinae were then transferred into either 35 mm petri dishes or 6-well plates containing Millicell-HA inserts (pore size 0.45 µm, Φ 30 mm; Millipore) (Figure2.4).

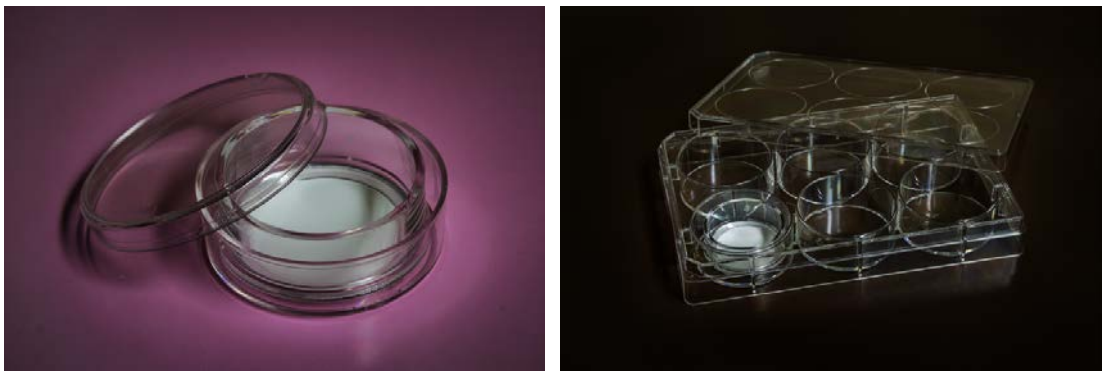

Figure 2.4: Millicell-HA inserts.

Retinae were mounted onto the membrane of the inserts in either one of two ways (Figure 2.5): A) flat mounted with the photoreceptors facing the filter and the ganglion cell layer facing up; B) following their natural curvature. In this preparation the photoreceptors faced up while the ganglion cells were sandwiched in the middle.



Figure 2.5: Schematic diagram of organotypic retinal whole-mount culture.

Afterwards, 1500 µl of modified DMEM medium (mDMEM) was added to the well. The cultures were kept at 37°C, 5% CO_2 and 95% humidity and 50% of the medium was changed every two days. Retinae were cultivated for 2, 4, 8, 12, and 16 days.

Modified DMEM (mDMEM)

42.25 ml	DMEM, High Glucose, GlutaMAX (Gibco)
0.5 ml	Antibiotic-Antimycotic, 100X (Gibco)
0.5 ml	Sodium-Pyruvate (Sigma-Aldrich)
0.5 ml	N2-Supplement, 100X (Invitrogen)
5 ml	FCS (Gibco/BRL)
1.25 ml	HEPES solution, 1 M, pH=7.4 (Sigma-Aldrich)

2.3.2.2 Immunocytochemistry

Retinal whole-mount cultures were fixed in 4% paraformaldehyde in 0.1 M phosphate buffer (PB) for 30 minutes at room temperature. Upon fixation, the cultures were washed in PB for 10 to 15 min. To section the whole-mount cultures, the retinae were cryoprotected by infiltration with 10% sucrose/PB for 2 hours and 30% sucrose/PB over-night, respectively. After being frozen in TissueTek (OCT; Fisher Scientific), retinal cultures were vertically sectioned (i.e. perpendicular to the layering) in a

thickness of 20 µm under optimum cutting temperature. Sections were collected on Superfrost plus glass slides (Thermo Scientific). Sections were blocked by incubation in CTA, and were then incubated overnight in the same solution containing the antibodies of interest. After washing in PB, sections were incubated with the appropriate fluorescent-labeled secondary antibody for 1 hour.

Control experiments included omission of the primary antibody and observation of only secondary antibodies labeled slides through the appropriate filter set. Sections were coverslipped using Aqua Polymount (Polysciences, Germany). The final analysis was performed using laser scanning confocal microscopy (Leica, see 2.3.5) using optimal settings.

Phosphate Buffer (0.1 M, PB)	
81 mM	Na_2HPO_4
19 mM	NaH_2PO_4

* in distilled water
* pH=7.4

Paraformaldehyde	
4 %	paraformaldehyde

* in 0.1 M PB

CTA	
5 %	Chemiblocker (Chemicon)
0.5 %	Triton-X 100 (Sigma)
0.05 %	NaN_3

* in 0.1 M PB

2.3.3 Dissociated retinal cell culture

2.3.3.1 Primary culture

Dissociated retinal cells were seeded onto 13 mm coverslips. Before seeding, coverslips were coated with 150 µl of a 0.1 mg/ml Poly-D-Lysine (PDL) solution at room temperature overnight. Following 2 times washing with sterile distilled water, coverslips were incubated in 100 µl of a 10 µg/ml Laminin solution at room

temperature for at least 3 hours. Laminin solution was aspirated immediately before seeding of cells.

C57BL/6 mice of postnatal day 2 to 4 (P2 to P4) were decapitated after deep anesthetization with isoflurane. The eyes were quickly enucleated and collected in Hank's. The front part of the eye (cornea, lens, and vitreous) was discarded and the retina was isolated from the pigment epithelium. The retinae were then transferred into a tube containing Calcium-Magnesium-free Hank's Balanced Salt Solution (CMF-Hank's; Sigma-Aldrich) and maintained for about 10 minutes. Following brief centrifugation and aspirating the supernatant, pre-warmed papain solution (20 units/ml in CMF-Hank's; Worthington, US) was applied and retinae were incubated for 20 minutes at 37°C. Afterwards, papain solution was removed and the retinae were washed twice with mDMEM to inactivate papain. Cells were gently dissociated by pipetting the retinae up and down through a 100 µl plastic tip (Nerbe Plus, Germany). When the tissue was fully dissociated, the cell suspension was adjusted by extra mDMEM to reach the concentration of 2000 cells/µl. For seeding, 150 µl of adjusted cell suspension containing 300000 cells was carefully added onto the coated surface of every coverslip in 15 mm wells and kept at 37°C, 5% CO_2 and 95% humidity for about 1 hour to allow cells to adhere. Finally, 350 µl of fresh mDMEM was added in order to increase the volume of the medium to 500 µl per well. Cultures were kept at 37°C, 5% CO_2 and 95% humidity, and 50% of the medium was changed every second day up to 4 weeks.

Poly-D-Lysine solution (0.1mg/ml, PDL)
5 mg PDL (Sigma-Aldrich)
50 ml distilled water

Laminin solution (10µg/ml)
100 µl Laminin (1 mg/ml, Sigma-Aldrich)
10 ml distilled water

Papain Solution (20 units/ml)
100 units Papain (Worthington)
5 ml CMF-Hank's

2.3.3.2 Immunocytochemistry

Immunocytochemistry for dissociated retinal cell cultures was performed on the glass coverslips and followed the same steps as described before (Chapter 2.3.2.2), except for the following modifications: 1) the fixation time was reduced to 10 minutes; 2) the incubation time was 1 hour for primary antibodies and 0.5 hour for secondary antibodies.

2.3.4 Organotypic retinal slice cultures

2.3.4.1 Primary culture

C57BL/6 mice at P8 were decapitated after deep anesthetization with isoflurane. The eyes were quickly enucleated and collected in Hank's. The front part of the eye (cornea, lens, and vitreous) was discarded and the retina was carefully isolated from the pigment epithelium. A tissue chopper (The Mickle Laboratory Engineering Co. Ltd., UK) was used to cut the retinae into vertical slices (perpendicular to the layering) with different thickness (150 µm or 250 µm). These slices were very carefully transferred into 35 mm petri dishes containing Millicell-HA inserts. In this preparation, slices attached with the cut surface to the filter and photoreceptors and ganglion cells faced either side of the slice. Afterwards, 1000 µl of mDMEM was added to the petri dishes. The cultures were kept at 37°C, 5% CO_2 and 95% humidity, and 50% of the medium was changed every two days. The retinae were cultivated for 2, 4, 6, and 8 days.

2.3.4.2 Immunocytochemistry

Retinal slice cultures were immunocytochemically stained intact on the filter. Staining procedure followed the same steps as described before (Chapter 2.3.2.2).

2.3.5 Native retina preparation and immunohistochemistry

C57BL/6 mice aged P8 to P24 were deeply anaesthetized with isoflurane and quickly

decapitated. The eyes were quickly enucleated and collected in Hank´s Balanced Salt Solution. The front part of the eye (cornea, lens, and vitreous) was discarded and the posterior part with the retina was fixed in 4% paraformaldehyde (in PB) for 30 minutes at room temperature. Upon fixation, the eye cups containing the retina were washed in PB for 10 to 15 minutes and, then cryoprotected by infiltration with 10% sucrose (in PB) for 2 hours and 30% sucrose (in PB) over-night, respectively. Thereafter, the retinae were carefully isolated from the eye cups and flat mounted on parafilm. After being frozen in TissueTek, retinae were vertically sectioned in a thickness of 20 µm under optimum cutting temperature. Sections were collected on Superfrost plus glass slides. Immunohistochemistry for native retinal sections was performed following the same steps as described in Chapter 2.3.2.2.

2.3.6 Confocal laser scanning microscopy

Immunofluorescence and differential interference contrast (DIC) images of retinal cultures and retinal sections were obtained by using a Leica TCS SP5II laser scanning confocal microscope (Leica Microsystems, Germany). The intensity of laser and filter settings were carefully controlled by the Leica LAS AF software. Wavelengths of 458 nm (for CFP) and 488 nm (for Cy2, GFP) generated by an argon laser and wavelengths of 543 nm (for Cy3), 594 nm (for Alexa594) and 633 nm (for Cy5, Alexa647, DyLight649, TO-PRO®3) generated by different HeNe lasers were used. All fluorescence micrographs were artificially colored. In addition, the sequential scanning mode was applied to rule out cross-talk between the fluorescence detection channels for samples with multiple stainings. Band pass filter of 465 - 490 nm for CFP, 500 - 540 nm for Cy2 and GFP, 555 - 605 nm for Cy3, 610 - 635 nm for Alexa594, and 650 - 750 nm for Cy5, Alexa647, DyLight649, TO-PRO®3 were used. Images were further processed in ImageJ and Adobe Photoshop (Adobe Systems, San Jose, CA) to optimize contrast and brightness. The layout was processed in Adobe Illustrator (Adobe Systems, San Jose, CA).

2.4 Adeno-associated viruses mediated transduction

All adeno-associated viruses (AAVs) used in this project were kindly provided by Prof. Arnd Baumann's lab (Table 2.1). AAV serotypes encoding green fluorescent protein (GFP) were used for initial testing of transduction efficiency. AAV2 encoding the cGMP sensor Cygnet-2.1 was used for Cygnet-2.1 expression in retinal cells. All viruses were stored in 40% iodixanol at - 20°C.

Table 2.2: AAVs used for transduction.

AAVs	Concentration (viral particles/µl)
AAV1-GFP	1.036×10^{9}
AAV2-GFP	1.780×10^{9}
AAV4-GFP	1.950×10^{9}
AAV6-GFP	3.666×10^{9}
AAV8-GFP	8.885×10^{9}
AAV9-GFP	1.072×10^{10}
AAV2-Cygnet-2.1	9.300×10^{7}

2.4.1 AAV mediated transduction of organotypic retinal whole-mount cultures

AAV mediated transduction in retinal whole-mount cultures was performed after two days in culture. Each AAV serotype was pre-diluted with mDMEM to obtain a concentration of 1×10^{10} vp/20 µl. For transduction, inserts with cultivated retinae were moved into dry and clean petri dishes. Then, 20 µl of the pre-diluted virus solution were directly pipetted onto the surface of each cultivated retina. Cultures were incubated with the virus solution at 37°C, 5% CO_2 and 95% humidity for 15 minutes. Thereafter, cultures were transferred back into the original culture plate with medium and were cultured for another 6 days. Then, the cultures were fixed for immunochemical studies.

2.4.2 AAV mediated transduction of dissociated retinal cell cultures

AAV mediated transduction on dissociated retinal cultures was performed two days after seeding. AAV serotypes were pre-diluted individually within mDMEM to obtain a concentration of 1×10^9 vp/300 µl. All cultures to be transduced were transferred into new dry and clean 4- or 24-well plates, depending on the number of cultures. Then, 300 µl of pre-diluted virus solution were added into each well. After two days, 200 µl of fresh mDMEM were added to each well. After another 6 to 8 days of cultivation, the cultures were used for imaging experiments or fixed for immunochemical studies.

2.4.3 AAV mediated transduction of FlpTS GC-A cells

AAV mediated transduction on dissociated retinal cultures was performed two days after seeding. AAV2-Cygnet-2.1 was pre-diluted with DH10 to obtain a concentration of 1×10^9 vp/300 µl. All cultures to be transduced were transferred into new dry and clean 4- or 24-well plates, depending on the number of cultures. Then, 300 µl of pre-diluted virus solution were added into each well and coverslips were cultured overnight. On the next day, extra 200 µl of fresh DH10 were added to each well. After another 3 to 4 days of cultivation, cultures were used for imaging experiments.

2.5 Ocular injection *in vivo*

2.5.1 Micro-injection system

Micro volumes were precisely delivered via a micro-injection system (Figure 2.6). This system was composed of a 10 µl-micro syringe (World Precision Instruments, Germany) connected with a 33-gauge beveled needle (World Precision Instruments, Germany) through a polyethylene tube (ID 0.38 mm; AgnTho's AB, Sweden). The syringe was mounted on and driven by an UltraMicroPump III (World Precision Instruments, Germany) which was precisely controlled by a SYS-MICRO4 controller (World Precision Instruments, Germany). The syringe, tube and needle were pre-filled

with mineral oil (Sigma-Aldrich). Before injection, about 5 µl of oil was displaced and the same volume of solution was sucked into the tube through the needle.



Figure 2.6: Micro-injection system for ocular injection.

2.5.2 Operation for ocular injection

C57BL/6 mice at postnatal day 5 (P5) were chosen for ocular injection. Mice were anesthetized by subcutaneous injection with a defined volume (10 µl/g body weight) of an anesthetic cocktail (Table 2.3).

Table 2.3: Prescription of anesthetic and antidote cocktail.

Anesthetic	
Medetomidine (1 mg/ml; Elanco, Germany)	50 µl
Midazolam (1 mg/ml; Actavis, Germany)	100 µl
Fentanyl (0.1 mg/ml; Janssen-CILAG, Germany)	100 µl
0.9% sterile NaCl (Berlin-Chemie, Germany)	750 µl
Antidote	
Atipamezole (5 mg/ml; Elanco, Germany)	50 µl
Flumazenil (0.1 mg/ml; Fresenius Kabi, Germany)	500 µl
Naloxone (0.4 mg/ml; ratiopharm, Germany)	300 µl
0.9% sterile NaCl	150 µl

* All pharmaceuticals were provided and controlled by the animal facility.

The entire operation was carried out under a dissecting microscope (Leica Microsystems, Germany). The pup was placed on a heating plate adjusted to 37°C. Once the pup was anesthetized, the skin that covered the eye was cut open with a scalpel blade along the fusion line of the two eyelids. The cutting was performed very gently without damaging the eye. A small incision was made in the sclera near the junction with the cornea using a 20-gauge needle and the 33-gauge beveled needle was inserted through the incision into the eye ball (Figure 2.7).

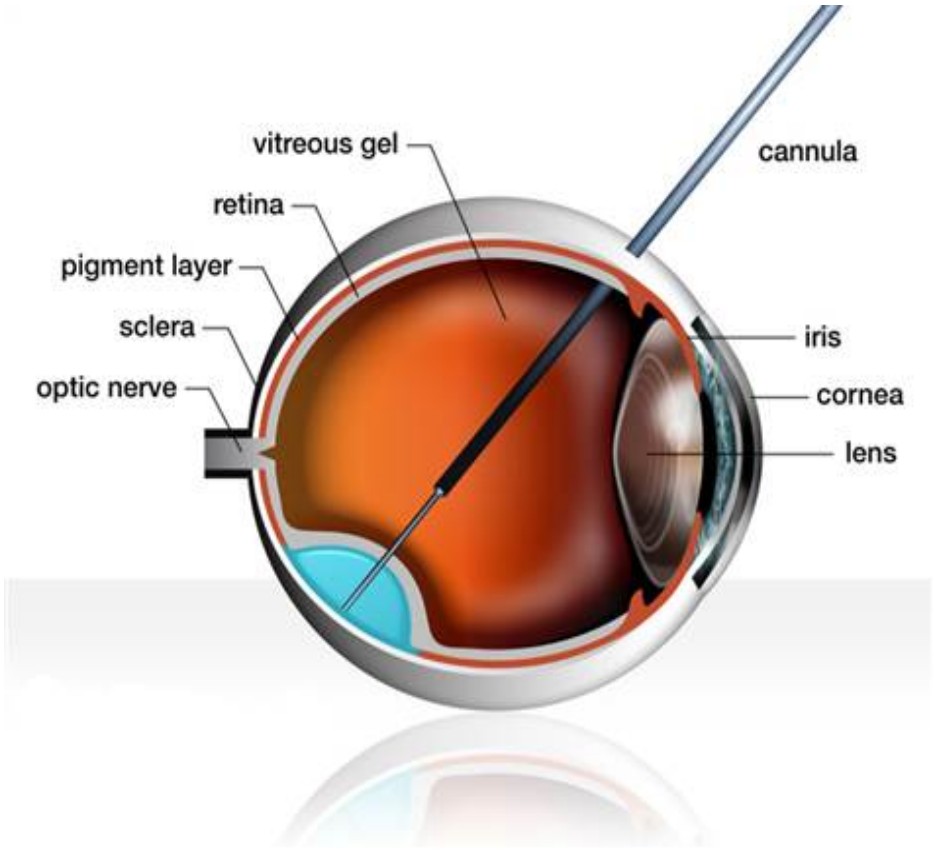

Figure 2.7: Rendering of a subretinal injection.
This image shows an artist's rendering of a surgery in which a solution is injected into the subretinal space. (AP / Moorfields Eye Hospital & University College London)
(http://media1.s-nbcnews.com/j/msnbc/Components/Photo_StoryLevel/080427/080427-vision-bcol-3p.grid-6x2.jpg)

0.5 µl of AAVs' stock solution (Table 2.2) were injected into the eye through the needle. At P5 the lens is still milky. Because the vision through the pupil was not clear, the exact injection position could not be monitored. For safety, before the injection was made the needle was slightly advanced backwards after reaching the bottom of

the eye. In that way, the viruses were injected as close to the retina as possible. After pulling out the needle a little amount of Refobacin Augensalbe (Merck) was smeared at the wound of the cover skin in order to reduce the risk of infection. A defined volume (10 µl/g body weight) of an antidote cocktail (Table 2.3) was injected subcutaneously. When the pups had recovered from anesthesia, they were returned to their mother.

2.5.3 Immunohistochemistry

Injected mice were kept for 4 to 8 weeks to allow for expression. Finally, mice were deeply anaesthetized with isoflurane and quickly decapitated. The eyes were quickly enucleated and collected in Hank´s. The front part (the cornea, lens, and vitreous) of the eye was discarded and the retina carefully isolated from the pigment epithelium. The following steps for immunohistochemistry were performed as described in chapter 2.3.2.2.

2.6 NO induced cGMP-immunoreactivity (cGMP-IR) in dissociated retinal cultures

Dissociated retinal cultures were used 3 to 4 days after seeding. Cultures were incubated in Ames' medium (Sigma-Aldrich, bubbled with 95% O_2 and 5% CO_2, pH 7.4) at room temperature for 10 minutes, which contained none or either one of the two NO donors: 100 µM S-nitroso-N-acetylpenicillamine (SNAP; Enzo) and 1 mM sodium nitroprusside dihydrate (SNP; Sigma-Aldrich).

After incubation, the cultures were fixed in 4% paraformaldehyde for 10 minutes at room temperature. Upon fixation, the cultures were immediately processed for immunocytochemistry following the protocol described in Chapter 2.3.3.2.

2.7 cGMP-imaging of dissociated retinal cultures upon transient transfection

Transient transfection of dissociated retinal cultures with Cygnet-2.1 was performed two days after seeding. The DNA was introduced into retinal cells using the Lipofectamine® 2000 Reagent. The transfection assay is described in Table 2.4.

Table 2.4: Transfection assay for retinal dissociated culture on a 13 mm coverslip.

Single-transfection	
DNA in H_2O	500 ng
Lipofectamine® 2000	1 µl
OPTI-MEM	100 µl

The assay was mixed gently and incubated for 30 minutes at room temperature. The culture medium was removed from the well and the DNA-Lipofectamine® 2000 complexes were directly pipetted onto the cells followed by incubation at 37°C, 5% CO_2 and 95% humidity for 3 hours. At the end of transfection, the solution was aspirated and the cells were incubated in fresh mDMEM (500 µl/well).

After 24 hours, the cultures could be used for imaging experiments.

The cGMP-imaging in dissociated retinal cultures followed the protocol described in 2.2.4 except that the incubation solution was replaced by Ames' medium. Solutions containing NO donors were prepared immediately before the imaging experiments.

2.8 Antibodies

Primary antibodies used in this study are described in Table 2.5.

Secondary antibodies used in this study are described in Table 2.6.

Table 2.5: List of primary antibodies.

Antibody	Antigen	Dilution	Species	Source
Blue opsin	blue-sensitive opsin	1:200	Goat polyclonal	Santa Cruz (sc-14365)
CaBP	Calbindin 28K	1:1000	Mouse monoclonal	Sigma (c-8666)
CaBP5	calcium binding protein 5	1:1600	Rabbit polyclonal	F. Haeseleer, Department of Ophthalmology, Seattle, WA
Calretinin	calretinin	1:10000	Rabbit polyclonal	Swant (7699/4)
cGMP	cGMP-formaldehyde-thyroglobulin complex	1:3000	Sheep polyclonal	Dr. Jan De Vente, The Rijksuniversiteit Limburg, The Netherlands
GAD65	glutamic acid decarboxylase isoform 65	1:4000	Mouse monoclonal	Abcam (ab26113)
GAD67	glutamic acid decarboxylase isoform 67	1:4000	Rabbit polyclonal	Chemicon (AB108)
GFAP	glial fibrillary acidic protein	1:400	Mouse monoclonal	Sigma-Aldrich (G3893)
GFP	green fluorescent protein	1:1000	Mouse monoclonal	Chemicon (MAB3580)
GFP	green fluorescent protein	1:8000	Rabbit polyclonal	Abcam (ab290)
GFP	green fluorescent protein	1:1000	Chicken polyclonal	Chemicon (AB16901)
GlyT1	glycine transporter 1	1:2000	Goat polyclonal	Chemicon (AB1770)
GS	glutamine synthetase	1:2000	Mouse monoclonal	BD Biosciences (610517)
NOS	neuronal nitric oxide synthase	1:4000	Rabbit polyclonal	Sigma (N7280)
PKARIIβ	protein kinase A, regulatory subunit IIβ	1:4000	Mouse monoclonal	BD Biosciences (P54720)
PKCα	protein kinase C, α isoform	1:2000	Mouse monoclonal	Transduction laboratories (P20420)
Recoverin	recoverin	1:2000	Rabbit polyclonal	Chemicon (AB5585)
Rhodopsin	rhodopsin	1:500	Mouse monoclonal	Dr. Robert S.Molday, The University of British Columbia

Antibody	Antigen	Dilution	Species	Source
sGC	soluble guanylate cyclase, subunit β1	1:500	Rabbit polyclonal	Cayman Chemicals, Ann Arbor, MI (160897)
Syt2	synaptic vesicle associated protein synaptotagmin-2	1:1000	Mouse monoclonal	Zebrafish International Resource Center (ZDB-ATB-081002-25)
TH	tyrosine hydroxylase	1:500	Chicken	Neuromics (CH23006)
TH	tyrosine hydroxylase	1:500	Mouse monoclonal	Sigma (T2928)

Table 2.6: List of secondary antibodies and nuclear stain.

Antibody	Dilution	Species	Source
Anti-chicken Cy™2	1:200	donkey	Dianova
Anti-chicken DyLight™649	1:800	goat	Dianova
Anti-goat Cy™2	1:400	donkey	Dianova
Anti-goat Cy™3	1:1000	donkey	Dianova
Anti-goat Alexa Fluor® 594	1:1000	donkey	Dianova
Anti-goat Alexa Fluor® 647	1:200	donkey	Invitrogen
Anti-mouse Cy™2	1:100	donkey	Dianova
Anti-mouse Cy™3	1:100	donkey	Dianova
Anti-mouse Alexa Fluor® 594	1:500	donkey	Dianova
Anti-mouse DyLight™649	1:500	donkey	Dianova
Anti-rabbit Cy™2	1:400	donkey	Dianova
Anti-rabbit Cy™3	1:500	donkey	Dianova
Anti-rabbit Alexa Fluor® 594	1:1000	donkey	Dianova
Anti-rabbit DyLight™649	1:500	donkey	Dianova
TO-PRO®3	1:1000	-	Invitrogen

3. RESULTS

The aim of this study was to establish methods that would allow to spatially and temporally monitor the dynamics of the second messenger cGMP in retinal neurons using the genetically encoded cGMP sensor Cygnet-2.1. The functionality of Cygnet-2.1 was first demonstrated in a cell model – the FlpTS GC-A cell line originated from the HEK-293 cell line. The most challenging aspect of the study is the expression of Cygnet-2.1 in the intact mouse retina *in vivo*. Recombinant adeno-associated viruses (AAVs) were chosen as gene ferries to deliver DNA into retinal cells. In a first step, different types of retina cultures were established and were used to characterize the performance of seven different AAV serotypes coding for GFP. Thereafter, six selected serotypes of AAVs were used to infect retinal cells *in vivo* via ocular injection and for each serotype transduction pattern and efficiency were characterized. Comparative analysis between the results obtained *in vitro* and *in vivo* determined AAV serotype II (AAV2) as a suitable vector to express Cygnet-2.1 in retinal cells. Finally, the functionality of Cygnet-2.1 expressed upon AAV2 transduction was further examined by cGMP-imaging in both retina cultures and FlpTS GC-A cells.

3.1 Characterization of Cygnet-2.1 in the model system FlpTS GC-A

3.1.1 Calcium-imaging in FlpTS GC-A cells

Cygnet-2.1 was characterized in the model cell line FlpTS GC-A. This cell line is derived from HEK-293 cells and expresses the particulate guanylate cyclase A (pGC-A) as well as a cyclic nucleotide-gated (CNG) channel composed of CNGA2 subunits. The atrial natriuretic peptide (ANP) activates the pGC-A which in turn synthesizes cGMP. A rise in intracellular cGMP leads to CNG channel activation and, hence, calcium influx. The changes in the intracellular calcium concentration can, therefore, be used to indirectly monitor the changes in the intracellular cGMP concentration.

In initial experiments, cells were incubated with the membrane permeable variant of the calcium indicator Fluo-4 for 30 to 40 minutes. Cells were transferred to the perfusion chamber of the imaging setup, constantly perfused with extracellular solution (ES) and the Fluo-4 fluorescence was detected using a camera. During recording, cells were superfused with ES containing 10 nM ANP for 1 minute. In Figure 3.1.1, the fluorescence signal of regions of interest (ROIs) recorded from three cells is plotted over time. The ROIs were defined to cover an individual cell entirely. The fluorescence signal is displayed as the change ΔF in fluorescence intensity divided by the initial fluorescence intensity F_0. A rapid increase in the fluorescence was detected approximately 20 seconds after the onset of ANP application. This delay was observed in all imaging experiments and is due to the time span needed to exchange the medium in the recording chamber. During the period of application, the fluorescence intensity decreased to a slightly lower level (about 88% of the peak). Upon washout of ANP, the fluorescence did not recover to the baseline level but remained at this elevated level until the end of the recording (5 minutes). In all traces, 0.16 Hz fluctuations can be observed. The fluctuations are perfectly synchronized between the cells and probably reflect a slight instability in the performance of the laser or the AOTF in the excitation pathway of the imaging setup.

As Fluo-4 acts as a calcium indicator, the increase in fluorescence intensity can be interpreted as a rise in the internal calcium concentration upon stimulation of the cell with ANP.

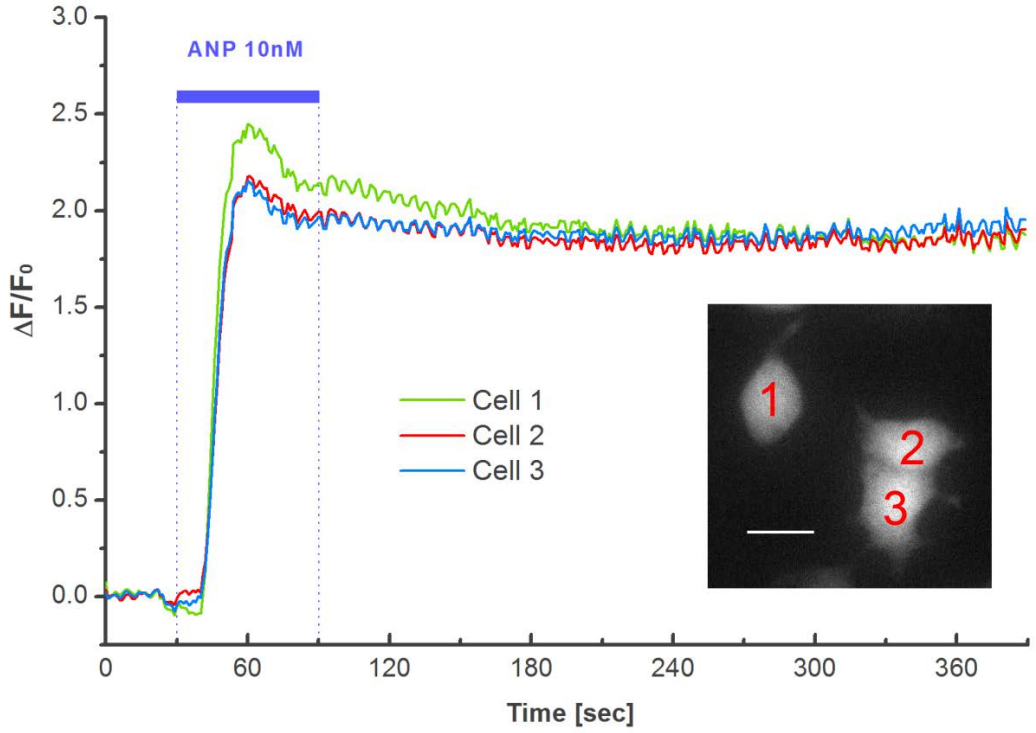

Figure 3.1.1: Fluorescence intensity of the calcium sensor Fluo-4 increased in FlpTS GC-A cells upon stimulation with ANP.

The fluorescence signal of three FlpTS GC-A cells loaded with Fluo-4 (indicated in the screenshot) is displayed. ANP (10 nM) was applied from 30 to 90 seconds. All cells showed a rapid increase of the Fluo-4 fluorescence, indicating a rise in the intracellular calcium concentration upon the stimulation with ANP. Interestingly, the fluorescence remained elevated after washing with ES for 5 minutes.

Scale bar = 20 µm. in screenshot

According to the signaling pathway of the FlpTS GC-A cells, the calcium influx is triggered by the opening of the CNG channels and, therefore, depends on the level of the intracellular cGMP concentration. The rise in the internal calcium concentration results from the activation of pGC-A by ANP. However, upon washout of ANP a decrease of the internal calcium concentration would have been expected as under other experimental paradigms calcium is readily cleared from the cytoplasm of HEK-293 cells (data not shown). One possible explanation would be that the cGMP concentration remains high even after ANP application was terminated, leading to a constant activation of CNG channels and, hence, constant influx of calcium. This hypothesis was tested by using the cGMP sensor Cygnet-2.1.

3.1.2 FRET-based cGMP-imaging in FlpTS GC-A cells

The cDNA encoding Cygnet-2.1 was transiently transfected into FlpTS GC-A cells by means of Lipofectamine® 2000 reagent. After expression for about 24 hours, cells were used for imaging.

Figure 3.1.2 shows one screenshot capturing two cells during an imaging experiment. Cygnet-2.1 is a FRET-based sensor. A beam splitter was used to separate the fluorescence signals into two parts: CFP fluorescence below 505 nm and YFP fluorescence above 505 nm. Both images were projected by the beam splitter side by side onto the camera chip. The upper part displays the image originating from CFP fluorescence; the lower part shows the identical image displaying YFP fluorescence. A healthy FlpTS GC-A cell transfected with Cygnet-2.1 usually shows the fluorescence mainly in the cytoplasm, while the nucleus is devoid of fluorescence.

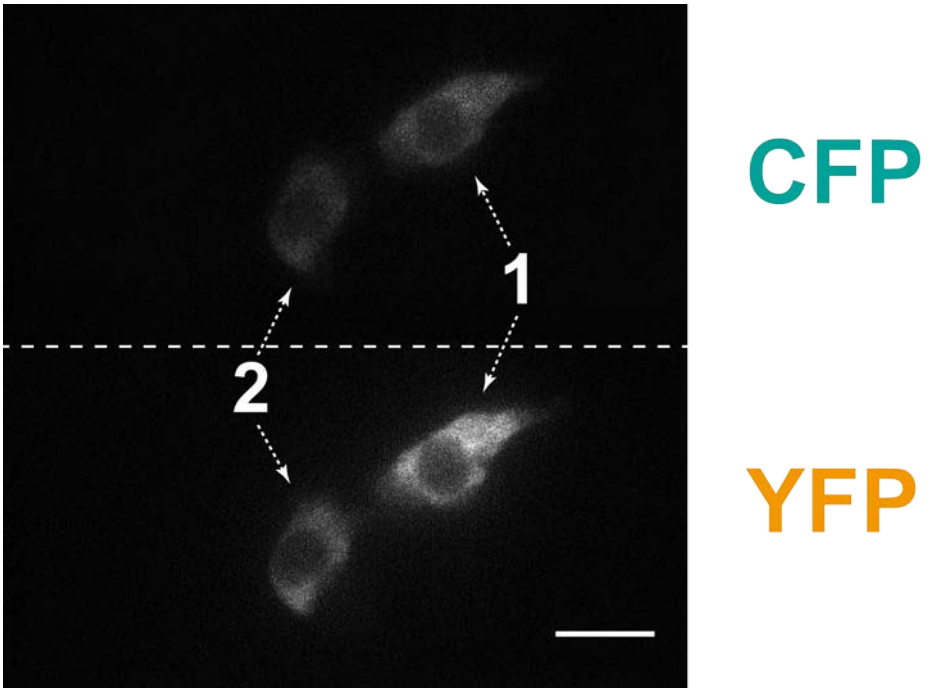

Figure 3.1.2: Screenshot from a FRET imaging experiment on FlpTS GC-A cells expressing Cygnet-2.1.

Two cells were captured. The upper panel (above the dashed line) represents the image in the CFP channel, while the lower panel (below the dashed line) reflects the image in the YFP channel. Note that fluorescence is only found in the cytoplasm of the cell.
Scale bar = 20 µm.

ROIs were adjusted to each cell and fluorescence intensity in both CFP and YFP channels was measured and plotted in artificial units over time. Figure 3.1.3 shows the result from cell 1.

During the whole recording, cells were constantly superfused with ES. The baseline intensity was stable during the ES perfusion. After the onset of ES containing 10 nM ANP, the CFP intensity increased while the YPF intensity decreased. The changes of CFP intensity and YFP intensity were mirror reversed. This is to be expected as binding of cGMP to the sensor Cygnet-2.1 reduces the efficiency of FRET between CFP and YFP. Similar to the calcium-imaging experiments as shown in Figure 3.1.1, the signals did not fully recover to baseline upon washout of ANP.

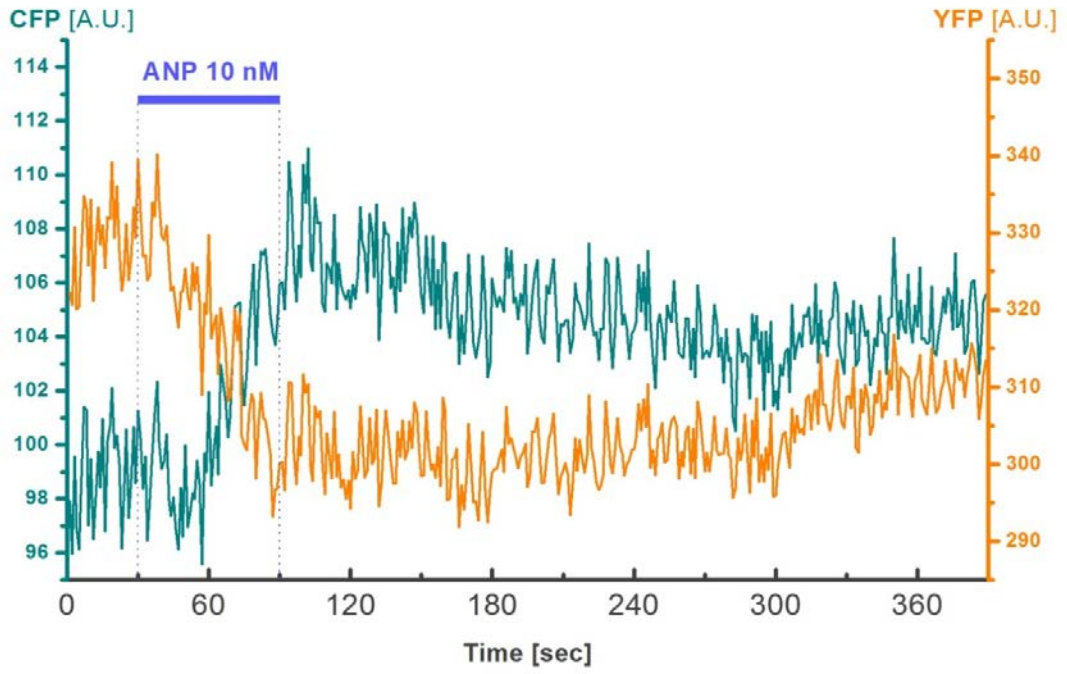

Figure 3.1.3: Fluorescence intensity of CFP and YFP for cell 1 during one recording.

CFP and YFP fluorescence was plotted in artificial units (A.U.) over time (CFP in cyan and YFP in orange). During the application of ANP (10 nM), the CFP fluorescence intensity increased, while the YFP fluorescence intensity decreased. The mirror reversed changes of CFP and YFP fluorescence are to be expected, if the FRET efficiency between the two fluorescent proteins is reduced by binding of cGMP to Cygnet-2.1. Note that the signals did not recover to baseline upon washout of ANP.

In the following, the signal was depicted as the ratio of CFP/YFP by dividing the CFP fluorescence intensity by the YFP fluorescence intensity. The ratiometric depiction also reduces artefacts that originate from instabilities of the excitation pathway of the imaging setup or from the movements of the cells during perfusion as fluorescence intensities of CFP and YFP are affected by such artefacts in the same way. In the ratiometric depiction (Figure 3.1.4), the curve of CFP/YFP is much smoother and less noisy than the original traces depicted in Figure 3.1.3.

As Cygnet-2.1 works as a FRET-based cGMP sensor, the reduction of FRET is due to the cGMP binding and, hence, the increase in the ratio of CFP/YFP can be interpreted as a rise in the intracellular cGMP concentration upon stimulation of the cell.

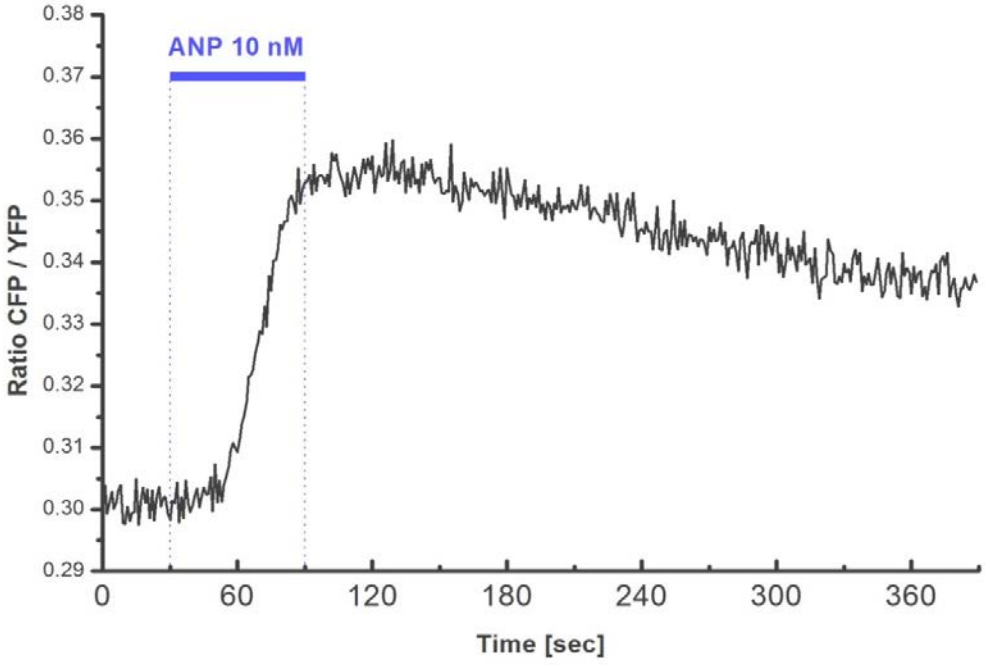

Figure 3.1.4: Ratio of CFP/YFP for cell 1 during one recording.
The ratio of CFP/YFP is plotted over time. A sharp increase was observed during the application of ANP, which can be interpreted as a reduction in FRET efficiency upon the binding of cGMP to the sensors and, therefore, as a rise in the cGMP concentration.

In Figure 3.1.4, the baseline ratio of CFP/YFP for cell 1 was around 0.3 before ANP application. Upon the stimulation with ANP, the ratio readily climbed to a plateau at around 0.355, representing an 18.3% change of the ratio (or FRET change).

Interestingly, upon washout of ANP the value of the ratio only slightly decreased but did not recover to the baseline level. This is reminiscent of the calcium imaging experiments that had revealed a prolonged increase in the intracellular calcium level (Figure 3.1.3).

In Figure 3.1.5, the FRET change for both cell 1 and cell 2 captured in Figure 3.1.2 was normalized as the change in CFP/YFP ratio (ΔR) divided by the initial ratio (R_0) and plotted over time. Both curves show a fast increase to about 0.18 upon the stimulation with ANP, which represents a change in FRET efficiency of 18%. Compared to cell 1, for cell 2 the cGMP increase upon ANP application was delayed for about 10 seconds. This difference might reflect differences between individual cells. In both cells the signal decreased very little upon washout of ANP.

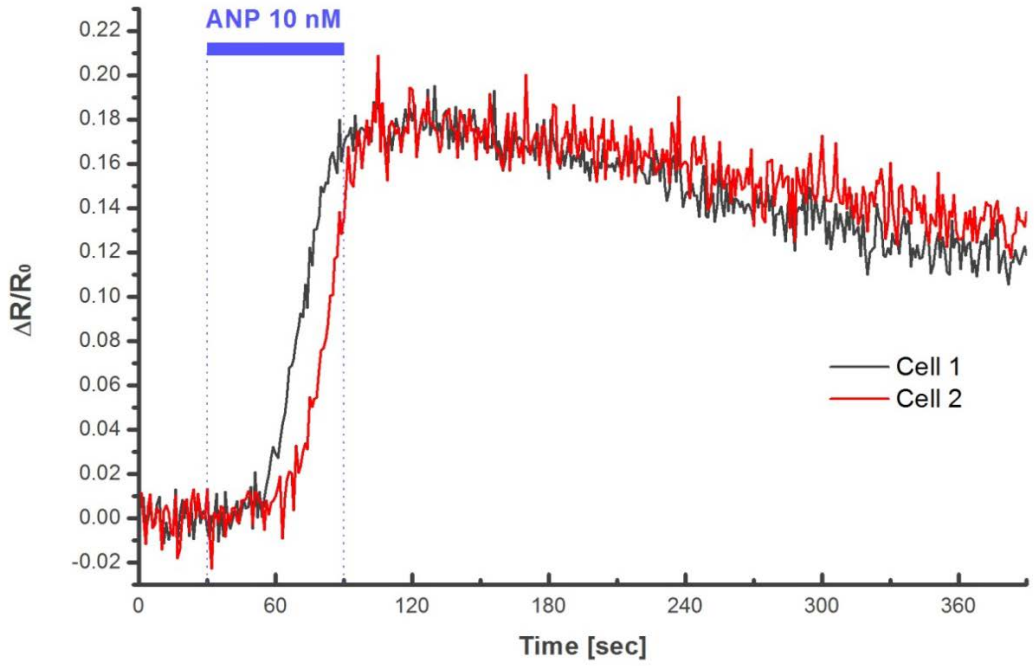

Figure 3.1.5: ANP stimulation increases cGMP concentration in FlpTS GC-A cells.
The FRET change observed in two FlpTS GC-A cells transiently transfected with Cygnet-2.1 was plotted over time. ANP (10 nM) was applied from 30 to 90 seconds. Both cells showed a fast increase ΔR of the ratio CFP/YFP to ~0.18 indicating a rise in the intracellular cGMP concentration upon stimulation with ANP. After a 5-minute washout, the ratios decreased by 0.06 for both cells but did not reach the baseline level by the end of the recording.

The slight decrease in both traces during the washing phase indicates that it takes a long time for the intracellular cGMP concentration to return to the baseline level. In the following experiments I changed the experimental parameters. First, the ANP concentration was reduced to 1 nM to avoid saturation of the response. A K_D value 0.1 to 1 nM has been described for the pGC-A (Jacobs et al., 1987; Pandey, 1997). Secondly, the ES washing time was extended to 10 minutes. The results for five cells are shown in Figure 3.1.6.

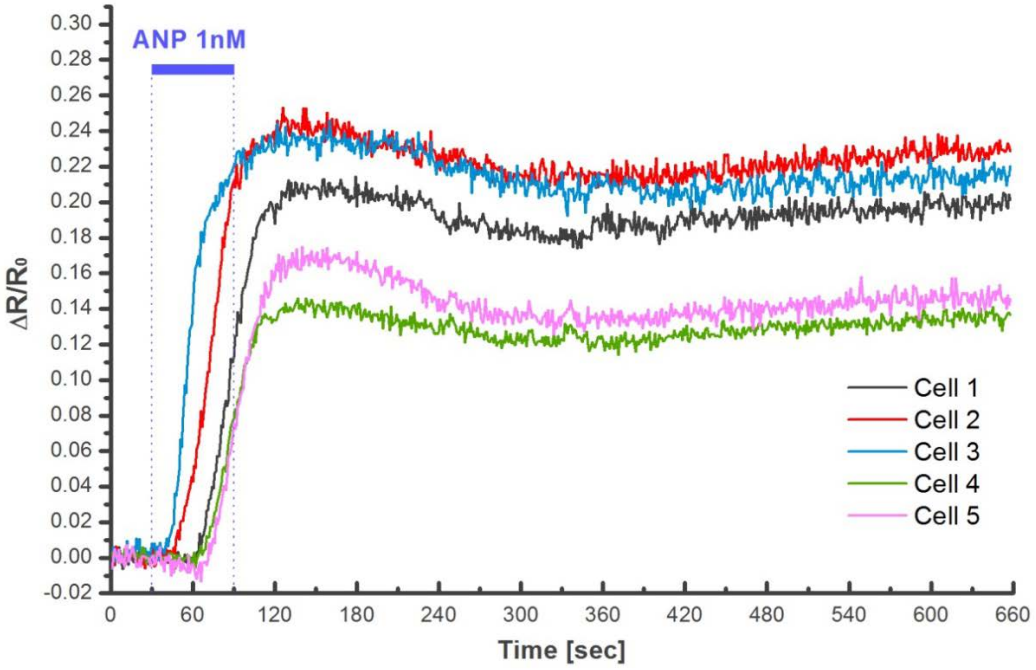

Figure 3.1.6: The fluorescence signals do not recover to baseline even with low ANP concentration and prolonged washout.

The FRET change of five FlpTS GC-A cells transiently transfected with Cygnet-2.1 was plotted over time. ANP (1 nM) was applied from 30 to 90 seconds. Upon the stimulation with ANP, the FRET change of Cygnet-2.1 indicated a rapid increase in the intracellular cGMP concentration in all cells. Despite washing for nearly 10 minutes, in none of the cells the signal recovered to the baseline level.

In Figure 3.1.6, five cells were recorded. For all cells, a rapid increase in cGMP concentration was observed during the application of 1 nM ANP. FRET changes were in the range of 14% to 24.5%, similar in amplitude to the responses observed upon the stimulation with 10 nM ANP (12% ~ 25%, n=22). Again, no recovery was observed

after washout of ANP.

Upon a further reduction in the ANP concentration to 0.5 nM, cellular responses became inconsistent. Some cells showed large responses, however with a long delay, while other cells did not respond at all (data not shown). Therefore, an ANP concentration of 1 nM was used in the following experiments.

In summary, the results indicated that upon stimulation of the pGC-A with ANP, the sensor Cygnet-2.1 displayed a fast increase in the ratio CFP/YFP, but the signal did not return to baseline levels even during prolonged washout phases. There are several explanations for this behavior.

1) The sensor may not reflect the change in the intracellular cGMP level properly. If the dissociation of cGMP from the sensor is slow, the cGMP-induced change in the sensor conformation and FRET rate might persist for a long time, even after the cGMP level has decreased.

2) ANP might bind to the pGC-A in a non-reversible or slowly reversible manner. Therefore, cGMP synthesis in the FlpTS GC-A cell line might continue during the washout phase.

3) The FlpTS GC-A cells might lack a phosphodiesterase capable of cleaving cGMP. As a consequence, the intracellular cGMP concentration would remain high even after washout of ANP.

The first possibility is rather unlikely. In the calcium-imaging experiments (Chapter 3.1.1), calcium levels were also found to remain elevated for a long time after washout of ANP. The second and third possibilities reflect problems unrelated to the functionality of Cygnet-2.1. Nevertheless, I tested between both possibilities by expressing the cGMP-specific phosphodiesterase type 5a (PDE5a) in FlpTS GC-A cells.

3.1.3 In the presence of the cGMP-specific PDE5a Cygnet-2.1 displays rapidly reversible signals in FlpTS GC-A cells

The cDNA encoding PDE5a was transiently transfected together with Cygnet-2.1 into FlpTS GC-A cells by the use of Lipofectamine® 2000 reagent. After 24 hours of expression, the cells were used for imaging experiments.

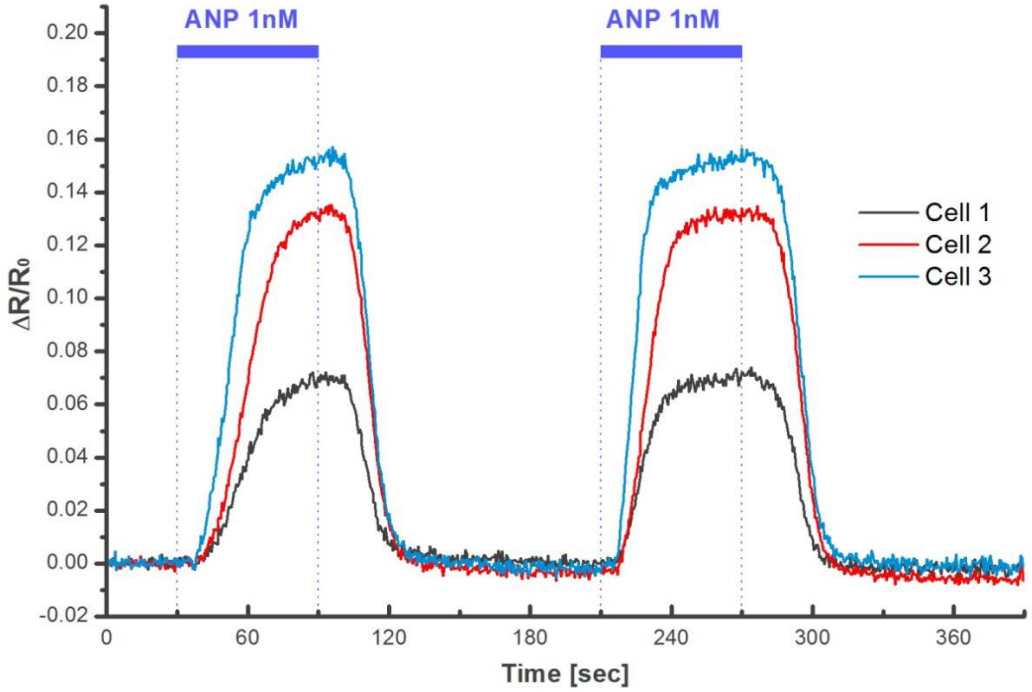

Figure 3.1.7: ANP-induced cGMP signal rapidly recovers to baseline in the presence of PDE5a.

The FRET change of three FlpTS GC-A cells transiently co-transfected with Cygnet-2.1 and PDE5a was plotted over time. ANP (1 nM) was applied during seconds 30 to 90 and 210 to 270. All cells showed rapid FRET changes after both onset and offset of ANP, which indicates the transient elevation of the intracellular cGMP concentration during the stimulation with ANP.

One of the experiments is shown in Figure 3.1.7. The FRET changes recorded from three FlpTS GC-A cells are plotted. Upon the stimulation with 1 nM ANP in all three cells a rapid FRET change albeit of different amplitudes was recorded. Around 15 seconds after the application of ANP had been stopped, the signal of all three cells quickly returned to the baseline level. Increase and decrease of the signals occurred in the same time range. These data suggest that the prolonged signals shown in Figure

3.1.5 and 3.1.6 reflect the prolonged increase in cGMP concentration due to the incapability of the endogenous phosphodiesterases to degrade cGMP. Upon expression of the cGMP degrading PDE5a, Cygnet-2.1 displays a fast dynamic response reflecting both cGMP binding and unbinding. During a second application of ANP, again the signal was fully reproducible. Although somewhat faster than during the first stimulation, similar amplitudes were reached during the second stimulation.

Similar experiments were performed using calcium imaging. For these experiments, FlpTS GC-A cells were transiently transfected with PDE5a. After being loaded with Fluo-4 for 30 to 40 minutes, cells were transferred into the recording chamber and used for calcium imaging according to the protocol shown in Figure 3.1.7.

The fluorescence intensity of two FlpTS GC-A cells was plotted over time (Figure 3.1.8). The two cells display very different calcium changes. Cell 1 displayed a calcium response similar to those shown in Figure 3.1.1. The calcium concentration sharply increased upon stimulation with 1 nM ANP, and remained elevated upon washout. During the second period of ANP stimulation the cell barely responded. In contrast, cell 2 responded with transient calcium elevations to both ANP applications. The discrepancy between cell 1 and 2 can be explained by the low transfection efficacy. Most probably, cell 1 did not express PDE5a, while cell 2 did.

Due to the low transfection efficiency, both PDE5a-expressing cells and none-PDE5a-expressing cells could be found in every recording. Among the whole population of the FlpTS GC-A cells recorded in this set of calcium-imaging experiments, about 42% of the cells (60/143) displayed permanent calcium elevations like cell 1, while 37% of the cells (53/143) displayed transient calcium elevations like cell 2. The remaining 21% cells (30/143) did not respond to ANP stimulation, probably due to a low expression of pGC-A.

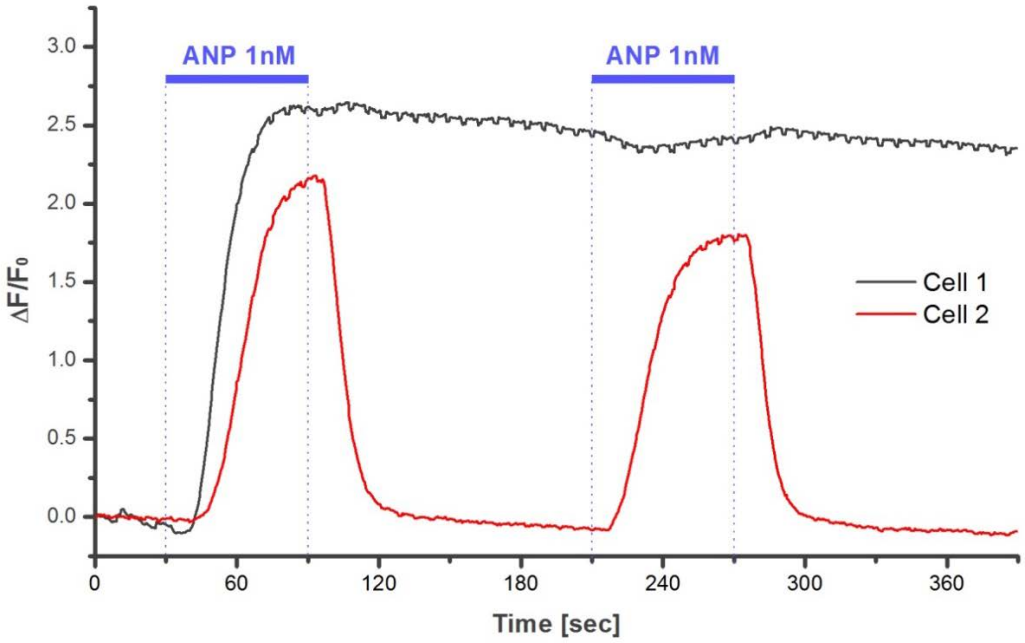

Figure 3.1.8: cGMP degradation by PDE5a in FlpTS GC-A cells results in transient calcium signals upon ANP stimulation.

The fluorescence signal of two FlpTS GC-A cells loaded with Fluo-4 is plotted over time. ANP (1 nM) was applied during seconds 30 to 90 and 210 to 270. Cell 1 (probably without PDE5a) showed a rapid increase of the Fluo-4 fluorescence, indicating a rise in the intracellular calcium concentration upon the first stimulation with ANP. Its fluorescence remained elevated until the end of the recording. Cell 2 (probably expressing PDE5a) showed transient increases of the Fluo-4 fluorescence, indicating transient elevation of the internal calcium concentration during the two applications of ANP.

3.1.4 Selectivity of Cygnet-2.1

In the following I tested whether the response of Cygnet-2.1 was specific for cGMP. The FlpTS GC-A cell line is a modified HEK-293 cell line and, therefore, expresses β-adrenergic receptors (βARs) (Krupinski et al., 1992). The βARs are linked to G_S proteins which in turn couple to adenylate cyclases. Agonists like noradrenaline (NA) activate βARs and, thus, cause a rise in the intracellular concentration of cAMP. Therefore, the response of Cygnet-2.1 to cAMP was tested in FlpTS GC-A cells co-transfected with Cygnet-2.1 and PDE5a. One of the recordings is shown Figure 3.1.9.

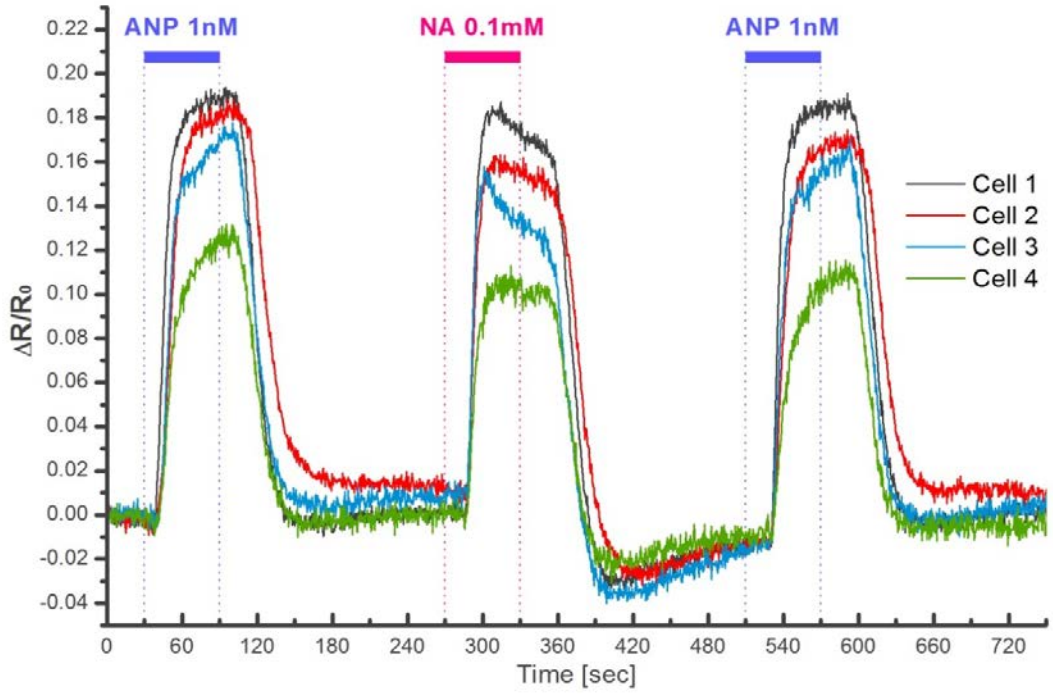

Figure 3.1.9: Cygnet-2.1 seems to respond to both cGMP and cAMP.

The FRET change of four FlpTS GC-A cells transiently co-transfected with Cygnet-2.1 and PDE5a was plotted over time. ANP (1 nM) was applied from 30 to 90 seconds and from 510 to 570 seconds. All cells showed transient FRET changes, indicating a transient elevation of the intracellular cGMP concentration during the application of ANP. NA (0.1 mM) was applied from 270 to 330 seconds. During application, a FRET change was recorded in all four cells that was similar in amplitude to the FRET change during ANP application. This suggests that Cygnet-2.1 responds to the increase in the internal cAMP concentration upon the stimulation with NA. After the washout of NA, an overshoot appears in all trances when the ratio recovers to the baseline.

In Figure 3.1.9, the recordings of four cells co-expressing Cygnet-2.1 and PDE5a are shown. During seconds 30 to 90, ANP (1 nM) was applied. A transient FRET change was recorded, indicating a quick increase and decrease of cGMP concentration in all four cells. After a 3-minute washout, NA (0.1 mM) was applied between seconds 270 and 330. Again, all four cells displayed transient FRET changes; however, the kinetics differed from those observed during ANP stimulation. ANP induced a sharp increase of the ratio CFP/YFP that was followed by a slow increase until the peak or a plateau was reached. Cells 3 and 4 did not reach a plateau during ANP application. In contrast, during NA application the peak was reached early followed by a plateau phase or even a decrease in the response. Furthermore, upon washout of NA, an overshoot was

always observed during which the ratio went below the baseline. After another 3-minute wash, ANP (1 nM) was applied again for 1 minute. The transient FRET change showed the same shape as during the first application of ANP.

Honda and his colleagues found that Cygnet-2.1 has a 500-fold higher affinity for cGMP than for cAMP (K_D (cGMP) = 600 nM, K_D (cAMP) = 300 µM; Honda et al., 2005). However, in the experiments shown in Figure 3.1.9, 1 nM ANP and 0.1 mM NA induced a similar response of the sensor, indicating that Cygnet-2.1 responded to increases of both cGMP and cAMP. The FRET change during NA application was nearly as strong as that during ANP application but differed slightly in the time course. If one assumes that the affinity of Cygnet-2.1 for cAMP is several hundred fold lower than its affinity for cGMP, one must conclude that the cAMP concentration upon stimulation with NA is several hundred fold higher than the cGMP concentration induced by ANP stimulation. Under such circumstances, Cygnet-2.1 probably shows little selectivity between cGMP and cAMP. As the selectivity of the sensor is a very important issue, one must use this sensor with great caution. The conditions in which the sensor can be used will be discussed in detail in Chapter 4.1.

Conclusion

In this chapter, I have shown that Cygnet-2.1 is capable of detecting changes in the intracellular cGMP concentration in FlpTS GC-A cells in a time-resolved manner. The fluorescence intensity of CFP and YFP changed in a mirror reversed way upon ANP stimulation, which is a result of the changed FRET efficiency due to cGMP binding to the sensor. The increased ratio of CFP/YFP reflects an elevation of the intracellular cGMP concentration. The fast responses upon cGMP binding and unbinding facilitate the visualization of dynamic changes, which makes the sensor qualified for studying cGMP metabolism both *in vitro* and *in vivo*.

3.2 Retinal culture

In my thesis I established different types of mouse primary retinal cultures. The aim was to use these cultures to establish virus mediated transduction and cGMP-imaging *in vitro.*

The first type of culture is the retinal whole-mount culture. Retinae of young mice were cultured intact. The advantage of this culture is the good preservation of the retinal layers and cell types *in vitro*. However, as the retina remains intact the different retinal cell types are not equally well accessible for viral transduction. The second approach was to culture dissociated retinal cells. The advantage of dissociated cell cultures is that all cells are equally accessible. As a disadvantage cultured cells may differ substantially from their counterparts *in vivo*, because their environment is drastically changed. The culture of retinal slices is a compromise as the accessibility of cells is better than in the whole-mount culture and the environment is less disturbed than in dissociated cell cultures. The three types of retinal cultures will be evaluated in this chapter.

3.2.1 Organotypic retinal whole-mount culture

The retinal whole-mount cultures were performed in two different ways: as folded and as flattened cultures. In brief, retinae from mice at postnatal day 8 (P8) were carefully isolated and placed onto a culture membrane. For folded cultures, the retinae were allowed to fold according to their natural curvature when they were put onto the membrane. Thus, the ganglion cell layer was sandwiched in the middle, and the photoreceptors of the lower part of the folded tissue touched the membrane whereas the photoreceptors of the upper part were exposed to the air, only covered by a thin film of liquid (see Figure 2.5). To obtain flattened cultures, retinae were flattened with the photoreceptors attaching the membrane whereas the ganglion cell layer was directed towards the air-medium interface (see Figure 2.5). It was crucial to not submerse the cultures in the culture medium but to maintain both flattened and folded

cultures at the air-medium interface in order to preserve the native structures of the tissue.

My aim was here to generate organotypic cultures that maintain native structures such as the typical retinal layering. When retinae from P8 mice are cultured, they are not yet fully mature at the day of cultivation. Therefore, it is also important to investigate whether retinae developed *in vitro* in a similar way as they do *in vivo*. These two aspects determine the quality of whole-mount cultures. To this end, both types of whole-mount cultures were characterized by cell type-specific immunochemical markers and compared to native retinae of the corresponding developmental stages. The results of my immunochemical studies are presented in the following figures (Figure 3.2.1 - Figure 3.2.6).

In each figure, the upper row shows vertical sections through native retinae of different postnatal stages: P8, P10, P12, P16, P20, and P24. Vertical sections of folded cultures are shown in the middle row and vertical sections of flattened cultures are depicted in the lower row. All cultured retinae were explanted at P8 and fixed after 2, 4, 8, 12, and 16 days of cultivation, respectively. Sections of native as well as cultured retinae were stained and analyzed by confocal laser scanning microscopy. The orange bars in the figures represent the position of the culture membrane and thus describe the orientation of the whole-mount during cultivation.

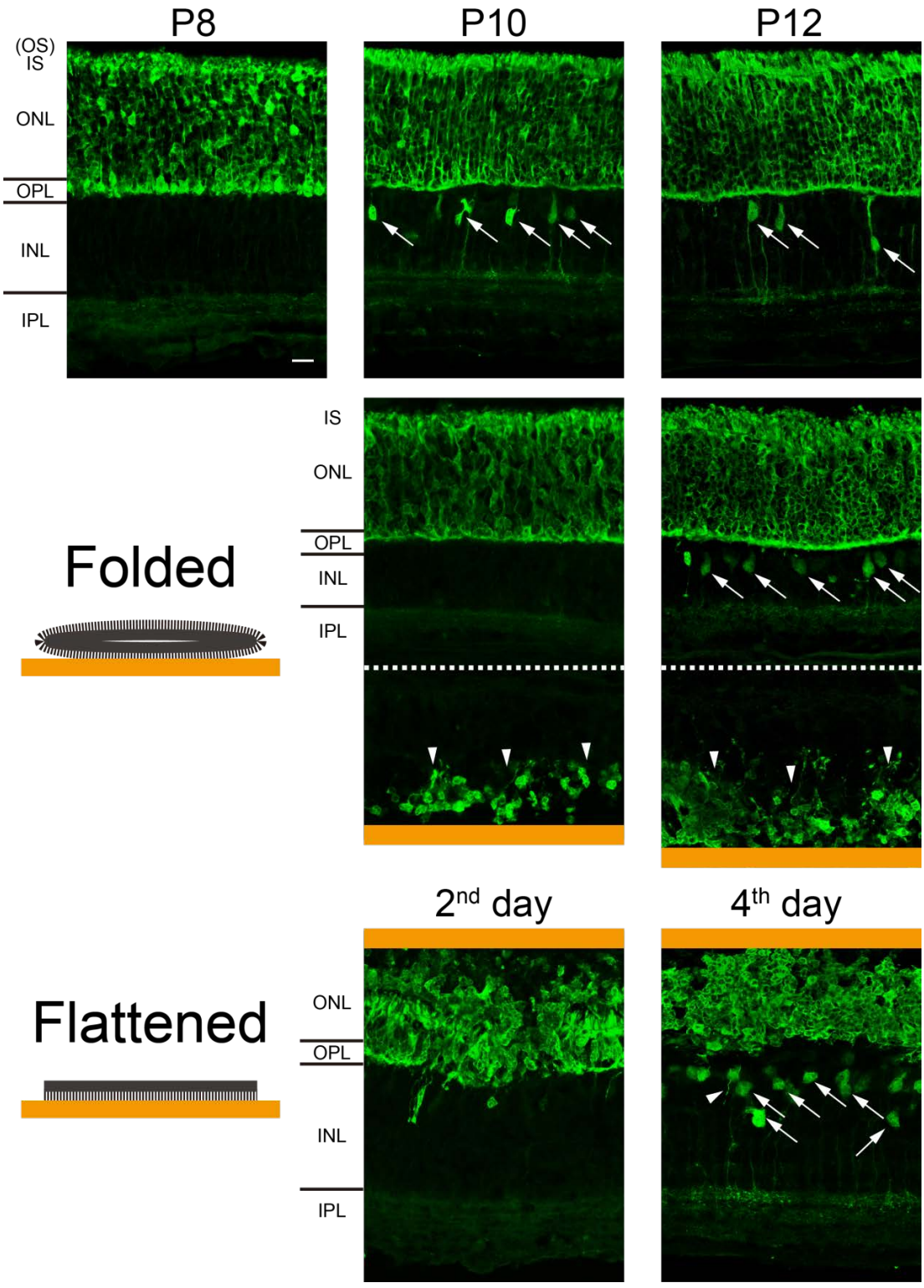

Figure 3.2.1: Recoverin label in vertical sections of native mouse retina and whole-mount retinal cultures.

Upper row: native retinae of P8, P10, P12, P16, P20, and P24 mice. Middle row: whole-mount cultures in the folded condition, lower row: whole-mount cultures in the flattened condition at 2nd, 4th, 8th, 12th, and 16th days of cultivation, respectively. All arrows mark recoverin-immunoreactive type 2 bipolar cells. The arrowheads in the upper row indicate the outer segments. Arrowheads in

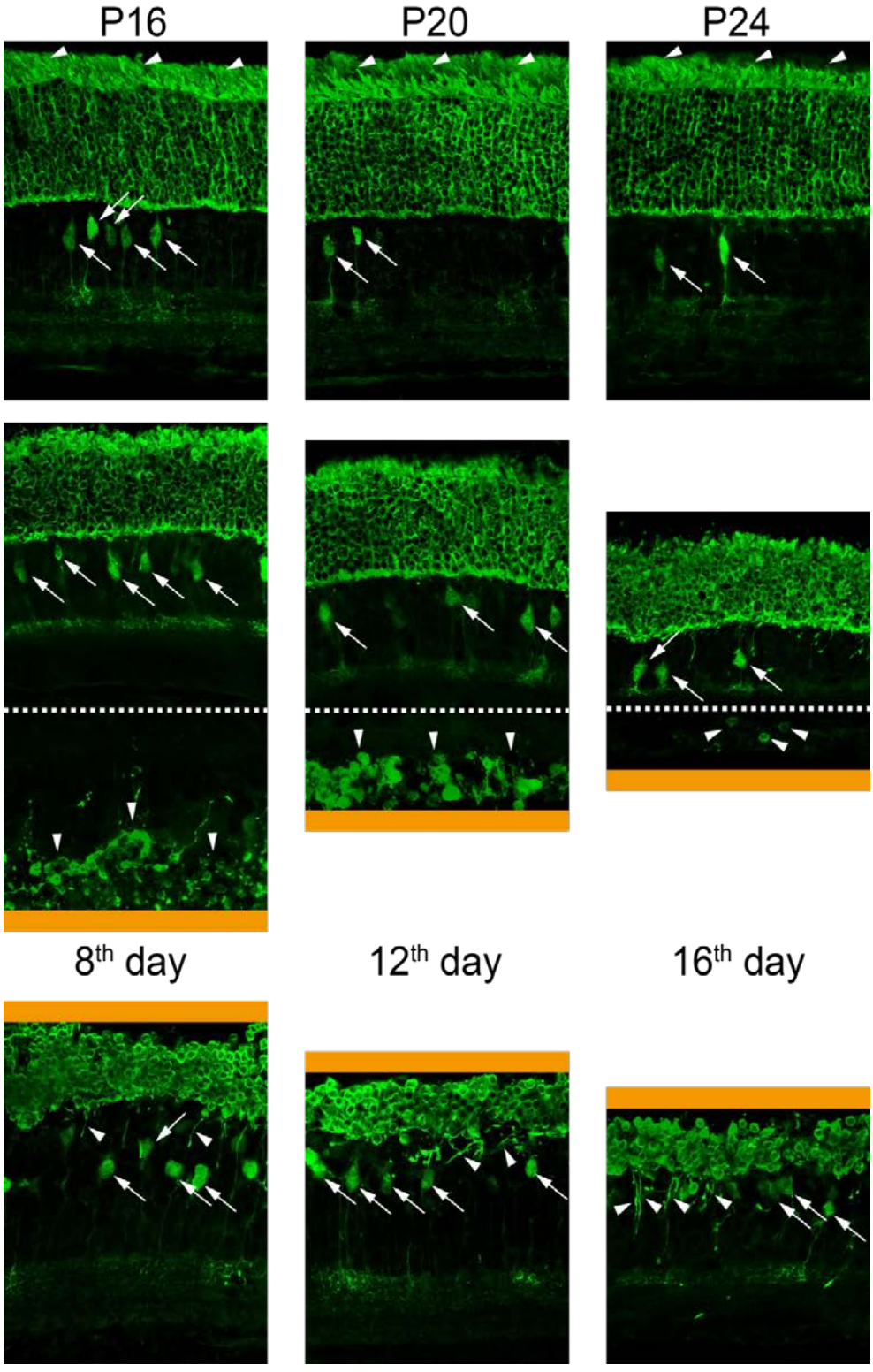

the middle row indicate the degenerated ONL in the lower part of the cultures. Arrowheads in the lower row indicate neurites that can be traced from photoreceptors into the INL. Orange bars represent the membrane. The dotted lines divide the upper and the lower parts of the cultures in the folded conditions.
Scale bar = 20 µm.

Figure 3.2.1 shows immunochemical stainings using antibodies against recoverin. Recoverin is a neuronal calcium-binding protein. In photoreceptors recoverin inhibits the rhodopsin kinase. Recoverin is a typical marker for both photoreceptor types but also for type 2 bipolar cells in the mouse retina (Dizhoor et al., 1991; Kawamura, 1993; Milam et al., 1993; Haverkamp and Wässle, 2000). The control stainings of native vertical sections (upper row) showed recoverin immunoreactivity (recoverin-IR) within the entire outer nuclear layer (ONL), where the somata of photoreceptors are located. In addition, the inner segments (IS) and the outer segments (OS) that developed after P12 (arrowheads) were recoverin-positive. The thickness of the ONL was appr. 100 µm including 13 ~ 15 rows of photoreceptor somata and did not change much from P8 to P24. Within the inner nuclear layer (INL), type 2 bipolar cells were detectable by recoverin-IR from P10 on (arrows).

In cultured retinae, the over-all structures were preserved under both folded and flattened conditions. However, degeneration was observed particularly in the part where the tissue had attached to the membrane. Degeneration was reflected by a reduced number of cells and a disturbed retinal organization.

In folded cultures (middle row), the lower retinal tissue (below the dotted line) degenerated rapidly. The ONL already started to disintegrate after two days of cultivation ("Folded", 2nd day, arrowheads) and degenerated further during the culture. After 16 days of cultivation, only few recoverin-positive cells remained in this part of the tissue ("Folded", 16th day, arrowheads). In contrast, the upper retinal tissue (above the dotted line) seemed to be unaffected during the first 4 culturing days. The thickness of the ONL was similar to that of the native retina at the corresponding stage. From the 8th day of cultivation, the ONL became progressively thinner: 8 ~ 10 rows of photoreceptor somata were observed on the 8th and 12th day *in vitro*, 6 ~ 8 rows on the 16th day. The inner segments were always shorter in cultured rods than in native ones and the outer segments were not clearly observed even in the later period of cultivation. Type 2 bipolar cells were detected by recoverin staining from the 4th day of cultivation on ("Folded", arrows). However, the axons of type 2 bipolar cells

became very short during the last stage of cultivation. Nevertheless, most of the general retinal morphology revealed with recoverin staining seemed to be conserved in the upper tissue part over 16 days of cultivation.

In flattened retinal cultures (lower row), the photoreceptors were attached to the membrane while the ganglion cells were exposed to the air. For better comparison the sections are shown in the same orientation as sections through the native retinae. The ONL started to degenerate early after culturing. It had disintegrated and reduced its thickness to about 80 µm (Flattened, 2nd day) already after 2 days of cultivation. On the 16th day the ONL eventually was reduced to a thickness of about 50 µm, corresponding to approximately half the thickness of a native ONL in a mature retina (compare P24, upper row). Not only the ONL, but also the outer plexiform layer (OPL) seemed to degenerate. The OPL was not a straight line and the border between the ONL and the INL become wavy on the 2nd culturing day. Some photoreceptor neurites even grew into the INL after 6 days of cultivation ("Flattened", 8th to 16th day, arrowheads). Nevertheless, recoverin-positive type 2 bipolar cells could be observed in the INL from the 4th day of cultivation on ("Flattened", 4th to 16th day, arrows) and thus appeared at the same time as in folded cultures.

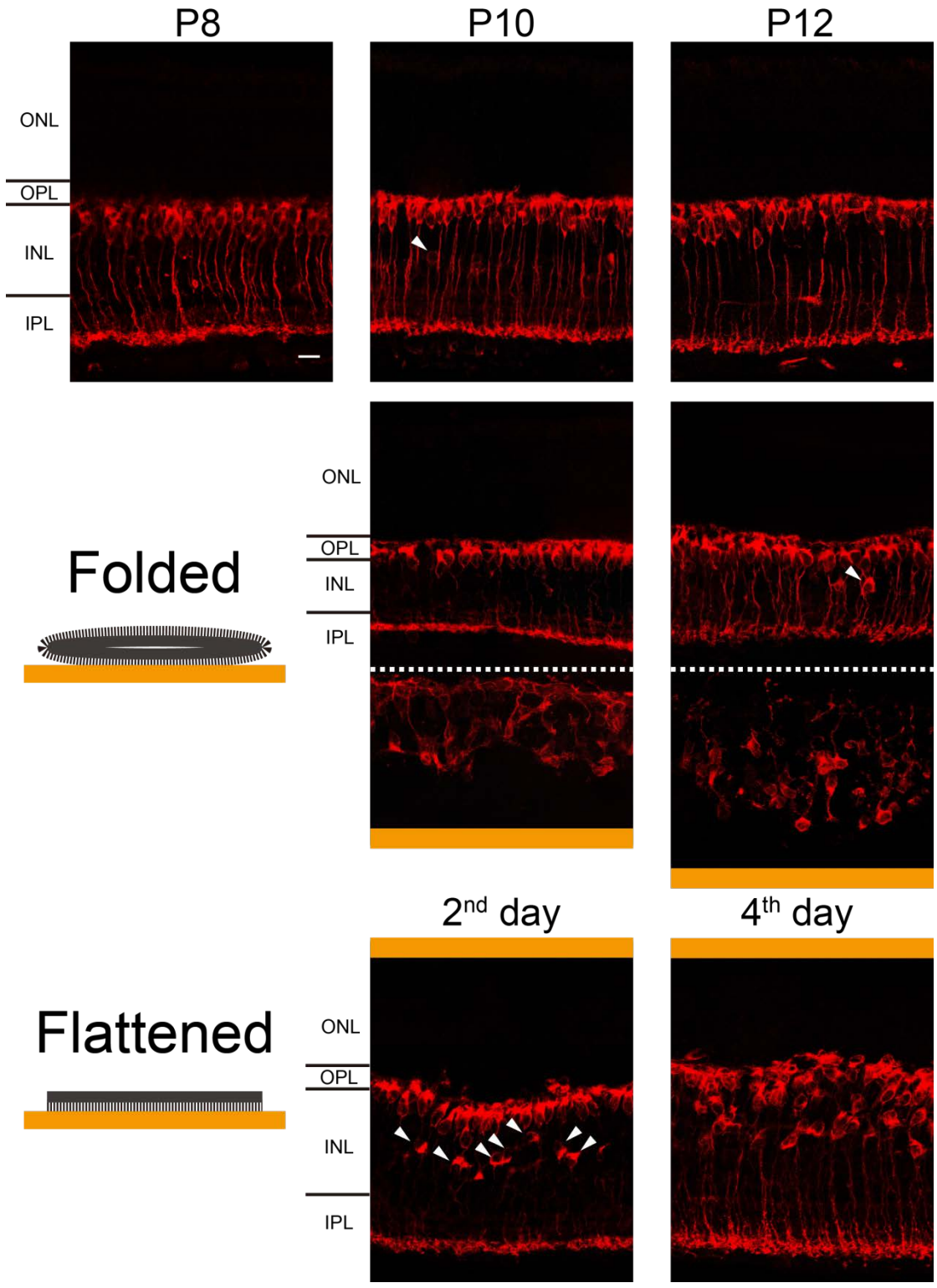

Figure 3.2.2: PKCα label in vertical sections of native mouse retina and whole-mount retinal cultures.

Upper row: native retinae of P8, P10, P12, P16, P20, and P24 mice. Middle row: whole-mount cultures in the folded condition, lower row: whole-mount cultures in the flattened condition at 2nd, 4th, 8th, 12th, and 16th days of cultivation, respectively. Arrowheads in the upper row mark few PKCα-immunoreactive amacrine cells in the native retina. Arrowheads in the middle row indicate

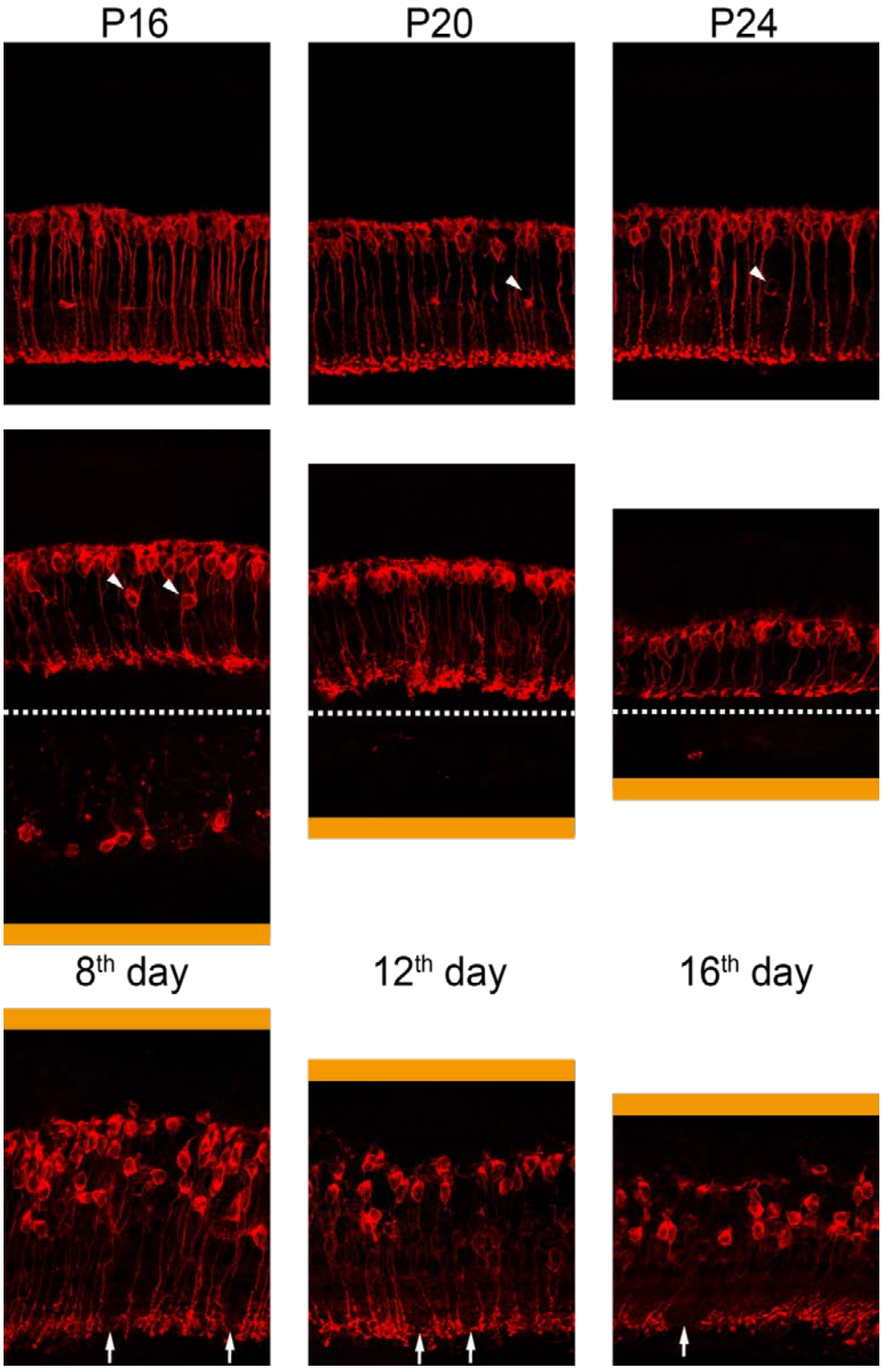

some misplaced rod bipolar cells in the upper part of the folded cultures. Arrows in the lower row mark some gaps among axon terminal systems, and arrowheads mark some misplaced rod bipolar cells in the flattened cultures. Orange bars represent the membrane. The dotted lines divide the upper and the lower parts of the cultures in the folded conditions.
Scale bar = 20 µm.

With the next stainings I focused on bipolar cells, the downstream targets of photoreceptors in the vertical pathway. Among all types of bipolar cells, rod bipolar cells come with the highest density. Figure 3.2.2 shows vertical sections of both native retinae and whole-mount cultures that were stained with antibodies against protein kinase Cα (PKCα). PKCα is the typical marker for rod bipolar cells in the mouse retina (Negishi et al., 1988; Greferath et al., 1990). As is shown in the native retina (upper row), rod bipolar cell somata usually sit in the uppermost row of the INL, next to the OPL; and their axons terminate in the innermost sub-layer of the IPL. In addition to rod bipolar cells, few somata (arrowheads) were found in the inner part of the INL. These cells clearly differ in size, shape and localization from rod bipolar cells and can be classified as amacrine cells (Haverkamp and Wässle, 2000). The morphology of rod bipolar cells and their PKCα-immunoreactivity (PKCα-IR) did not change during development from P8 to P24.

In the folded cultures (middle row), the upper parts (above the dotted line) displayed relatively well-arranged PKCα-positive rod bipolar cell bodies during the whole culturing period. The somata of rod bipolar cells were located in the uppermost layer of the INL; except for very few misplaced ones (arrowheads) that were identified by their axons and axon terminals. However, the axon terminals of rod bipolar cells seemed to degenerate slightly. After the first 4 days of cultivation, the axon terminal systems displayed more diffuse staining patterns. At the 16th culturing day, an overall shortening of the rod bipolar cells could be observed as the total thickness of INL plus IPL had been reduced by nearly 50% compared to native tissue at P24 (upper row). Again in the lower parts of the cultures (below the dotted line), a fast and strong degeneration was observed leading to a disorganized staining pattern. The number of PKCα-positive cells was rapidly reduced during culturing. After 8 days of cultivation nearly no PKCα-immunoreactive cells could be observed in the lower part.

In the flattened retinal cultures, the somata of rod bipolar cells became progressively misplaced. After 2 days of cultivation, some misplaced somata (arrowheads) could be observed. At later stages the majority of the rod bipolar cell bodies moved to the inner

part of the INL. In addition, the number of PKCα-positive somata progressively decreased after 8 days of cultivation. Accordingly, some gaps (arrows) were found in the axon terminal system layer at the same time. Nevertheless, the axon terminal systems displayed staining patterns similar to that found in the upper part of the folded cultures (comparing “Folded”, middle row).

In the both folded and flattened cultures, PKCα-IR in the axon of rod bipolar cell was weaker during the first 2 days of cultivation. Only somata, dendrites and axon terminals were strongly immunoreactive, while the axons were hardly visible in the PKCα-staining (“Folded” and “Flattened”, 2nd day). Starting from the 4th culturing day, PKCα-IR was observed throughout the entire bipolar cell.

Another bipolar cell marker - calcium binding protein 5 (CaBP5) for type 3, type 5, and rod bipolar cells - was also used in immunochemistry. These types of bipolar cells were observed in both folded and flattened cultures (data not shown).

Horizontal cells are interneurons that form lateral connections in the OPL. For mouse horizontal cells, the calcium binding protein (CaBP, also called calbindin) is a reliable marker (Röhrenbeck et al., 1987). In Figure 3.2.3, sections of native retinae and whole-mount cultures were immunochemically stained for CaBP. In the native retina (upper row), CaBP-immunoreactivity (CaBP-IR) was found in horizontal cells (arrows) whose somata and neurites were immunoreactive. In addition, amacrine cells (arrowheads) at the inner margin of the INL and displaced amacrine cells (arrowheads) in the ganglion cell layer (GCL) also showed CaBP-IR. Two labeled prominent strata in the IPL were formed by the dendrites of CaBP-positive amacrine cells. During maturation, CaBP-IR in horizontal cells was progressively increasing until P16, while CaBP-IR in amacrine cells and their dendritic strata was gradually decreasing (P8 ~ P24, upper row). All micrographs in Figure 3.2.3 were stained under identical conditions and scanned using the same microscope settings.

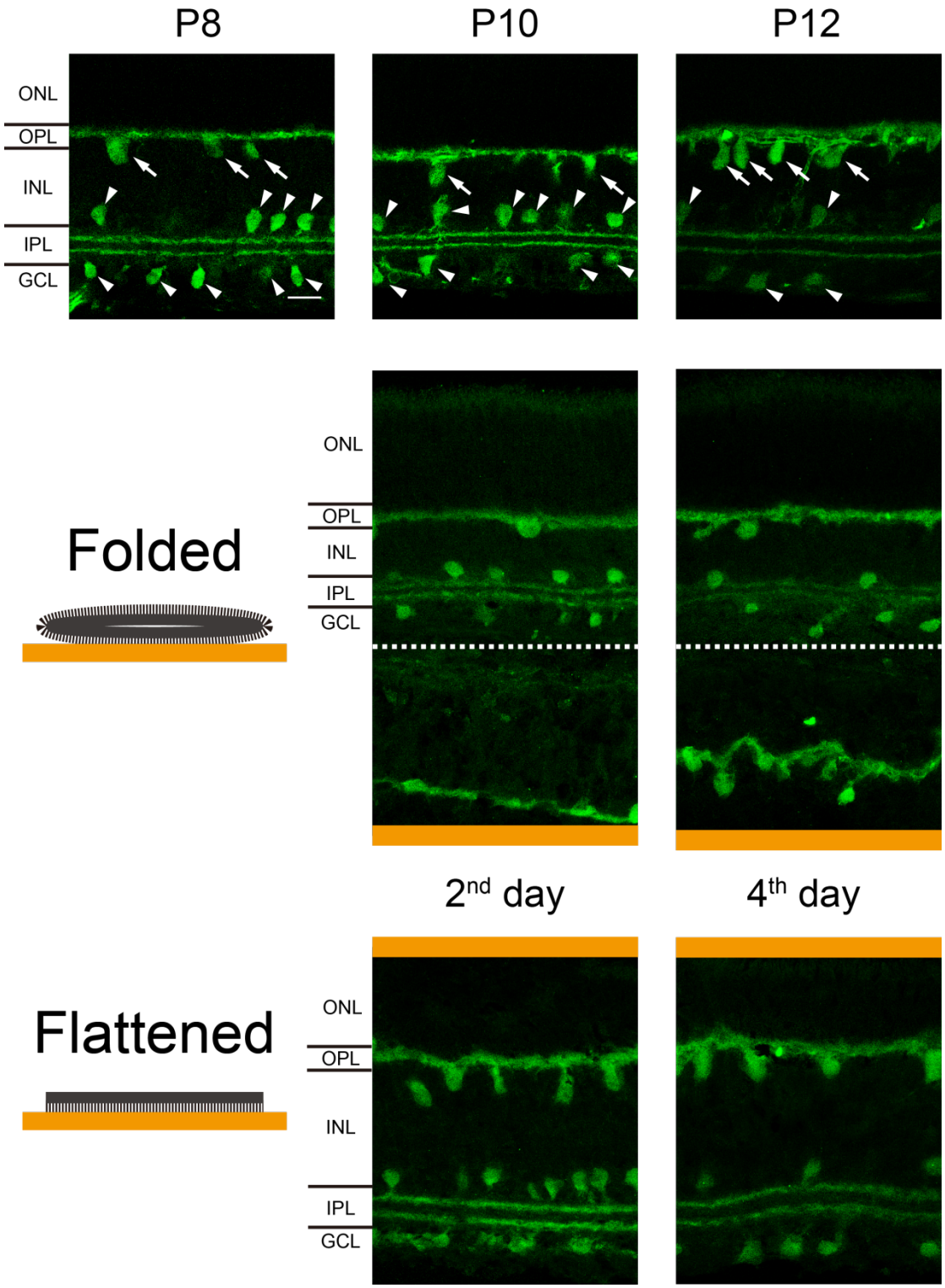

Figure 3.2.3: CaBP label in vertical sections of native mouse retina and whole-mount retinal cultures.

Upper row: native retinae of P8, P10, P12, P16, P20, and P24 mice. Middle row: whole-mount cultures in the folded condition, lower row: whole-mount cultures in the flattened condition at 2nd, 4th, 8th, 12th, and 16th days of cultivation, respectively. In the upper row, arrows indicate

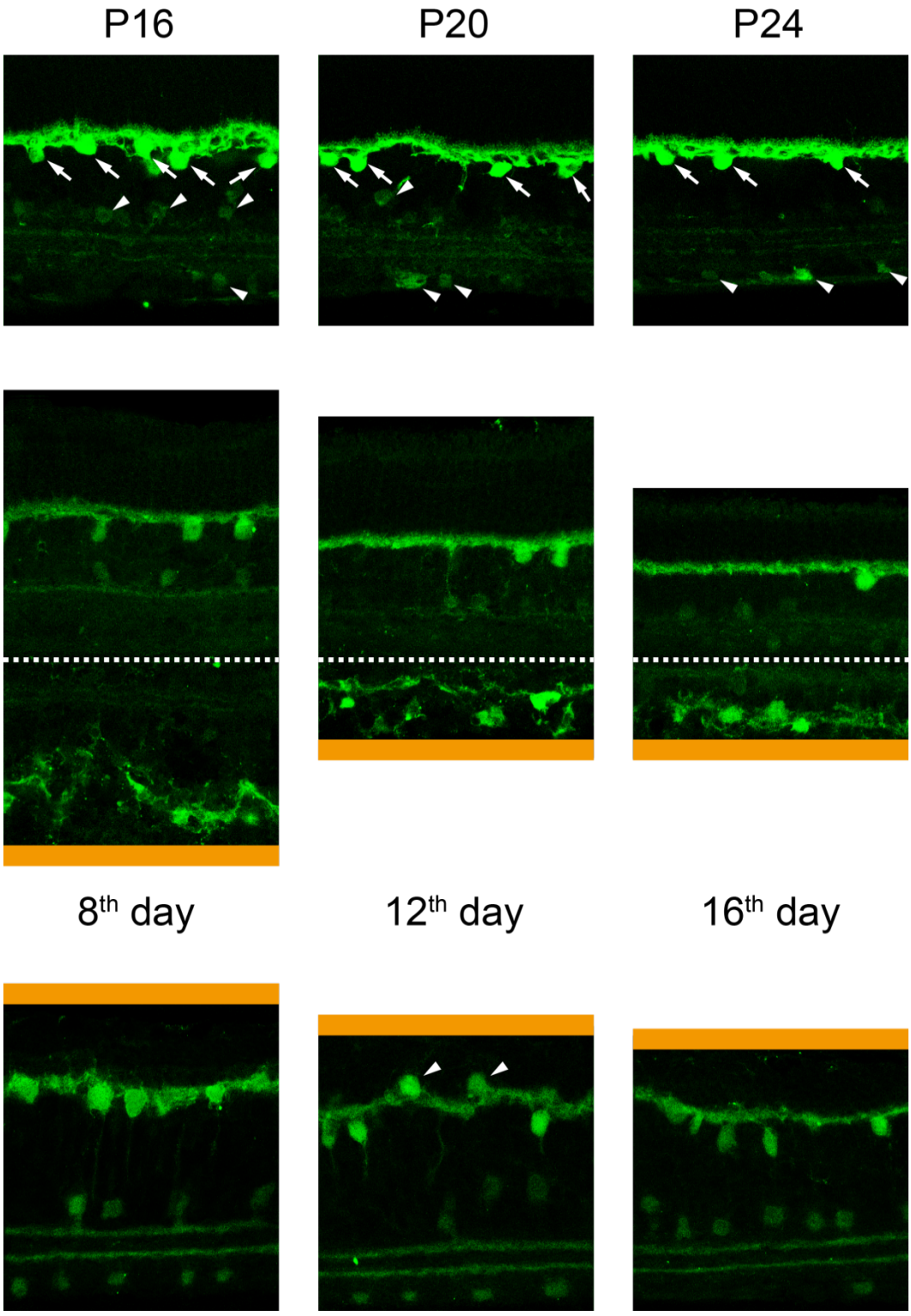

CaBP-immunoreactive horizontal cells and arrowheads indicate CaBP-immunoreactive amacrine cells both in the INL and in the GCL. In the lower row, arrowheads indicate two horizontal cells misplaced to the ONL. Orange bars represent the membrane. The dotted lines divide the upper and the lower parts of the cultures in the folded conditions.
Scale bar = 20 µm.

In folded culturing conditions (middle row), the staining in the upper part (above the dotted line) strongly resembled the staining in the native retinae. However, the staining seemed more diffuse. While under native conditions, CaBP-IR in horizontal cells increased with age, in the cultures no changes in CaBP expression in horizontal cells were observed during cultivation (compare to native retina at P8 to P24, upper row). On the other side, CaBP-positive amacrine cells showed a similar decrease in immunoreactivity as observed in native retina. In the lower part of the culture (below the dotted line), strong degeneration similar to that found in previous stainings (Figure 3.2.1 & Figure 3.2.2) was observed.

In the flattened cultures (lower row), the outer retina showed a certain degree of degeneration. The OPL became more wavy and in the later culturing stages, some horizontal cell bodies ("Flattened", 12th day, arrowheads) were found misplaced to the ONL. In contrast, the staining pattern for CaBP-positive amacrine cells was surprisingly good. Amacrine cells in both the INL and the GCL and their strata in the IPL were well preserved even after 16 days in culture. Their CaBP expression was higher than in native retina (comparing P8 to P24, upper row).

The following immunostainings will focus on certain types of amacrine cells that can be labeled with antibodies against calretinin during cultivation. Antibodies against calretinin do not only label many amacrine cells and ganglion cells, but also three characteristic strata in the IPL of the mouse retina. The outermost and innermost strata are identical to those stained by the CaBP antibodies (see Figure 3.2.3, upper row) and are formed by the dendrites of cholinergic amacrine cells (Haverkamp and Wässle, 2000).

Figure 3.2.4 shows vertical sections of native retinae and whole-mount retinal cultures, which were stained with antibodies against calretinin. Calretinin-immunoreactivity (calretinin-IR) was only found in the inner part of the retina. In native retinae (upper row), many somata in the INL and in the GCL and processes in the IPL were immunoreactive. In P8 retina, calretinin-IR was strongest in many big neurons (long arrows) in the GCL, but weaker in many neurons in the INL. Based on the large size

of the somata in the GCL, they are probably ganglion cells. Also bundles of ganglion cell axons (arrowheads) are positive for calretinin. In the IPL, strongest immunoreactivity was found in a thick continuous band. Starting from P10, there was a progressive increase in the number of strongly calretinin-immunoreactive amacrine cells (short arrows) in the INL and displaced amacrine cells (short arrows) in the GCL that have relatively small somata compared to the ganglion cells. Most notably, three distinct calretinin-positive strata (arrowheads) in the IPL developed.

When the retinae were cultured in the folded condition (middle row), the calretinin-positive amacrine cells degenerated strongly not only in the lower, but also in the upper part of the cultures. During the first 2 days of cultivation, the number of calretinin-positive cells in the GCL was greatly reduced, while the amacrine cells in the INL seemed to survive better. In the IPL, the staining pattern was less clear than in native retina. On the 16th culturing day, only one calretinin-positive band was observed in the IPL near the border to the INL.

In contrast, in flattened retinal cultures (lower row), calretinin-immunoreactive amacrine cells seemed to be well preserved. In addition, three calretinin-positive strata in the IPL were recognized even after 16 days *in vitro* (arrowheads), except that the middle stratum was weaker than the other two.

In addition to calretinin, stainings (data not shown) with antibodies against glutamic acid decarboxylase (GAD, including GAD65 & GAD67), glycine transporter 1 (GlyT1) and tyrosine hydroxylase (TH) revealed GABAergic amacrine cells, glycinergic amacrine cells and dopaminergic amacrine cells (Nguyen-Legros et al., 1997; Haverkamp and Wässle, 2000), respectively. All these types of amacrine cells could be identified in both types of whole-mount cultures. These stainings corroborated the finding that the inner retina including IPL and GCL degenerated fast in the folded cultures while it was better preserved in the flattened cultures.

The health status of nerve tissue can also be determined by the properties of the neuron supporting cells, glia cells. Upon injury or during degeneration, often, glia cells become activated.

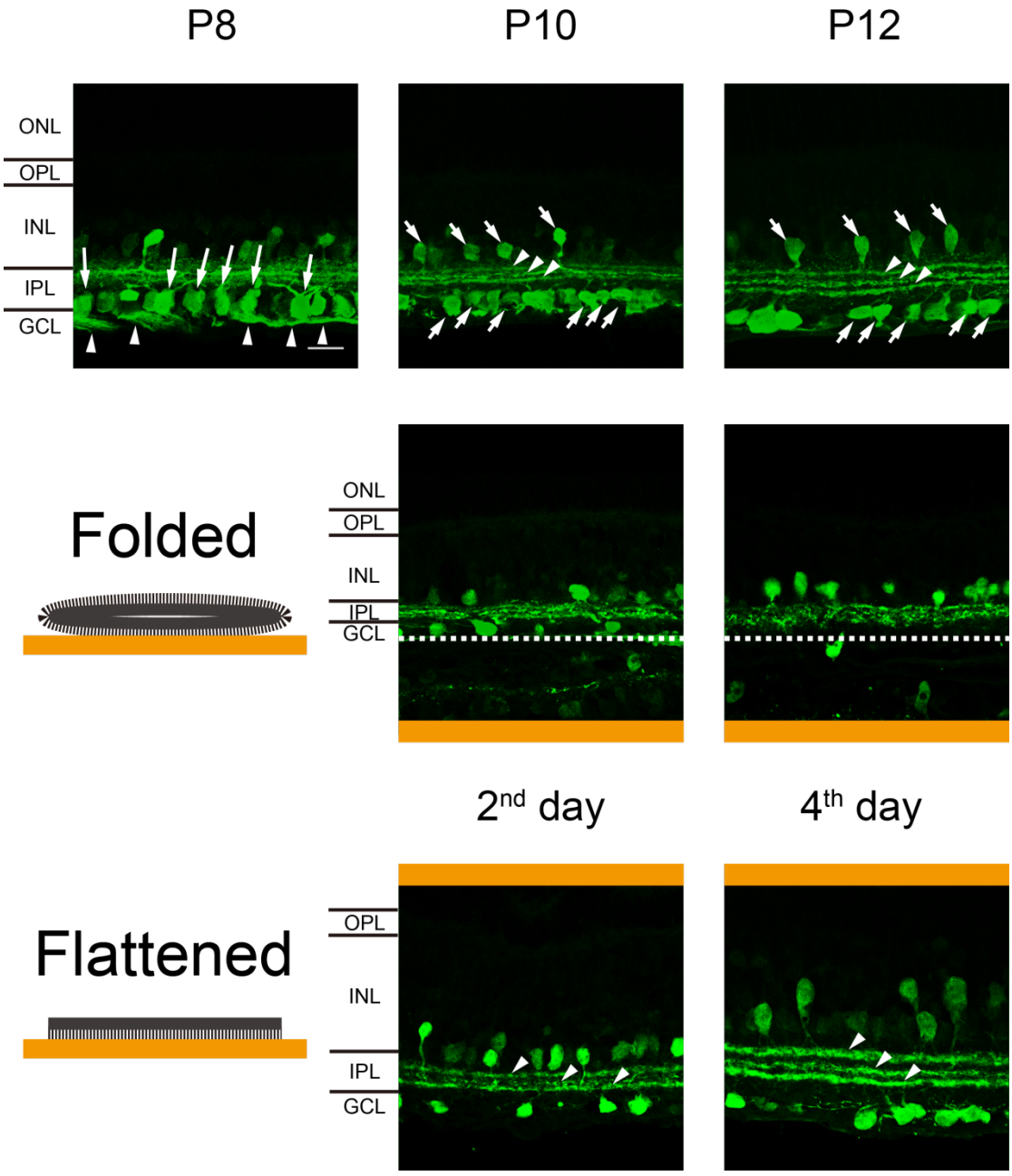

Figure 3.2.4: Calretinin label in vertical sections of native mouse retina and whole-mount retinal cultures.

Upper row: native retinae of P8, P10, P12, P16, P20, and P24 mice. Middle row: whole-mount cultures in the folded condition, lower row: whole-mount cultures in the flattened condition at 2nd, 4th, 8th, 12th, and 16th days of cultivation, respectively. All arrowheads indicate the three distinct

In the retina, three types of glia cells are found: astrocytes can be stained by antibodies against glial fibrillary acidic protein (GFAP). Müller cells and microglia are negative for GFAP. Under neurodegenerative conditions however, Müller cells

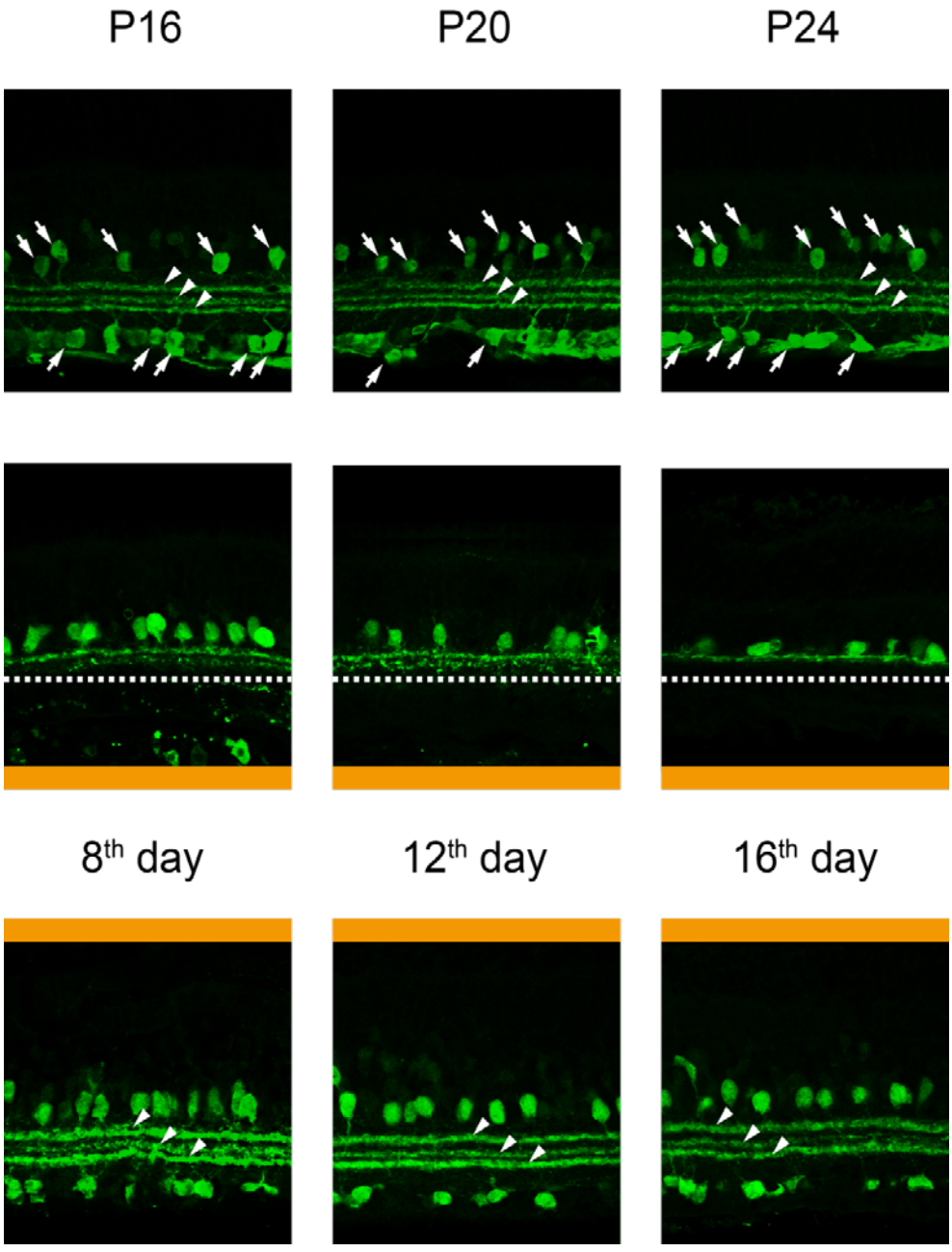

strata in the IPL. In the upper row, long arrows indicate immunoreactive ganglion cells in the GCL from P8 retina and the short arrows indicate immunoreactive amacrine cells both in the INL and in the GCL. Orange bars represent the membrane. The dotted lines divide the upper and the lower parts of the cultures in the folded conditions.
Scale bar = 20 µm.

express GFAP. Figure 3.2.5 shows sections labeled for GFAP from native retina and from whole-mount cultures. GFAP-immunoreactivity (GFAP-IR) in the native retina (upper row) was strong in astrocytes that are mainly found in the nerve fiber layer (NFL) and sometimes in the GCL. Arrows indicate some blood vessels that were stained by the secondary antibody against mouse primary antibodies. Müller cells expressed little or no GFAP at all. In cultured retinae, GFAP expression was immediately up-regulated, independent of the culturing conditions. In both folded and flattened cultures (middle row & lower row), GFAP-IR was initially enhanced in the NFL after 2 days of cultivation. Then, fibers running vertically through the retina towards the ONL became strongly GFAP-immunoreactive. These fibers are Müller cell processes. On the 8th days of cultivation, GFAP seemed to be fully expressed. Müller cells remained GFAP-immunoreactive throughout the entire culturing time. Strangely, in the lower part of the folded culture, GFAP-IR was much weaker and the onset of GFAP expression seemed to be delayed. As is known from previous stainings (Figure 3.2.1 - Figure 3.2.4), the lower part degenerated very rapidly in culture. Probably, GFAP expression could be up-regulated only when the retinal tissue was still preserved and maintained. Thus, the lower part of the folded cultures might degenerate too fast for Müller cells to become reactive and express GFAP. From day 12 on, GFAP-IR was also found in the lower part.

In this project, the main research interests are focused on the NO-cGMP pathway in the mouse retina. NO is synthesized by NO-synthase (NOS). Amacrine cells containing NOS and releasing NO are found in the mouse retina. Hence, it was important to know whether NOS-immunoreactive cells were also found in whole-mount cultures and if NOS-positive cells retained their typical morphology.

Figure 3.2.6 shows the stainings with antibodies against NOS. In the native tissue (upper row), NOS-immunoreactivity (NOS-IR) was found only in amacrine cells. Two types of NOS-amacrine cells were identified. One type (arrows) with strong immunoreactivity had a large elongated soma and one thick primary neurite ramifying around the middle of the IPL. This type of NOS-positive cells was present in all

postnatal stages (P8 to P24) of the native retina. Another type of NOS cells (arrow heads) was small in size and situated very close to the border of the IPL. This cell type only became weakly immunoreactive after P10. Starting from P12, many processes throughout the entire thickness of the IPL were visible in the staining. The processes observed only at the later stages might arise from the small NOS-amacrine cells. Both types of cells can be found in the INL and the GCL. However, the NOS-immunoreactive amacrine cells represent only a small population of amacrine cells.

NOS-IR was also found in amacrine cells in both folded and flattened whole-mount cultures. As mentioned above, the inner retina degenerated faster in the folded culturing conditions while it could be preserved longer in the flattened culturing conditions. Thus, not surprisingly in the upper part of folded cultures (middle row), NOS-staining appeared degenerated. The sparse NOS-immunoreactive processes in the IPL and the number of cells continuously lessened after explanting the retina.

NOS-amacrine cells in the flattened cultured retinae (lower row) were preserved, which was expected according to the previous results from calretinin-staining. Two days after explanting, the inner retina showed a similar NOS-staining pattern as the native retina of a P10 mouse. After the 8th culturing day, many NOS-immunoreactive interlaced processes through the entire IPL were observed. Both types of NOS-amacrine cells were observed during all culturing stages in the flattened cultures. However, the number of displaced NOS-amacrine cells in the GCL strongly decreased while the number of NOS-amacrine cells in the INL seemed to increase.

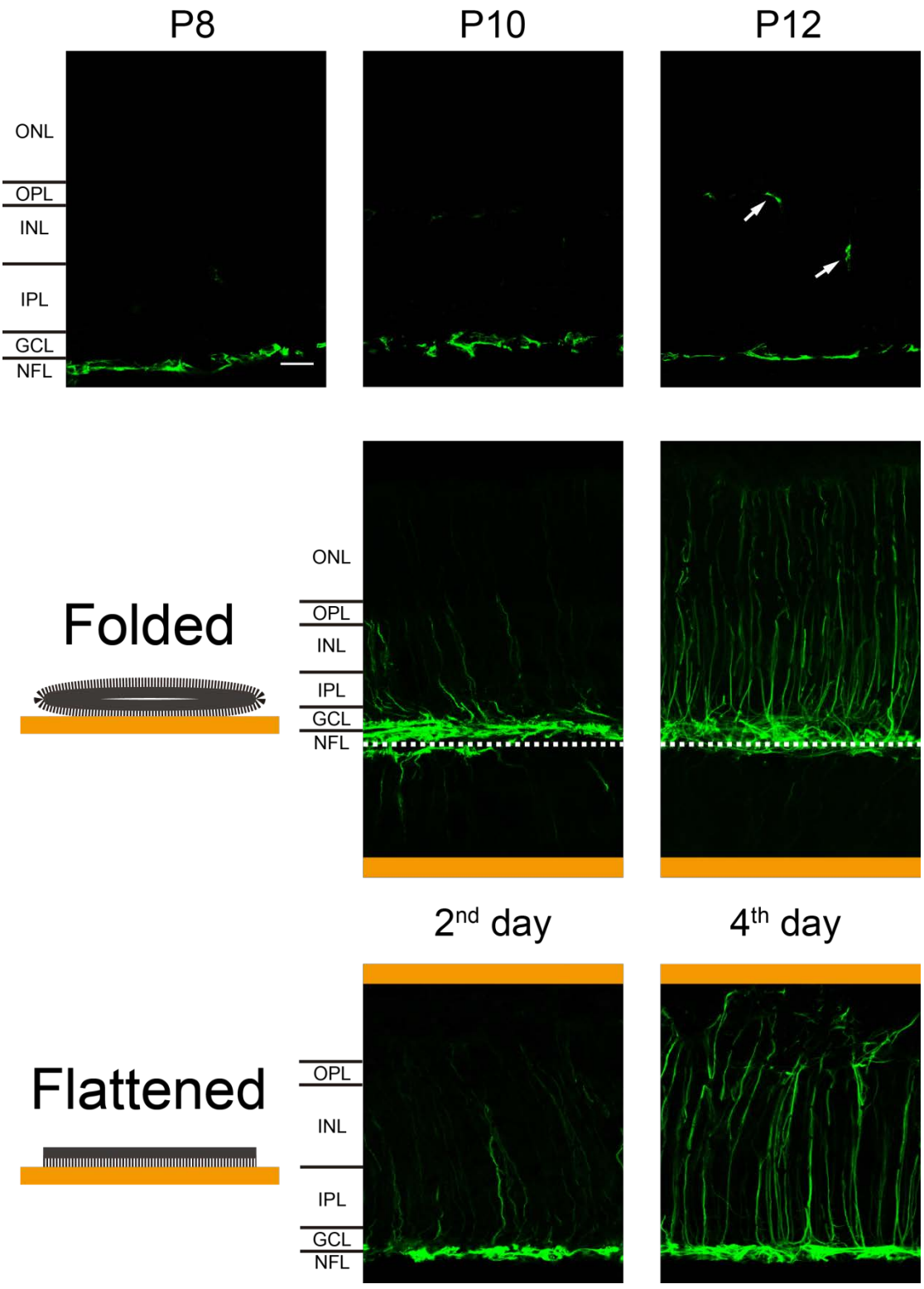

Figure 3.2.5: GFAP label in vertical sections of native mouse retina and whole-mount retinal cultures.

Upper row: native retinae of P8, P10, P12, P16, P20, and P24 mice. Middle row: whole-mount cultures in the folded condition, lower row: whole-mount cultures in the flattened condition at 2nd, 4th, 8th, 12th, and 16th days of cultivation, respectively. The arrowheads in the upper row indicate

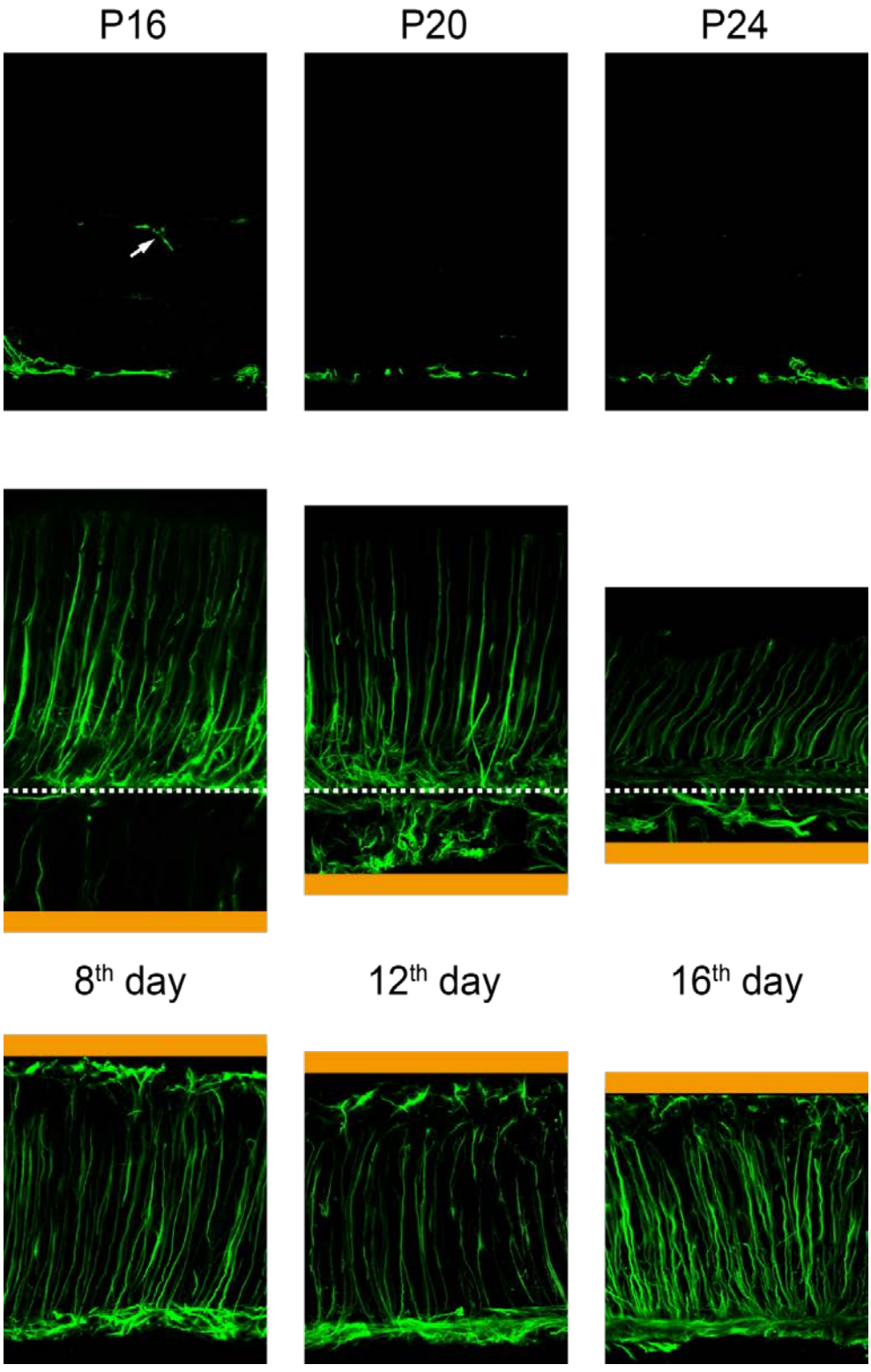

blood vessels stained by the secondary antibody against mouse primary antibodies. Orange bars represent the membrane. The dotted lines divide the upper and the lower parts of the cultures in the folded conditions.
Scale bar = 20 µm.

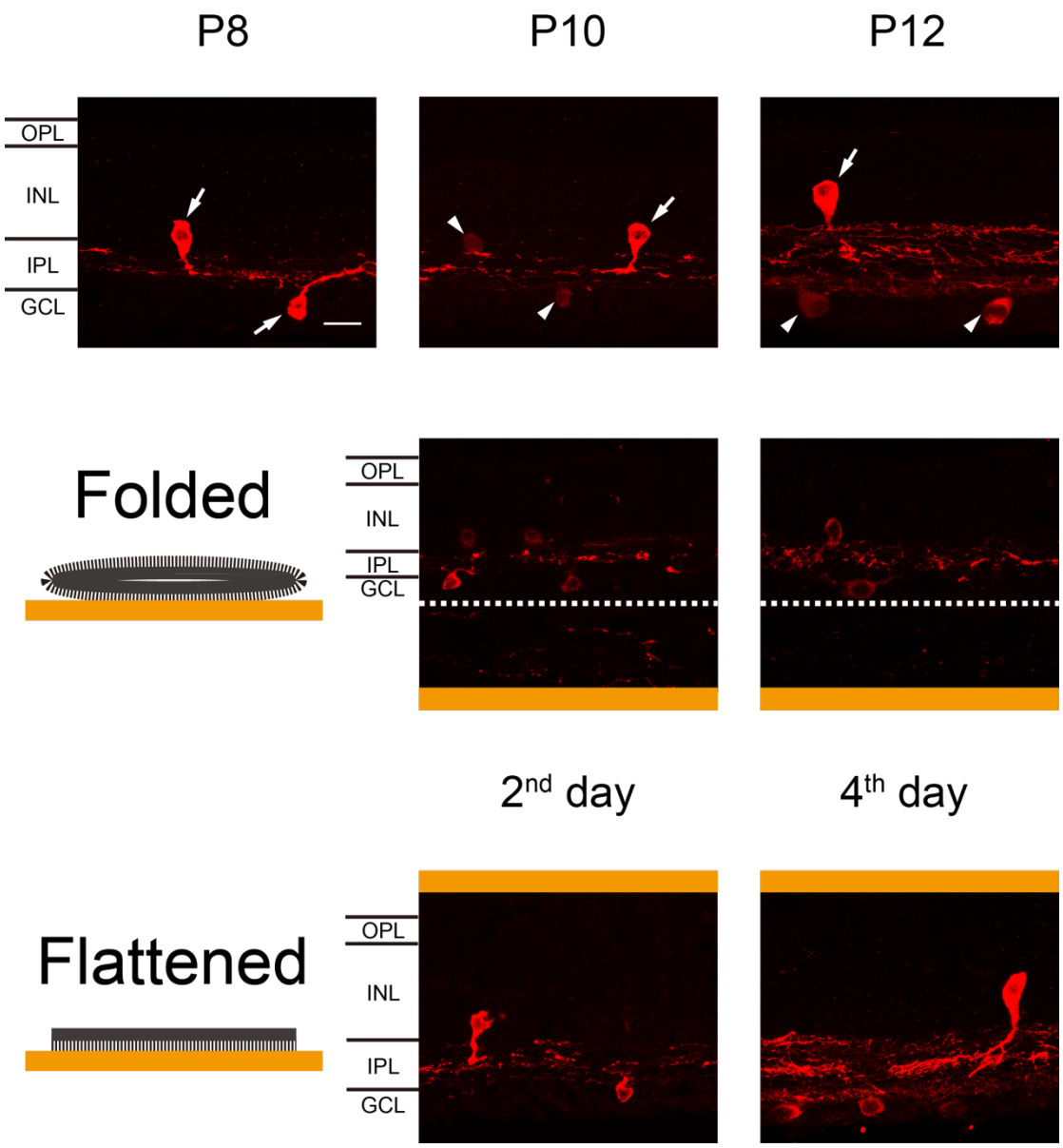

Figure 3.2.6: Nitric oxide synthase label in vertical sections of native mouse retina and whole-mount retinal cultures.

Upper row: native retinae of P8, P10, P12, P16, P20, and P24 mice. Middle row: whole-mount cultures in the folded condition, lower row: whole-mount cultures in the flattened condition at 2nd, 4th, 8th, 12th, and 16th days of cultivation, respectively. In the upper row, arrows indicate strongly

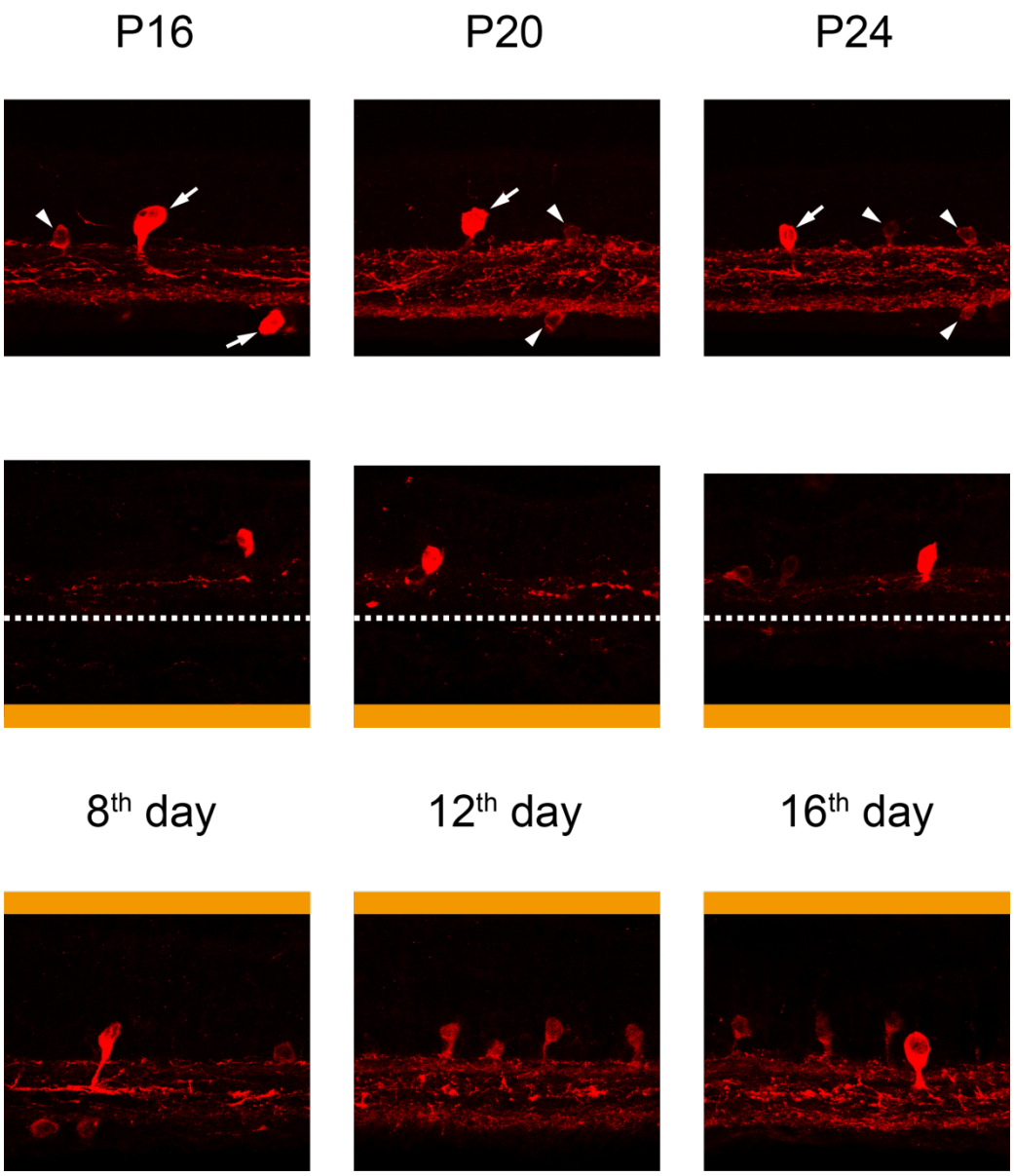

immunoreactive amacrine cells with large somata; and arrowheads indicate weakly immunoreactive amacrine cells with small stomata. Orange bars represent the membrane. The dotted lines divide the upper and the lower parts of the cultures in the folded conditions.

Scale bar = 20 µm.

Conclusion for organotypic retinal whole-mount cultures

The way the retina is placed on the culture membrane strongly affects the survival of the retina and its development during cultivation. When the retina is folded according to its natural curvature, the lower part degenerates rapidly. The upper part of the tissue facing the air-medium interface can be cultured longer. In the upper part, ONL, OPL and INL develop structures similar to those found *in vivo*. However, the inner part of the upper cultures, especially the GCL and the ON-sublayers of the IPL, degenerates much faster. In flat-mounted retinal cultures with photoreceptors attaching membrane, the outer parts of the retina including the ONL, the OPL and the outer margin of the INL start to degenerate rapidly, while the inner parts including the inner margin of the INL, the IPL and the GCL appear better preserved during cultivation. For experiments that focus on the bipolar cells and their synaptic connection with photoreceptors, it is suggested to use the folded culture method. However, if experiments aim to investigate processes in the IPL and the GCL, the flattened culture method is the better choice. As in both types of whole-mount cultures morphological and immunoreactive features of cells are best retained between the 4th and 8th culturing day, this time window is suggested for experiments.

Generally after 8 days *in vitro*, cultures show some kind of degeneration. Therefore, in either folded or flattened culturing condition, it is strongly suggested that cultivation does not exceed 8 days.

3.2.2 Dissociated retinal cell culture

Retinae from young mice between P2 to P4 were used for the dissociated retinal cultures. Upon isolation from the eyecup, the retinae were incubated with papain and cells were dissociated by trituration. Cells were seeded onto pre-coated coverslips and cultured for up to 4 weeks. Cultures between the 8th and the 14th day of cultivation were characterized by reliable immunomarkers for different retinal cell types. The results are presented in this chapter.

Markers were chosen to cover as many retinal cell types as possible: recoverin for photoreceptors; CaBP for horizontal cells; synaptotagmin-2 (Syt2), CaBP5, and PKCα for bipolar cells; GAD67 and GlyT1 for amacrine cells, and GFAP for glia cells. In dissociated cultures, the environment of the cells differs strongly from the native conditions. Therefore, cells will differ morphologically from their counterparts in the intact retina. Moreover, it cannot be ruled out that some markers might yield different staining patterns than in the intact retina.

Figure 3.2.7 displays one retinal culture triple-stained with antibodies against recoverin, rhodopsin, and blue opsin. As shown in Figure 3.2.1, recoverin is expressed mainly in photoreceptors and also in type 2 bipolar cells in the mouse retina. In panel A, many recoverin-positive cell bodies and their neurites were revealed. Most of them resemble mouse photoreceptors as they have relatively small somata (6 to 7 µm in diameter). In some cells, the somata were stained inhomogeneously by the recoverin antibodies (appearing as unstained “bubbles”, arrowheads in the inserted figure of panel A), which is a characteristic of the recoverin staining for cultured photoreceptors. Moreover, in contrast to other neurons found in the cultures, the small recoverin-positive cells grew only few fine neurites with a maximum length of 45 µm. The very specific markers rhodopsin for rods and blue opsin for early developing cones are shown in panel B and C, respectively. Rhodopsin and opsin are usually expressed in the outer segments of either type of photoreceptors. Surprisingly, while rhodopsin-immunoreactivity (rhodopsin-IR) and blue opsin-immunoreactivity (blue opsin-IR) were found in few cells, the majority of the recoverin-positive cells were not labeled by these markers. Only one cell (red arrows) in panel B displayed rhodopsin-IR and two cells (blue arrows) in panel D exhibited blue opsin-IR. Furthermore, the outer segments cannot be identified in cells of dissociated cultures. These results suggest that many photoreceptors did not develop outer segments and stopped expressing rhodopsin or opsin, respectively, during culturing. Therefore, in dissociated cultures photoreceptors can only be identified based on the morphology (small cell body, one or few short neurites) and recoverin-IR.

In addition, recoverin-positive cells with larger soma size (around 8 to 9 µm in diameter, white arrows in panel A), were observed in this kind of culture. These bigger cells might represent type 2 bipolar cells according to the size and their recoverin-IR. However, these cells do not always display a clear bipolar morphology.

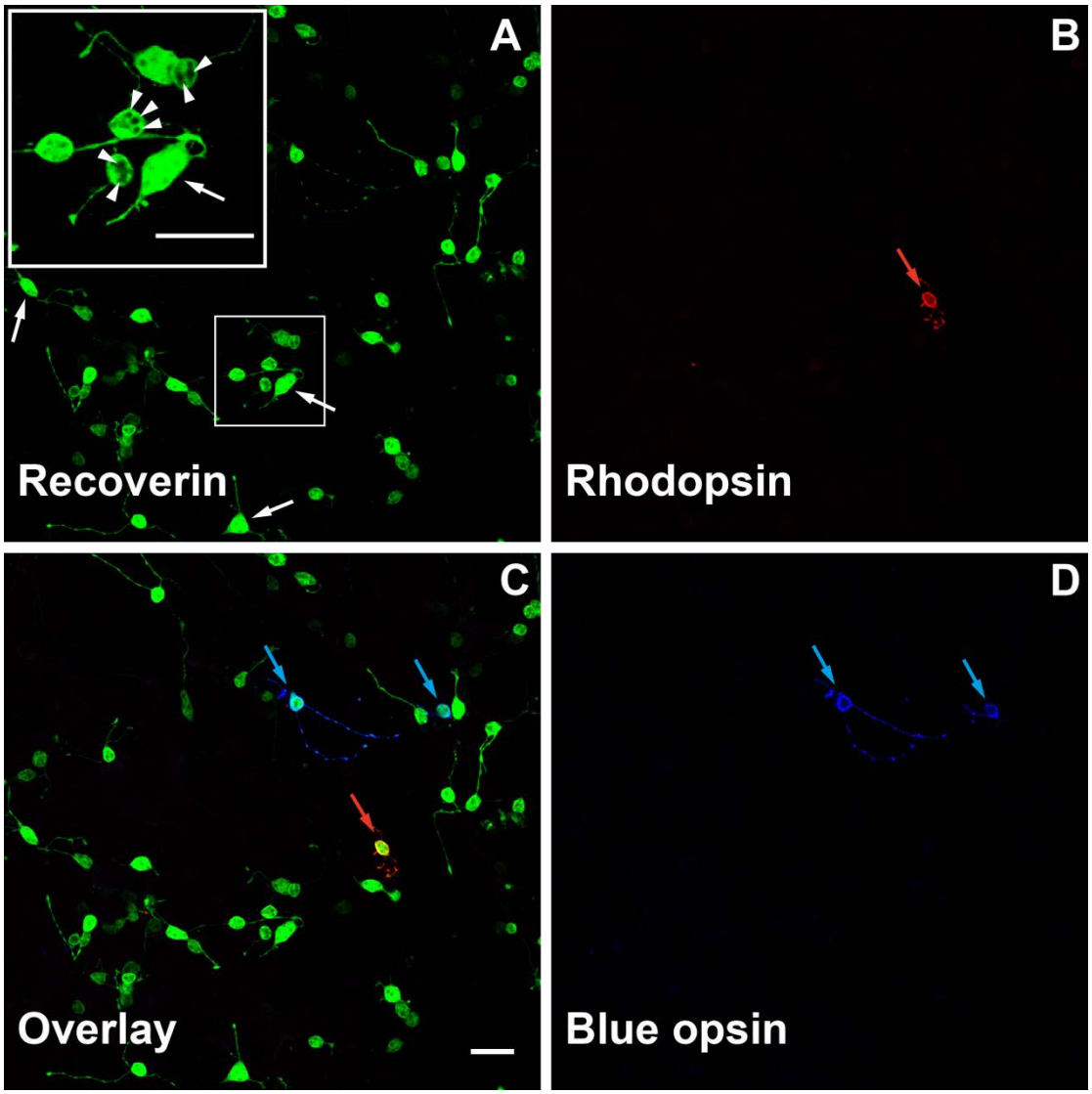

Figure 3.2.7: Identification of photoreceptors in dissociated retinal cultures.
Dissociated retinal cultures were stained with immunochemical markers for recoverin (green), rhodopsin (red), and blue opsin (blue). The inserted panel is a higher magnification of the marked area of panel A. White arrowheads mark the "bubbles" in the photoreceptor somata and white arrows mark cells that are presumably type 2 bipolar cells. Rhodopsin-immunoreactive cells and blue opsin-immunoreactive cells are indicated by a red arrow and blue arrows respectively.
Scale bar = 20 µm.

Figure 3.2.8 focuses on neurons postsynaptic to photoreceptors in the native retina: horizontal cells and bipolar cells. Immunochemical staining for CaBP on a dissociated culture is shown in panel A. As shown in Figure 3.2.2, strong CaBP-IR is a reliable marker for horizontal cells. Figure 3.2.8 A shows a strongly stained cell with a large soma (~15 µm in diameter, arrow). Some thick projections (arrowheads) grow out and further bifurcate into many fine processes that spread widely in the surrounding area. Actually, only a part of the dendritic tree is displayed here. Normally, these branches extend to several hundred micrometers. These features agree with the morphology of horizontal cells *in vivo* forming far reaching lateral connections (Peichl and Gonzalez-Soriano, 1994). Moreover, the CaBP-immunoreactive cells were rare in the cultures, which agrees well with the relatively small number of horizontal cells in the retina. However, CaBP expression is also found in amacrine cells (see Figure 3.2.4) identified as cholinergic amacrine cells (Haverkamp and Wässle, 2000). To rule out that the CaBP-positive cells in the cultures were amacrine cells, a double-staining was performed. The staining for calretinin that is found in many amacrine cells including cholinergic amacrine cells is shown in red in the overlay (panel B). One strong calretinin-immunoreactive cell (red, long arrow) was found on the right to the CaBP-positive cell (green, short arrow). Clearly, there is no colocalization of the two markers. Therefore, the cells with CaBP-IR are identified as horizontal cells in dissociated cultures.

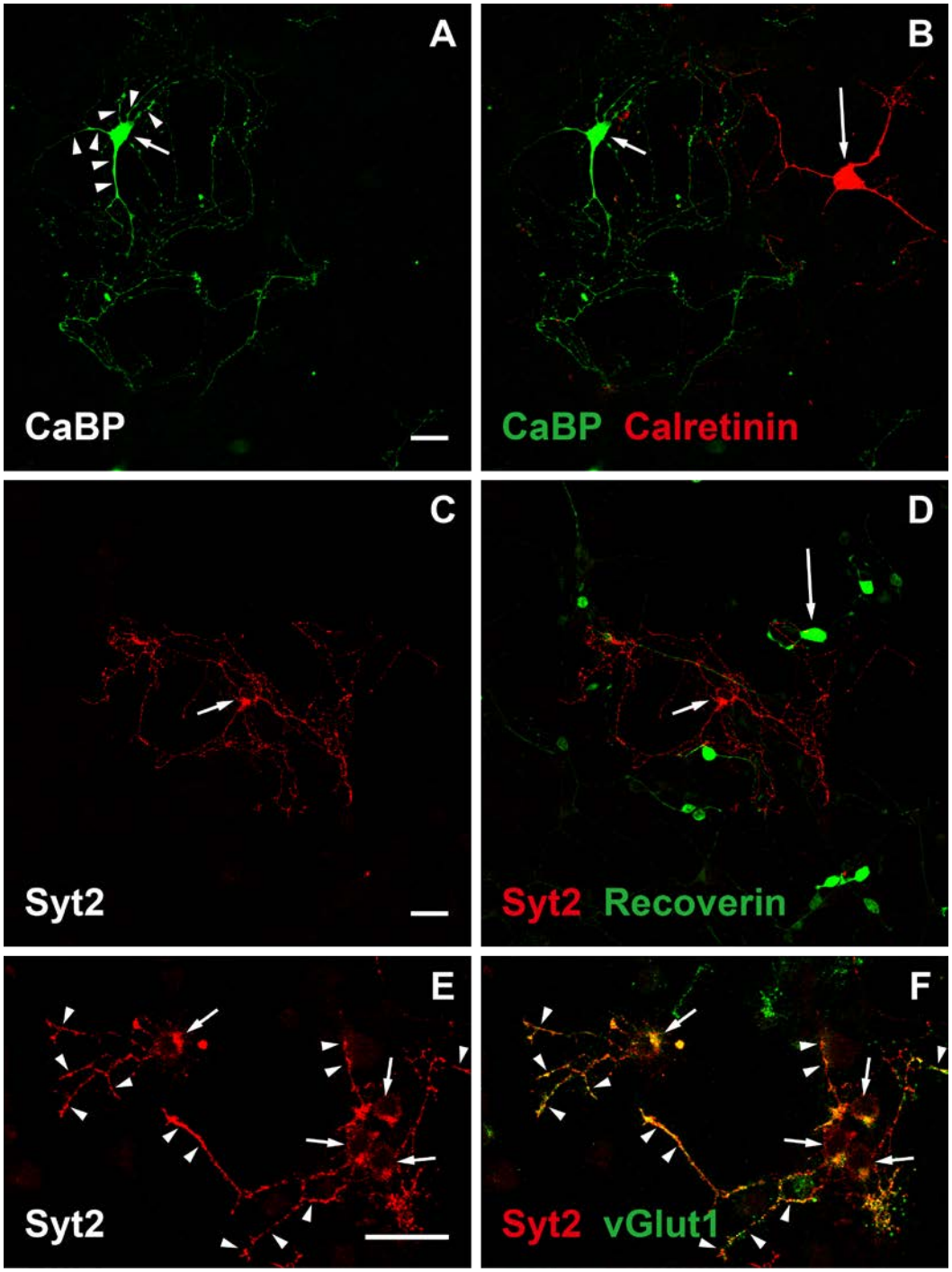

Figure 3.2.8: Identification of horizontal cells and bipolar cells in dissociated retinal cultures.

Dissociated retinal cultures were stained with antibodies against CaBP (A & B, green), calretinin (B, red), Syt2 (C, D, E & F, red), recoverin (D, green) and vGlut1 (F, green). A & B: Short arrows indicate CaBP-immunoreactive somata. Arrowheads indicate CaBP-immunoreactive thick neurites. Long arrow indicates calretinin-immunoreactive soma. C, D, E & F: Short arrows indicate Syt2- immunoreactive somata. Long arrow indicates a big recoverin-immunoreactive cell. Arrowheads indicate neurites co-stained by antibodies against Syt2 and vGlut1.
Scale bar = 20 µm.

Surprisingly, some antibodies used in native mouse retina as reliable bipolar cell marker such as PKCα for rod bipolar cells and CaBP5 for type 3, 5, and rod bipolar cells showed weak or variable stainings in the dissociated cultures. PKCα-IR was barely found in the cultures, while the immunoreactivity for CaBP5 was very faint (data not shown). The antibodies against the synaptic vesicle associated protein synaptotagmin-2 (Syt2) shows strong stainings. Syt2 was reported to be expressed in type 2 and 6 bipolar cell axon terminal systems and also horizontal cell terminals in the mouse retina (Fox and Sanes, 2007; Wässle et al., 2009). Using Syt2 antibodies, two kinds of cells were stained. Wide-field cells with big somata (about 15 µm in diameter) and very long neurites were found (data not shown). They were very rare. All three features indicate that they were horizontal cells. Double-staining of Syt2 with the horizontal cell marker CaBP was not possible as both antibodies were raised in mouse. The more commonly found Syt2-positive cells might be bipolar cells. A Syt2 immunoreactive cell is shown in Figure 3.2.8 C. Its neurites are strongly immunoreactive. While from the morphology this cell does not appear bipolar at all, two morphological features indicate that this cell might be a bipolar cell rather than a horizontal cell. First, the soma is quite small (arrow, only about 8 µm in diameter). Second, the neurites are quite short (about 80 µm in radius), which is clearly much shorter than the projections from the horizontal cell in panel A. Most of the Syt2-positive cells found in dissociated cultures had similar features as the one shown in Figure 3.2.8 C. In Figure 3.2.8 D, no cell was co-stained in the double-labeling for recoverin and for Syt2. The larger recoverin-positive cell (long arrow) does not appear to be Syt2-IR. As this cell is much larger than a photoreceptor, it might represent a type 2 bipolar cells (compare Figure 3.2.1 & Figure 3.2.7) and hence, should be Syt2-positive (Haverkamp and Wässle, 2000; Wässle et al., 2009). One might conclude that either type 2 bipolar cells cease to express Syt2 in dissociated cultures, or, alternatively, that cells other than photoreceptors and type 2 bipolar cells express recoverin in dissociated cultures. Double-labeling using antibodies against Syt2 and against the vesicular glutamate transporter 1 (vGlut1) was performed to confirm that the small Syt2-positive cells were bipolar cells. vGlut1 is expressed in photoreceptor

terminals and bipolar cell axon terminals in the mouse retina (Haverkamp et al., 2003). Figure 3.2.8 E shows four small-field cells with Syt2-IR, whose somata are indicated by arrows. In the overlay F, co-expression of Syt2 and vGlut1 can be observed. The neurites (arrowheads) appear yellow due to the co-staining. Therefore, the small-field Syt2 immunoreactive cells probably are type 6 bipolar cells. But not all of them were found to be vGlut1-immunoreactive (data not shown), which might imply some type 6 bipolar cells cease to express vGlut1 in dissociated cultivation.

As a summary for cultured bipolar cells, their morphology mostly remodeled into multipolar forms and their functional properties also showed variable changes

Figure 3.2.9 mainly focuses on different amacrine cell markers (panel A ~ C). Amacrine cells are the inhibitory interneurons in the retina. They can be further divided into many subtypes according to their neurotransmitters and molecular components. The two major neurotransmitters are γ-aminobutyric acid (GABA) and glycine. GABAergic and glycinergic amacrine cells each represent 40 to 50% of the whole amacrine cell population in the mouse retina (Marc, 1988; Pourcho, 1996; Nguyen-Legros et al., 1997; Pow and Hendrickson, 1999; Lin and Masland, 2006). The key enzyme that catalyzes the decarboxylation of glutamate to GABA and CO_2 in GABAergic neurons is glutamic acid decarboxylase (GAD). In this study, an antibody against glutamic acid decarboxylase isoform 67 (GAD67) was selected as a marker for GABAergic amacrine cells. In panel A of Figure 3.2.9, some cell bodies (arrows) are immunoreactive for GAD67. Their somata had diameters of 10 to 12 µm, similar to the size of amacrine cells. Also numerous far reaching GAD67-immunoreactive processes can be observed. In the native retina, GABAergic amacrine cells are wide-field amacrine cells (Vaney, 1990; MacNeil and Masland, 1998; Lin and Masland, 2006), which agrees well with the morphology of GAD67-immunoreactive cells in the dissociated cultures. Thus, I consider all these GAD67-positive cells as GABAergic amacrine cells.

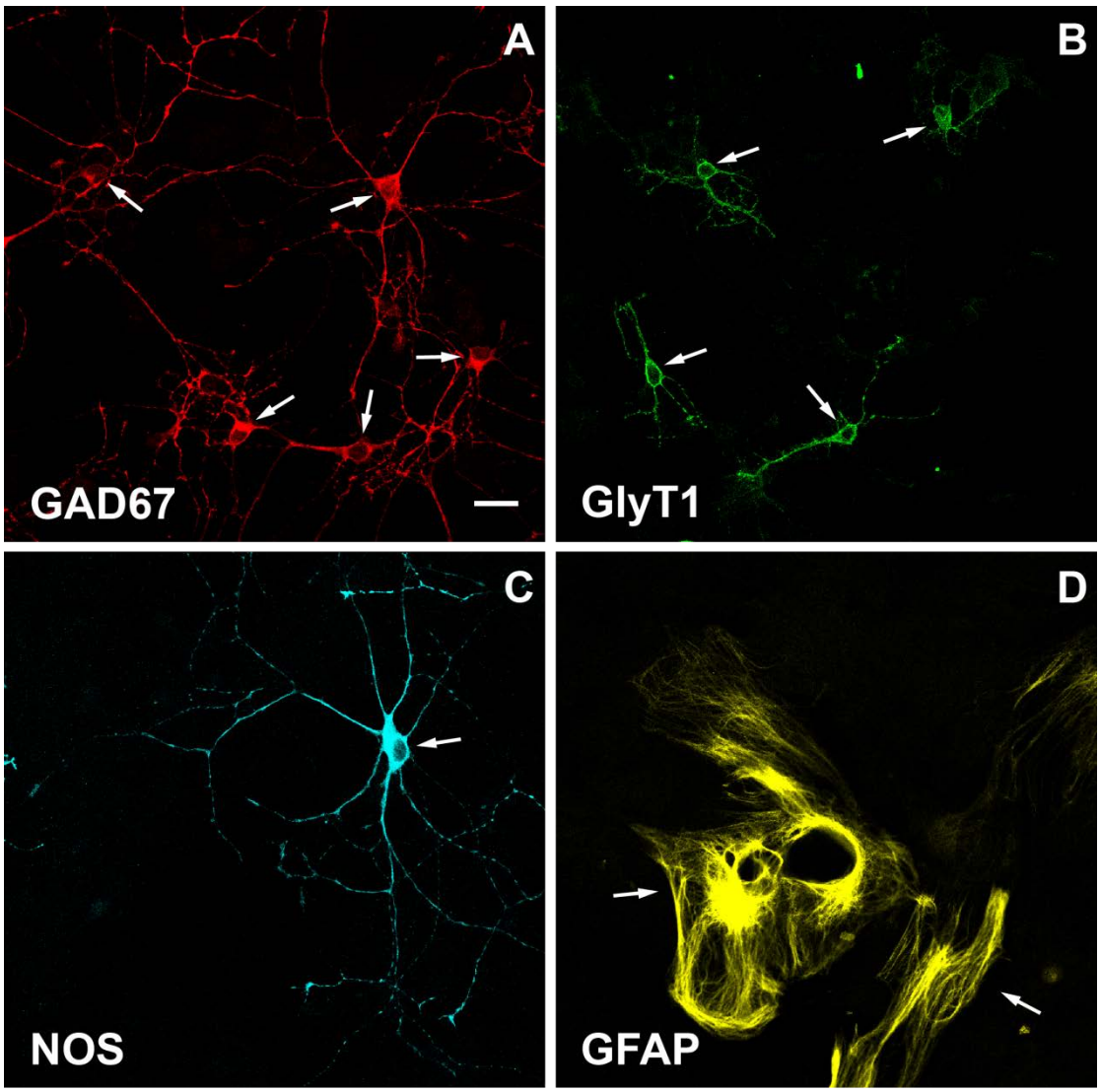

Figure 3.2.9: Identification of amacrine cells and glia cells in dissociated retinal cultures.

Dissociated retinal cultures were stained with immunochemical markers for GAD67 (A, red), GlyT1 (B, green), NOS (C, cyan) and GFAP (D, yellow). All immunoreactive somata are marked with arrows.

Scale bar = 20 µm.

Another major group of amacrine is glycinergic. These cells can be labeled with antibodies against glycine or against the glycine transporter (Menger et al., 1998; Pow and Hendrickson, 1999; Haverkamp and Wässle, 2000). Therefore, the antibody against the glycine transporter 1 (GlyT1) was used to identify glycinergic amacrine cells. Figure 3.2.9 B shows four GlyT1-immunoreactive cells with their somata (arrows) and neurites. The staining appears membrane-associated, which was

expected as glycine transporters are located in the membrane of glycinergic cells. The GlyT1-positive processes are clearly shorter than the neurites of the GABAergic amacrine cells. The longest neurites of these glycinergic cells were about ~50 µm in length. In the mammalian retina, glycinergic amacrine cells are mostly small-field amacrine cells (Pourcho and Goebel, 1985; Menger et al., 1998). Therefore, the features of these cultured cells in panel B fit to those of glycinergic amacrine cells.

Figure 3.2.9 C shows a staining with an antibody against NO-synthase (NOS). In agreement with the rather small population of NOS-positive amacrine cells *in vivo*, the number of NOS-positive cells in dissociated retinal cultures was also found to be relatively small. In this panel, one cell shows strong immunoreactivity in its cell body and neurites. Although there are two types of NOS-positive amacrine cells in the native retina as shown in Figure 3.2.6, only one type was found in the dissociated cultures, which has a big soma (arrow) and neurites extending several hundred micrometers.

Panel D of Figure 3.2.9 shows a culture stained for GFAP. It was observed that glia cells were important in all dissociated retinal cultures. Glia cells grew below the cultured neurons and formed a homogenous cellular support for them. The dissociated retinal neurons survived only on this layer of glia cells. Glia cells were found all over the cover slips. In contrast, GFAP-IR is surprisingly rarely found in the dissociated cultures. In Figure 3.2.9 D, two glia cells (arrows) exhibit GFAP-IR. In the normal healthy retina, only astrocytes express GFAP. The cells with GFAP-IR might be astrocytes. Antibodies against glutamine synthetase (GS), a specific marker for Müller cells (Linser et al., 1984), did not reveal immunoreactive cells (data not shown). The unstained glia cells might be Müller cells whose expression pattern has changed due to the culturing conditions.

Conclusion for dissociated retinal cell cultures

The dissociated mouse retinal culture was established successfully. Retinal neurons could survive for more than 4 weeks on coated coverslips *in vitro*. However, the

number of cultured cells decreased with the duration of the culture. Therefore, the best time window for experiments on these cultures would be from the 2nd day after seeding until the 14th day. Photoreceptors, horizontal cells, bipolar cells, and amacrine cells were identified in cultures, although some types of cells appeared to differ morphologically from their counterparts *in vivo*. The heterogeneous population indicated a good quality of the cultures. Furthermore, the present of NO-positive cells might offer an additional platform for investigations of the NO-cGMP pathway in these retinal cultures.

3.2.3 Organotypic retinal slice culture

The third type of retinal culture can be considered as a compromise: it makes the retinal neurons similarly accessible as in the dissociated culture while attempting to preserve the retinal structure as much as possible.

For this type of culture, isolated retinae from P8 mice were sliced and slices were cultured up to 8 days. Slices were sectioned at a minimum thickness of 150 μm and a maximum thickness of 250 μm. Cultures were characterized by the same immunochemical markers as described for other culture types.

Generally spoken, the retinal architecture was not well retained in the slice cultures. Immunochemical studies on 150 μm retinal slices are shown in Figure 3.2.10. The recoverin-label in the first row indicate the changes of photoreceptors: photoreceptors were initially found in a limited area during the first four days of culturing (Figure 3.2.10, recoverin, 2nd & 4th day) but then grew into a loose pattern (Figure 3.2.10, recoverin, 6th & 8th day). The second row shows PKCα-staining. No PKCα-IR was observed in the first 4 days after seeding (Figure 3.2.10, PKCα, 2nd & 4th day). This is most surprising, as strong PKCα-IR is found in the retina at P8 (see Figure 3.2.2) the stage that was chosen for cultivation. From the 6th day on, PKCα-IR was found weakly in some cells but became more prominent on the 8th day. The calretinin staining in the third row shows amacrine cells with large somata and long neurites in all stages of cultivation. However, no structure was observed that reminded of an IPL,

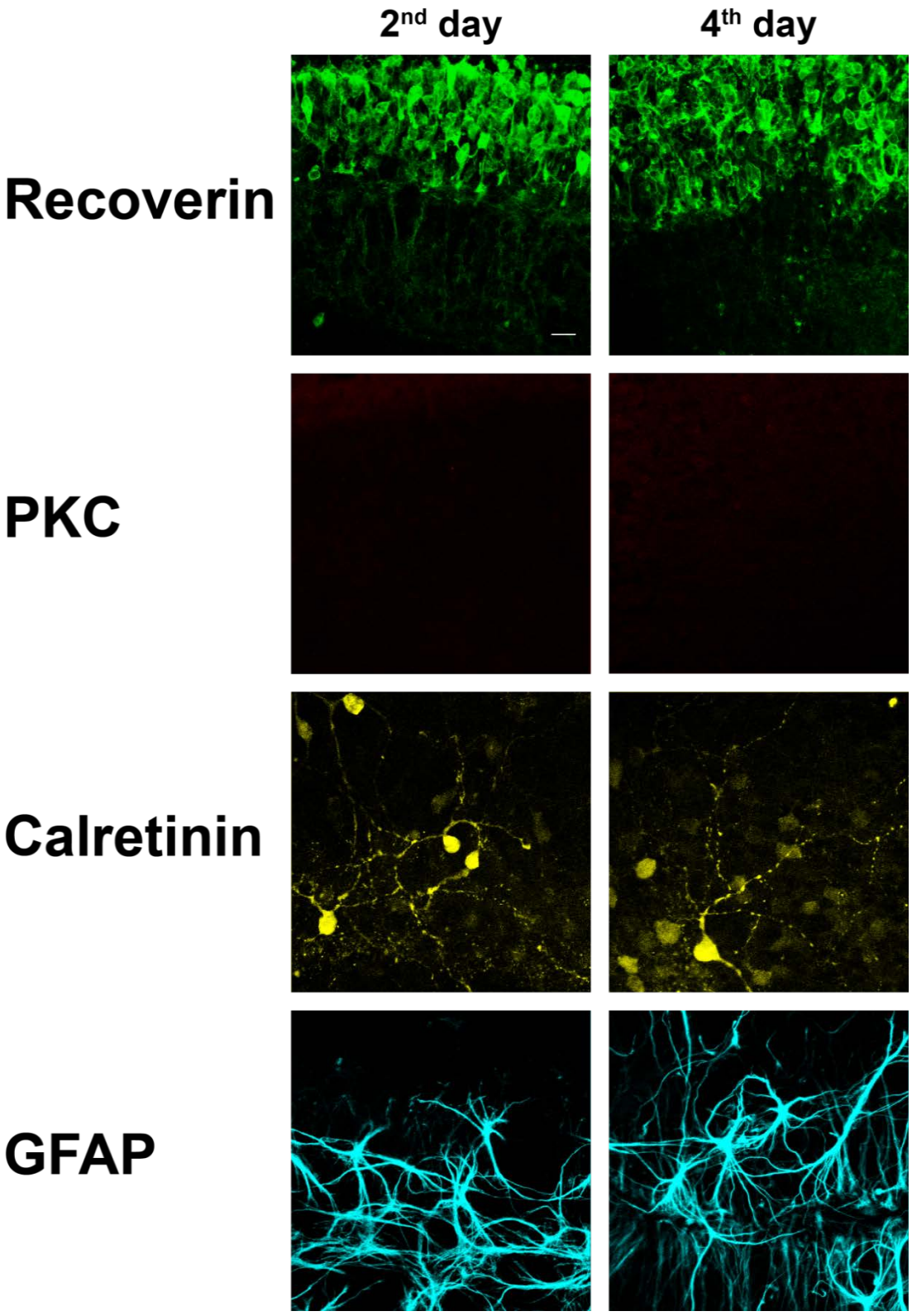

Figure 3.2.10: Immunochemical characterization of 150 µm-thick retinal slice cultures.

150 µm-thick retinal slice cultures at 2nd, 4th, 6th and 8th days of cultivation were immunostained

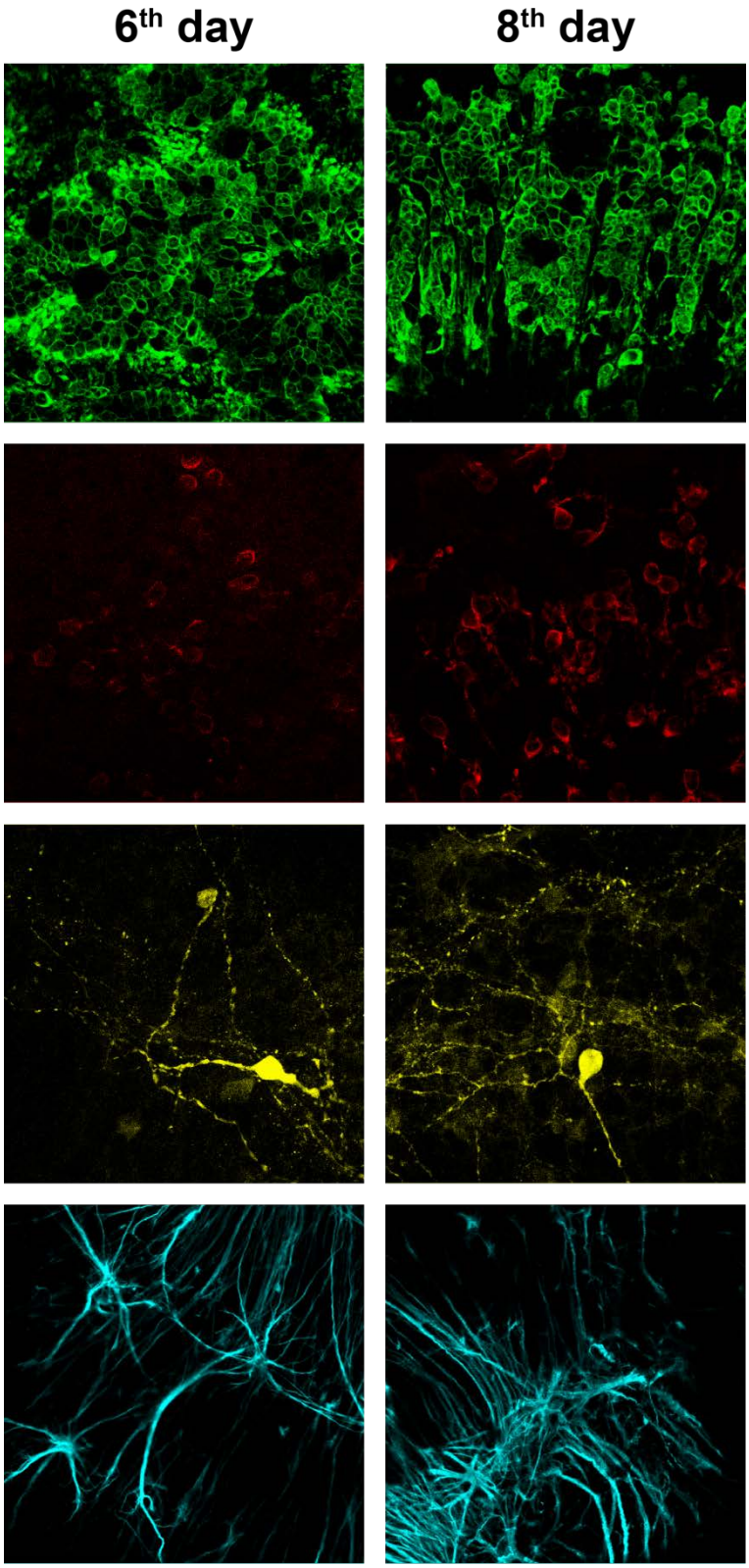

with antibodies against recoverin (first row, green), PKCα (second row, red), calretinin (third row, yellow) and GFAP (bottom row, cyan). Scale bar = 20 µm.

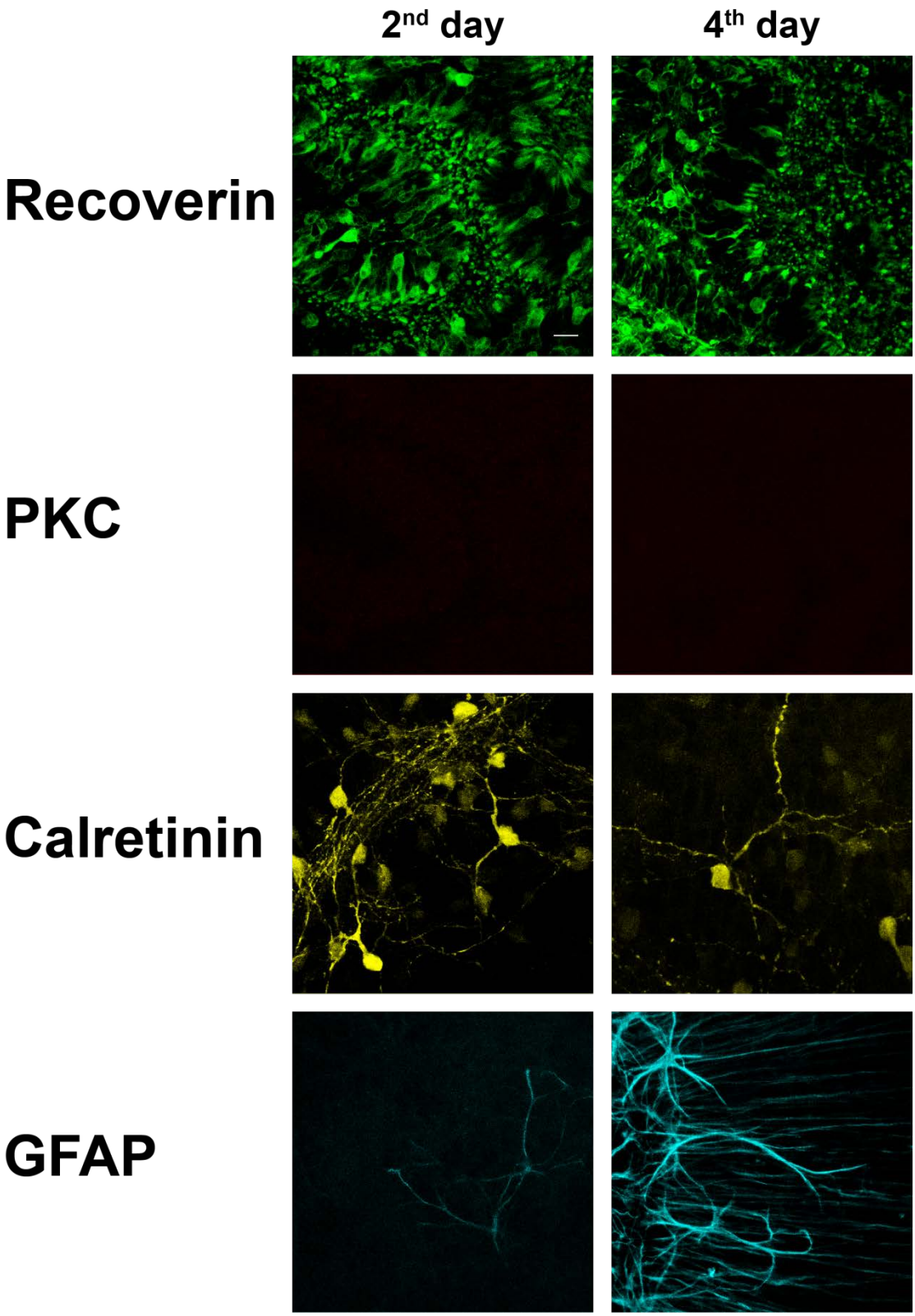

Figure 3.2.11: Immunochemical characterization of 250 µm-thick retinal slice cultures.

250 µm-thick retinal slice cultures at 2nd, 4th, 6th and 8th days of cultivation were immunostained

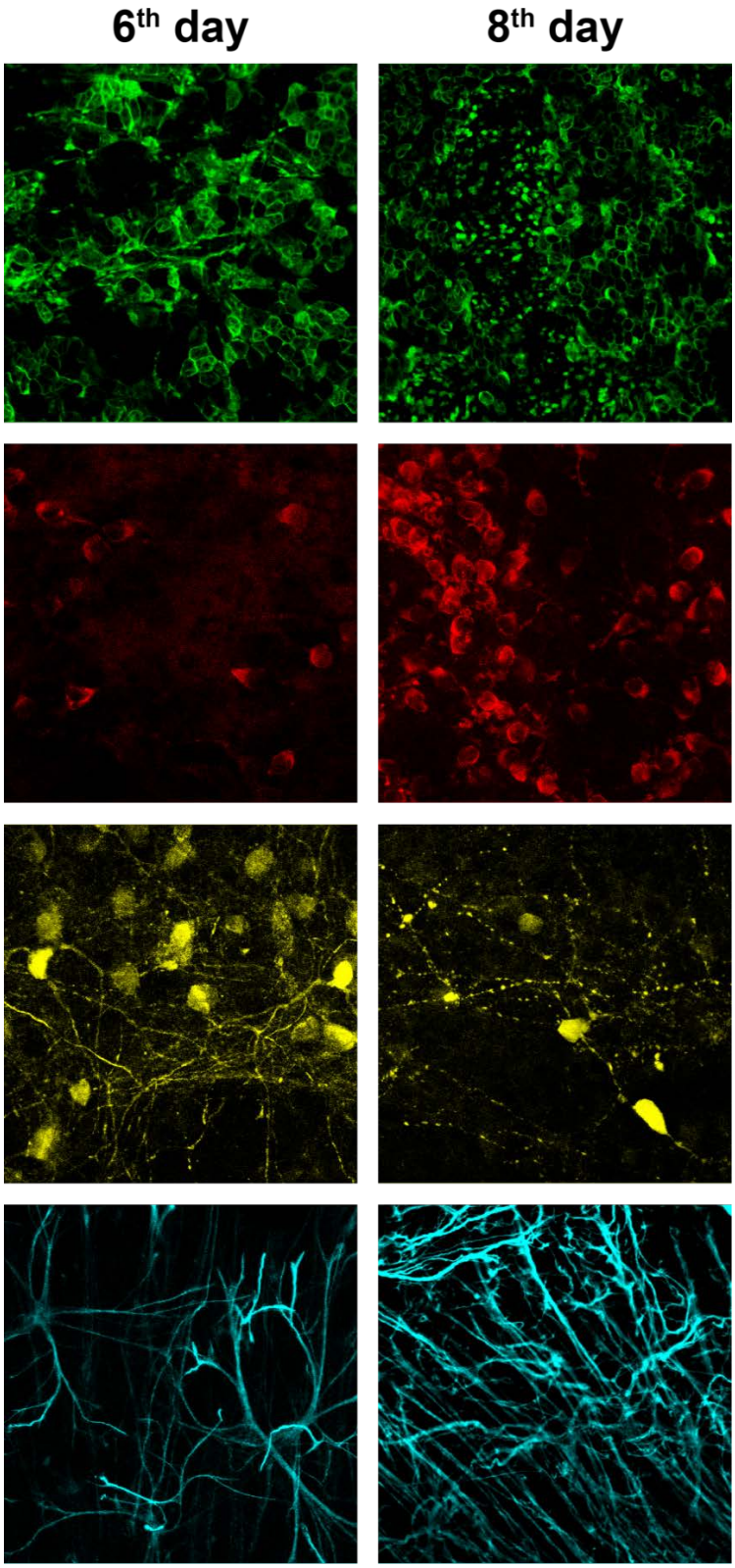

with antibodies against recoverin (first row, green), PKCα (second row, red), calretinin (third row, yellow) and GFAP (bottom row, cyan). Scale bar = 20 µm

not to mention three distinct calretinin-immunoreactive bands. The last row of GFAP-staining shows strong immunoreactive fibers in all stages.

Increasing the thickness of the retinal slices to 250 μm did not improve the tissue preservation (Figure 3.2.11). Many disorganized photoreceptors were found in the recoverin-staining in all periods of culturing (first row). Again, PKCα expression was delayed (second row). Amacrine cells visualized using calretinin-staining showed unorganized distribution during the whole culturing period (third row). Strangely, two days after seeding, GFAP was not expressed as strongly as it was found in 150 μm s1ice cultures. GFAP-IR increased from the 4th day of culturing.

Conclusion for organotypic retinal slice cultures

The overall results indicated an extremely fast degeneration of the retina structure in retinal slice cultures, which was independent of the original thickness of the slice. Besides, the properties of some types of cells were also changed. For example, rod bipolar cells could temporarily stop synthesizing PKCα when the culturing was initiated. Therefore, the sliced retinae are not able to preserve native structures in culture. So this type of cultures is not suggested for further experiments that require a well preserved retinal network.

3.3 AAV-mediated transduction *in vitro*

3.3.1 AAV-mediated transduction in dissociated retinal cell cultures

In this project, adeno-associated viruses (AAVs) were used as gene ferry to introduce foreign genes into retinal neurons. Seven different serotypes of AAVs were available: AAV1, AAV2, AAV4, AAV5, AAV6, AAV8, and AAV9. Different serotypes have been shown to have different transduction efficiency for different cell types. The selectivity of these viruses is most probably due to the receptor-mediated endocytosis of the target cells (Michelfelder and Trepel, 2009; Agbandje-McKenna and Kleinschmidt,

2011). To evaluate the transduction efficiency on retinal cells, AAVs were used, which carry the cDNA for the enhanced green fluorescent protein (GFP; AAVs-GFP) under the control of a cytomegalovirus (CMV) promoter. Usually two days after seeding, viruses were added directly into the culture medium of dissociated retinal cultures. Cells were cultured for another 6 to 8 days before being fixed and analyzed by immunocytochemistry.

For the initial testing, TO-PRO3 was used to stain nuclei for cell counting. Figure 3.3.1 gives an overview on the transduction efficiency for different serotypes of AAVs. To enable a better comparison of the strength of expression, GFP was not visualized via immunocytochemistry using antibodies against GFP. Rather, the endogenous fluorescence of GFP was detected in all transduction experiments using the same settings of the microscope. The total number of cells in the same field is shown by the nuclear stain in blue. The overlays reveal the transduction rate of the seven different AAV serotypes in the cultures.

In dissociated cultures transduced by AAV1-GFP (Figure 3.3.1, A1 - A3), GFP expression was found in many cells. A few cells showed large somata (arrows) while the rest of the cells were smaller in size. The intensity of the green fluorescence differed from one cell to another. In the most intensely fluorescing cells, also the thick neurites (arrowheads) protruding from the soma could be observed. A similar expression pattern was found in AAV2-GFP infected cultures (Figure 3.3.1, B1 - B3). For example, two bright cells (arrows) are found in panel B1 together with several small cells, some of which have bright fluorescence and some of which are faint. In cultures incubated with AAV4-GFP (Figure 3.3.1, C1 - C3), only cells with small cell bodies were transduced. No larger cell was found that expressed GFP. AAV5-GFP (Figure 3.3.1, D1 - D3) gave the lowest transduction efficiency. Only few cells expressed GFP at a very low level as seen in D1. Based on this observation, AAV5 was omitted from further tests.

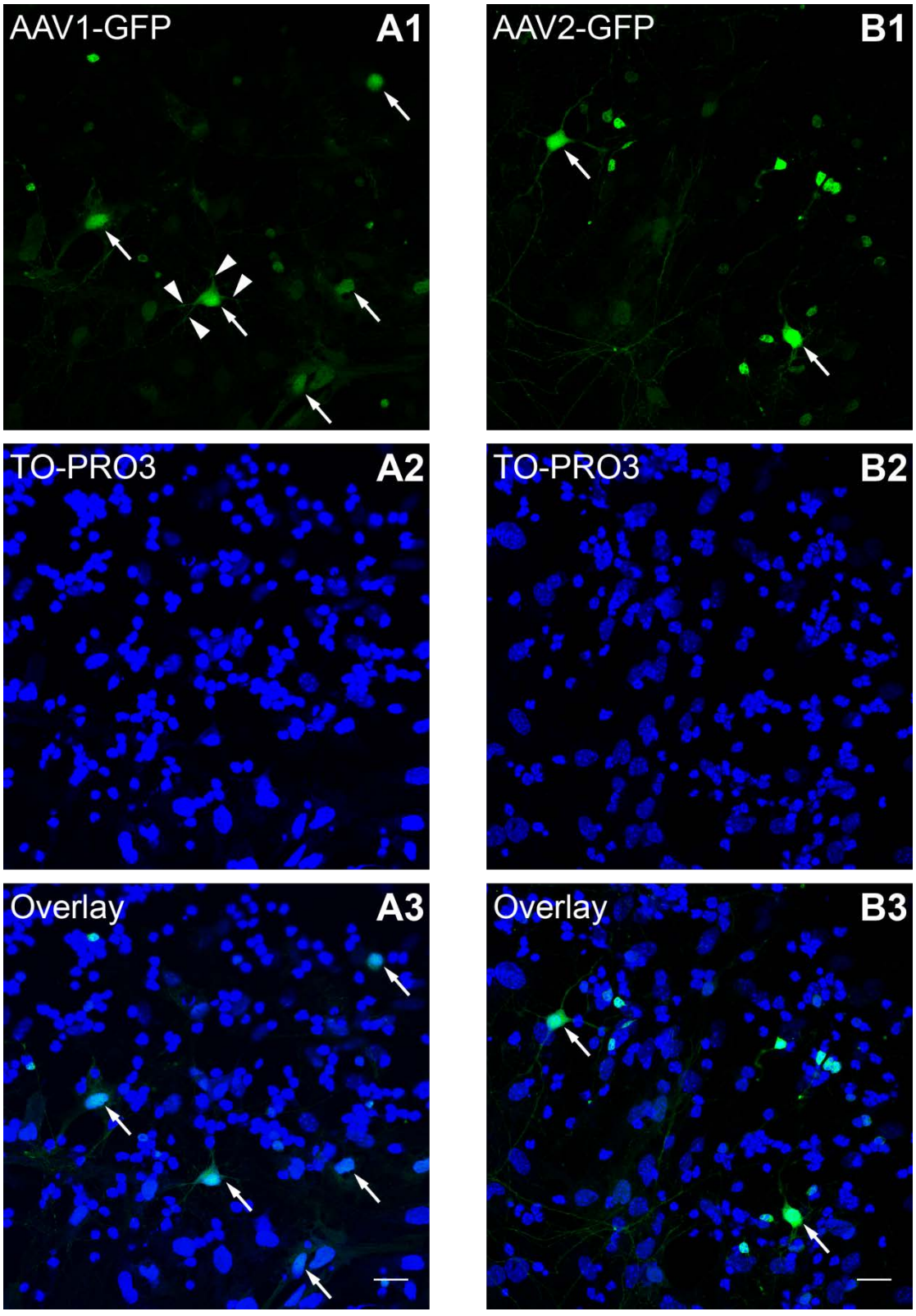

Figure 3.3.1: GFP expression in dissociated retinal cultures upon transduction by AAVs.

Dissociated retinal cultures were transduced by AAV1-GFP (A1 - A3), AAV2-GFP (B1 - B3), AAV4-GFP (C1 - C3), AAV5-GFP (D1 - D3), AAV6-GFP (E1 - E3), AAV8-GFP (F1 - F3), and

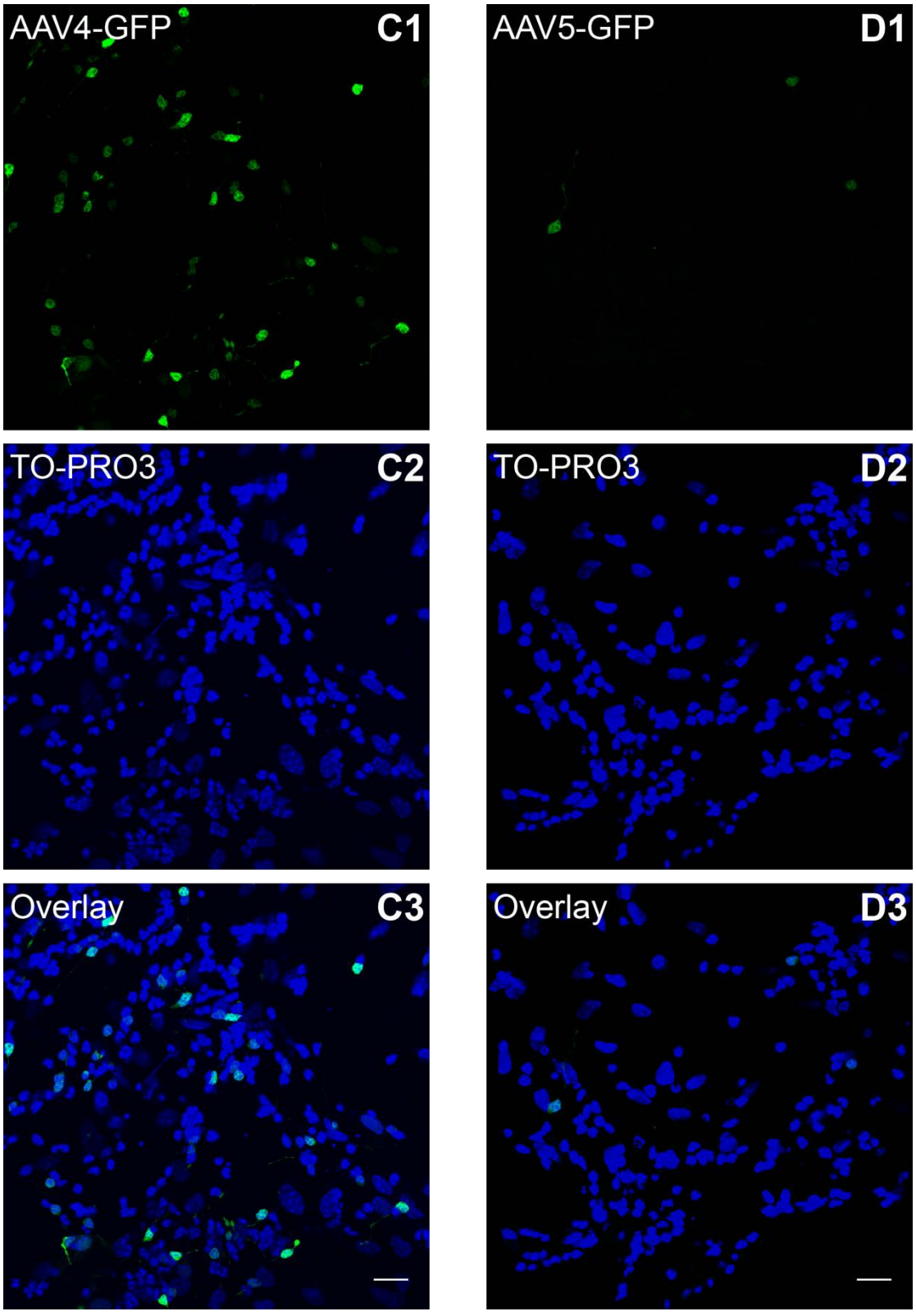

AAV9-GFP (G1 – G3). The green fluorescence represents endogenous GFP fluorescence. Cell nuclei were stained by TO-PRO3 (blue). All arrows indicate large neurons expressing GFP. Arrowheads indicate neurites.
Scale bar = 20 µm

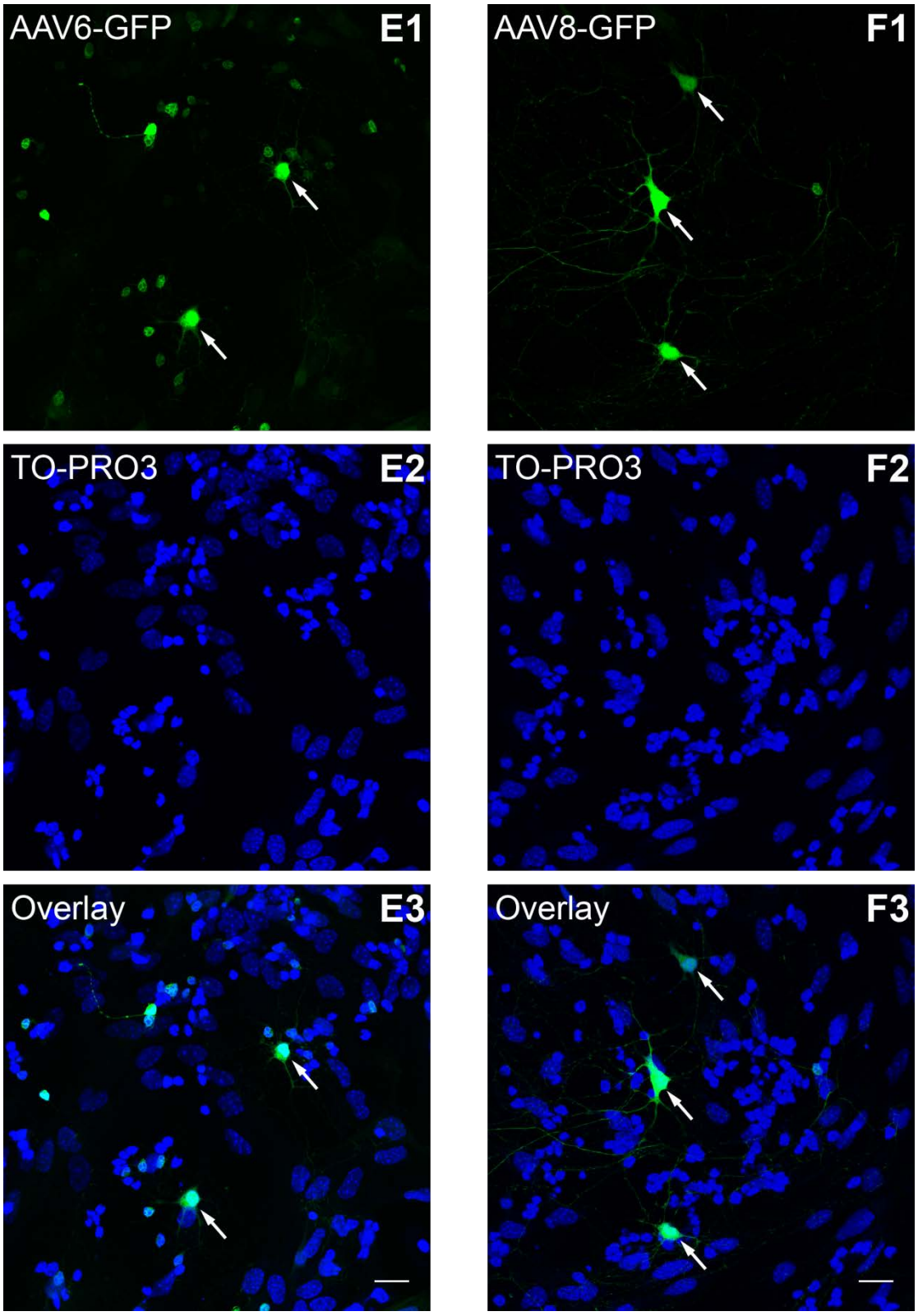
AAV6-GFP
E1
AAV8-GFP
F1
TO-PRO3
E2
TO-PRO3
F2
Overlay
E3
Overlay
F3

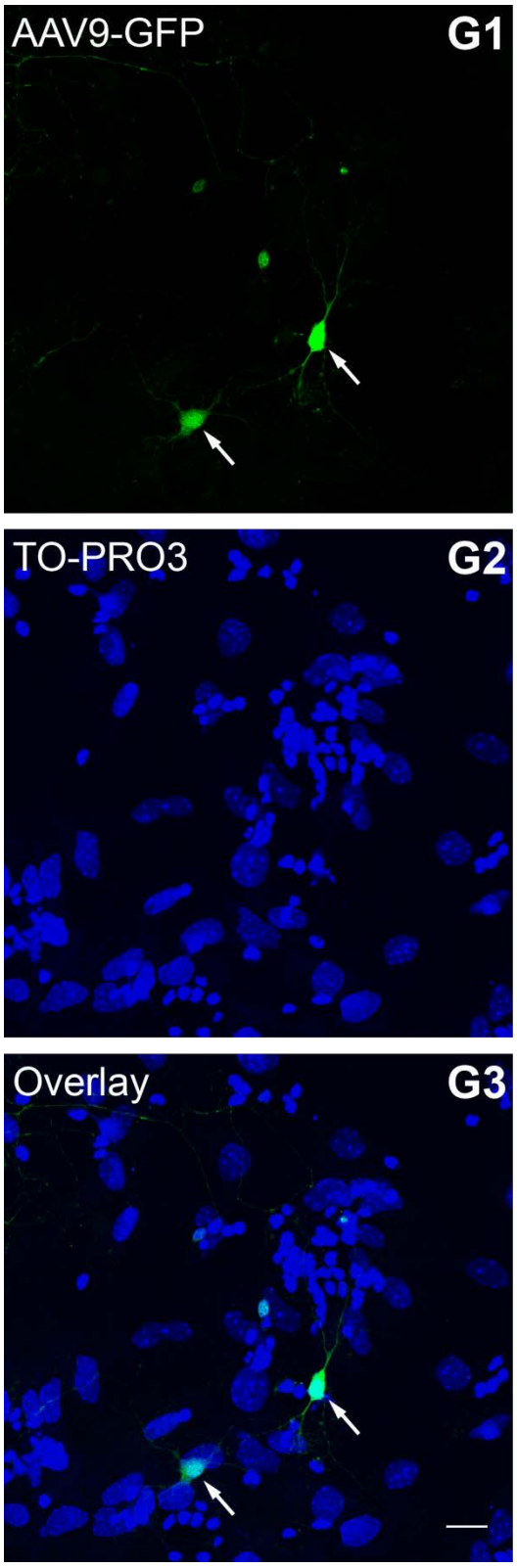
AAV9-GFP
G1
TO-PRO3
G2
Overlay
G3

The infection pattern of AAV6-GFP (Figure 3.3.1, E1 - E3) was similar to that found in AAV1- and AAV2-infected cultures. In Figure 3.3.1 E1, two big cells (arrows) and a few small cells can be observed. Many of them have high GFP intensity reflecting a high expression level. In cultures transduced by AAV8 (Figure 3.3.1, F1 - F3) and AAV9 (Figure 3.3.1, G1 - G3) only few cells expressed GFP. However, these cells were usually large in size and had high expression levels. Additionally, GFP-expressing glia cells were found in all AAV-transduced cultures (data not shown).

In general, all AAV serotypes transduced retinal neurons in dissociated cultures. However, different AAV serotypes yielded different transduction patterns and expression levels. As dissociated retinal cultures comprise a large variety of neuronal types, the transduction efficiency should not be determined simply on the percentage of transduced cells. In the following experiments, transduced cultures were counterstained with cell type specific markers.

Figure 3.3.2 compares the detection of GFP based on its endogenous fluorescence (green, A) and on the immunocytochemical staining using antibodies against GFP (red, B). The number of cells that can be detected using immunocytochemistry is larger than the number of cells that are visualized by endogenous GFP fluorescence. Some cells that can barely be detected based on the endogenous GFP fluorescence are marked by arrowheads. The advantage of the immunocytochemical detection is twofold: it reveals cells with low expression level and it visualizes neurites. This finding was observed in all transductions independent of the AAV serotype. There are two possible reasons for this difference. First, due to the amplification step in indirect immunochemistry, several fluorescent molecules bind via secondary antibodies to each GFP molecule, resulting in a superior sensitivity of this method compared to the detection of endogenous fluorescence. Second, however, it cannot be ruled out that some GFP molecules are not functional and, therefore, do not emit fluorescence but can be detected by antibodies. Thus, immunolabeling with antibodies against GFP was employed for cell type identification.

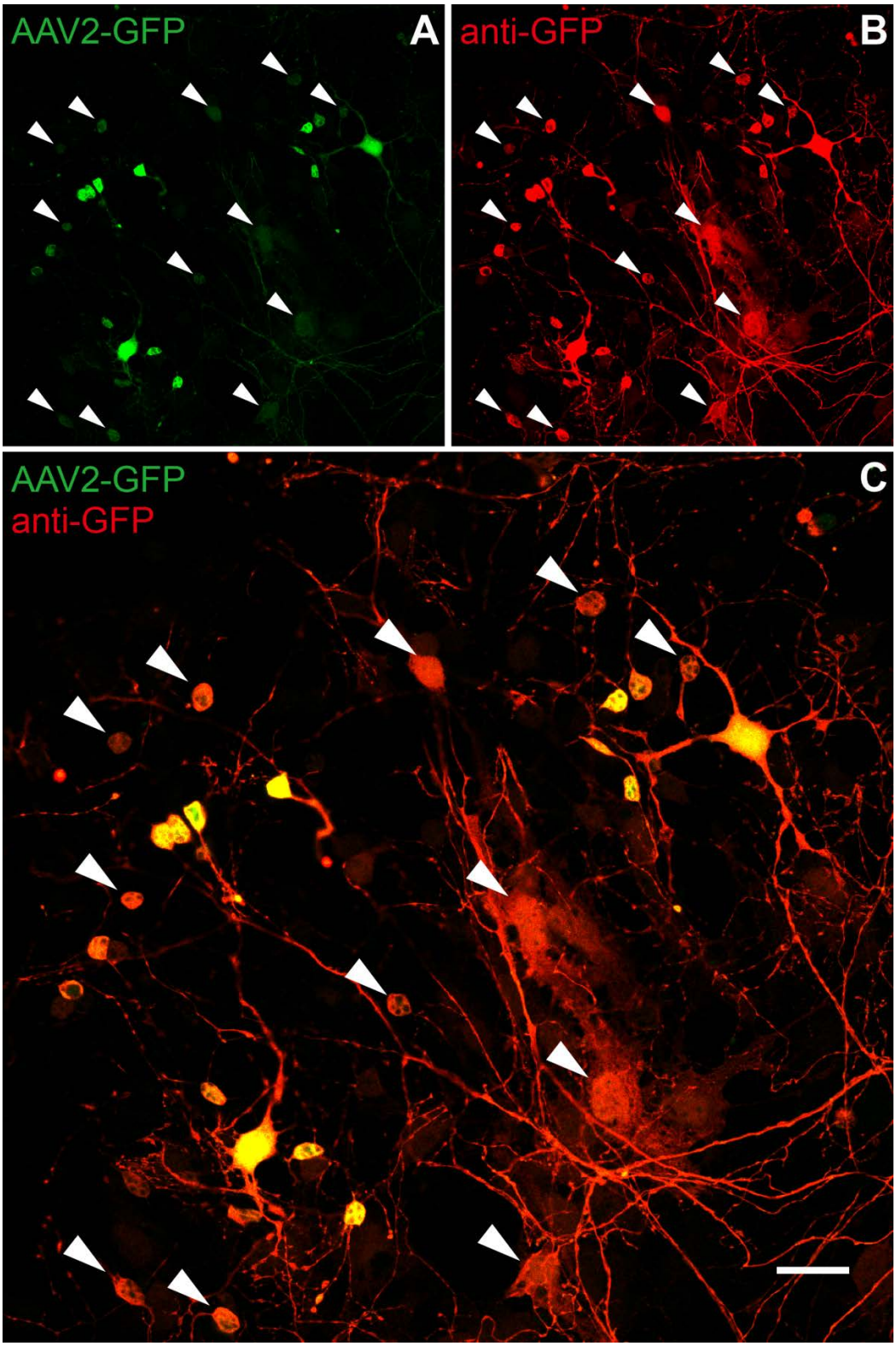

Figure 3.3.2: Comparison of immunostaining for GFP with GFP fluorescence.

Dissociated retinal cultures transduced by AAV2-GFP were immunostained for GFP in red. The green fluorescence represents endogenous GFP fluorescence. Arrowheads indicate cells that show strong GFP-IR, but low GFP fluorescence.

Scale bar = 20 µm.

In the following figures, counterstainings were performed systematically that covered nearly all neuronal types except for ganglion cells using reliable markers: recoverin for photoreceptors, CaBP for horizontal cells, Syt2 for type 6 bipolar cells, GlyT1 for glycinergic amacrine cells, GAD67 for GABAergic amacrine cells and NOS for NOS amacrine cells.

Figure 3.3.3 gives an example of the cultures transduced by AAV2-GFP showing a double staining with antibodies against GFP in green and recoverin, the photoreceptor marker, in red. Prominent GFP expression was found in two cells with big somata and weaker expression was observed in many smaller cells (Figure 3.3.3 A). In the recoverin-staining many cells with small cell bodies were observed (Figure 3.3.3 B). In the overlay (Figure 3.3.3 C), the double-labelled small cells in yellow (arrows) can be identified as photoreceptors based on their recoverin immunoreactivity. But not all the recoverin-positive cells were infected. On average only about 10% (16/156) of the recoverin-immunoreactive cells were transduced by AAV2. On the other side, there were green cells that were negative for recoverin, which implies that AAV2 not only infects photoreceptors but also other types of retinal neurons.

For better comparison, the following counterstainings shown in this section were all taken from cultures infected by AAV2-GFP. The results of the remaining AAV serotypes will be presented in Table 3.3.1.

The double-staining for anti-GFP in green and CaBP in red is shown in Figure 3.3.4. In the anti-GFP micrograph (Figure 3.3.4 A), several cells show GFP expression upon AAV2-GFP transduction. In particular, two cells with big somata (arrows) are strongly immunoreactive for GFP. In the CaBP-staining (Figure 3.3.4 B), these two cells (arrows) are also visible, resulting in a yellow appearance in the overlay (Figure 3.3.4 C). The statistical analysis from independent cultures yielded a transduction rate of 100% (55/55) for CaBP-positive cells. AAV2 seems to be quite efficient to target large retinal neurons with CaBP-IR, most likely horizontal cells.

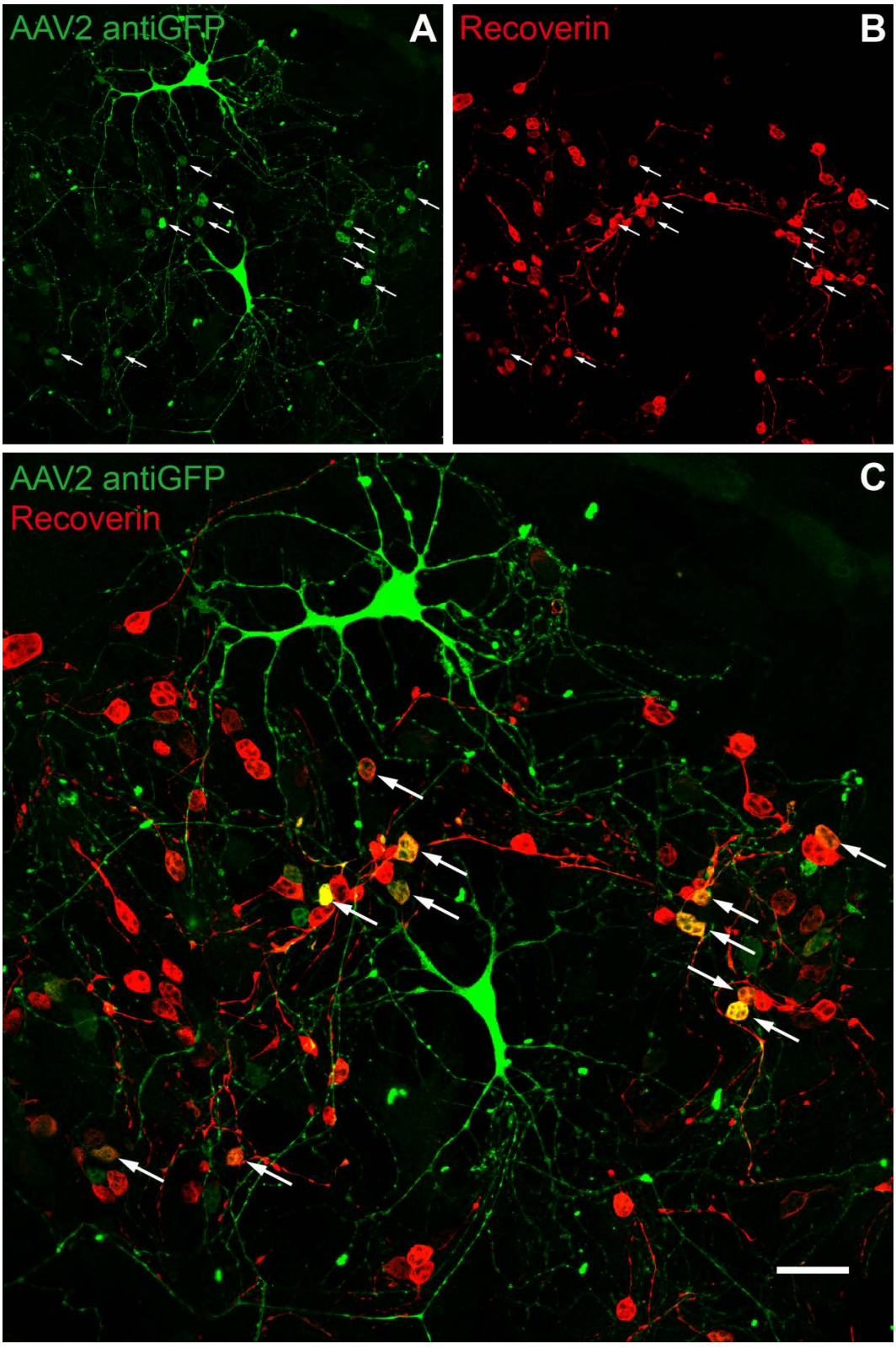

Figure 3.3.3: Identification of photoreceptors in AAV2-GFP transduced cultures.
Dissociated retinal cultures transduced by AAV2-GFP were immunostained for GFP in green and for recoverin in red. Arrows indicate infected cells immunoreactive for recoverin.
Scale bar = 20 µm.

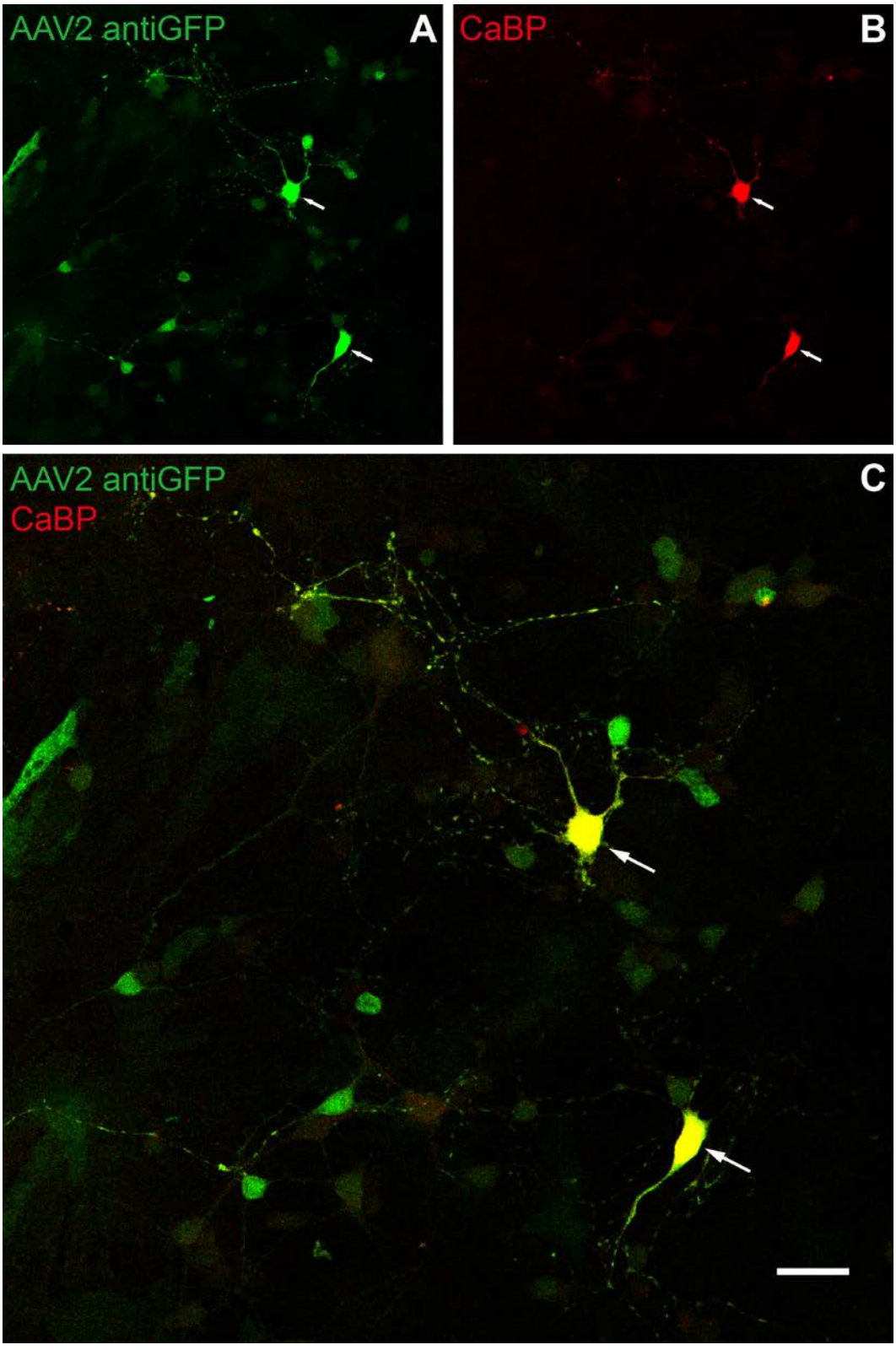

Figure 3.3.4: Identification of horizontal cells in AAV2-GFP transduced cultures.

Dissociated retinal cultures transduced by AAV2-GFP were immunostained for GFP in green and for CaBP in red to identify horizontal cells. Arrows indicate infected cells immunoreactive for CaBP.

Scale bar = 20 µm.

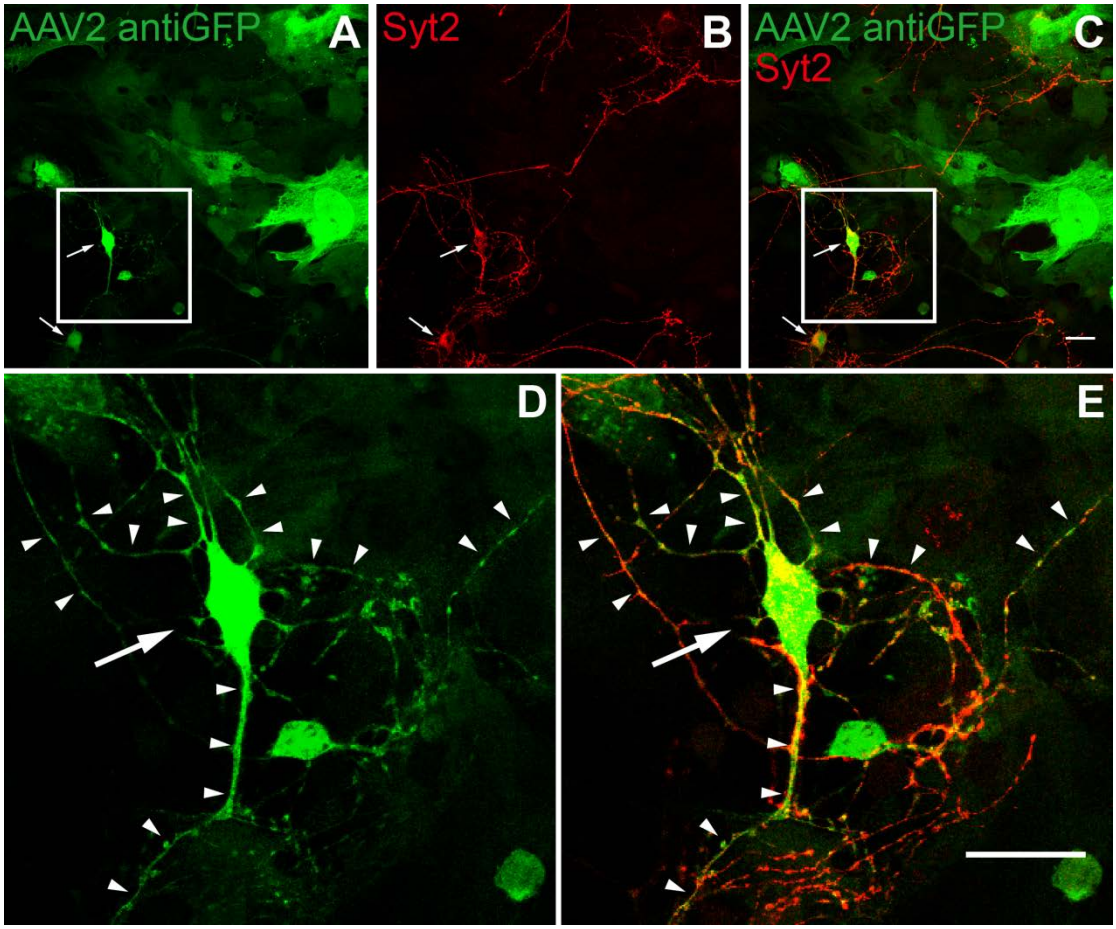

Figure 3.3.5: Identification of type 6 bipolar cells in AAV2-GFP transduced cultures.

Dissociated retinal cultures transduced by AAV2-GFP were immunostained for GFP in green and for Syt2 in red. Arrows indicate infected cells immunoreactive for Syt2. Two lower panels show higher magnifications of the marked area. Arrowheads indicate neurites of the cell.
Scale bar = 20 µm.

The type 6 bipolar cell marker Syt2 (red) and anti-GFP (green) were combined in the next staining. As seen in Figure 3.3.5 B, Syt2-IR was strong in the neurites of the cells and weak in their somata. However, somata (arrows) could be identified by carefully tracing the neurites. In this particular field of view, in addition to some neurons, very large and flat cells were observed in the GFP staining (Figure 3.3.5 A). Those large and flat cells are glia cells expressing GFP. Of the several GFP expressing neurons, two (arrows) were also found in the Syt2 staining. The marked area is shown at higher magnification in the lower images (Figure 3.3.5 D & E). It is clearly visible that the

processes (arrowheads) are immunoreactive for both antibodies. By counting the cells with Syt2-IR from several cultures, it was found that 98% (45/46) of Syt2-positive cells expressed GFP. The only Syt2-positive GFP-negative cell is shown in Figure 3.3.6 (arrow). No GFP expression was observed in soma or neurites.

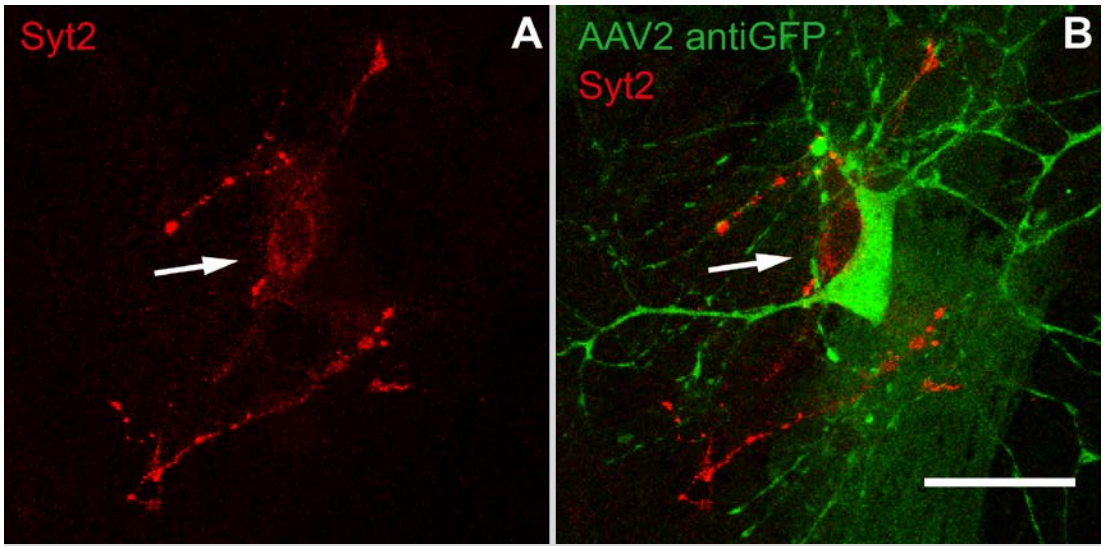

Figure 3.3.6: A Syt2-immunoreactive cell that did not express GFP upon AAV2 transduction.

Dissociated retinal cultures transduced by AAV2-GFP were immunostained for GFP in green and for Syt2 in red. Arrow indicates a Syt2-positive cell that is negative for GFP.
Scale bar = 20 µm.

The transduction efficiency was also determined for amacrine cells. Antibodies against GlyT1 were chosen for glycinergic amacrine cells (Figure 3.3.7, A: GFP in green, B: GlyT1 in red). Six cells were labeled for GlyT1-IR. Five of them (arrows) were positive for GFP, while one cell (arrowhead) was negative. The overlay (Figure 3.3.7 C) nicely presents five positive cells whose green somata are wrapped by a yellow ring. In total, about 80% (53/66 GlyT1-positive cells) expressed GFP. AAV2 is well suited to transduce glycinergic amacrine cells.

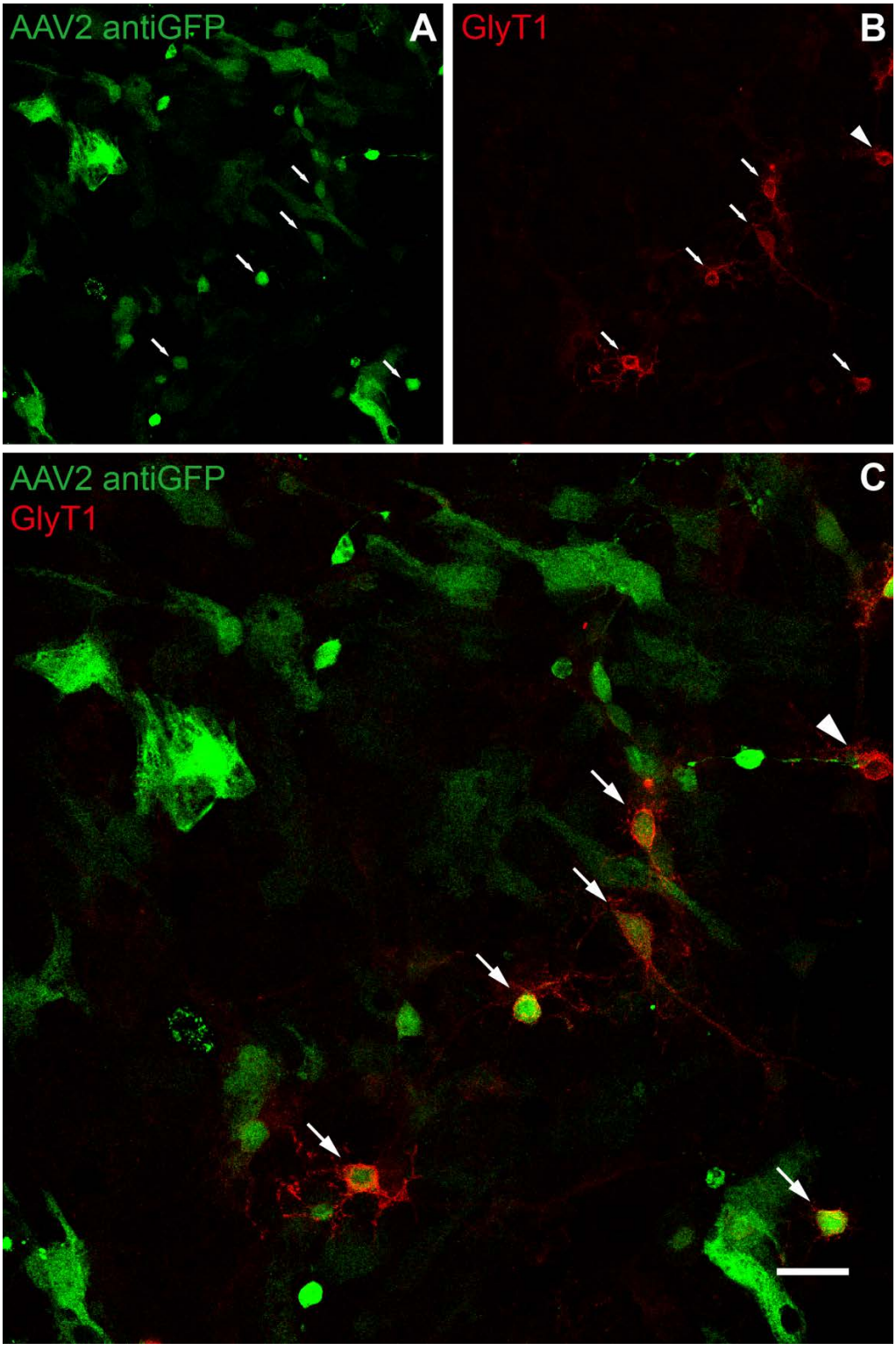

Figure 3.3.7: Identification of glycinergic amacrine cells among AAV2-GFP transduced cells.

Dissociated retinal cultures transduced by AAV2-GFP were immunostained for GFP in green and for GlyT1 in red. Arrows indicate infected cells immunoreactive for GlyT1. Arrowhead indicates a GlyT1-positive cell that is negative for GFP.

Scale bar = 20 µm.

GABAergic amacrine cells were labeled by antibodies against GAD67. GAD67-staining revealed four GABAergic cells in the image (Figure 3.3.8 B, red), which were immunoreactive in their cytosol and numerous neurites. Five neurons in the same field showed GFP-expression (Figure 3.3.8 A). Only two of them (arrows) were double labeled for GAD67, leading to a yellow appearance in the overlay (Figure 3.3.8 C). In total, 56 out of 72 GAD67-positive cells (nearly 80%), were transduced by AAV2.

The last cell type that was tested for GFP expression was the NOS-positive amacrine cell. Two examples are presented in Figure 3.3.9, where GFP-IR is in green and NOS-IR is in red. In panel A, one NOS-immunoreactive cell (arrow) was found to express GFP. In panel B, another NOS-immunoreactive cell (arrowhead) found in the same culture was negative for GFP-IR. Roughly 50% (14/29) of the NOS-positive cells were GFP-positive.

The transduction efficiency and specificity was determined for all AAV serotypes used in this study. Data are presented in Table 3.3.1. In this table, the first horizontal line lists the serotypes of AAVs, and the first vertical column lists the antibodies that were used for cell type identification. The transduction efficiency is given in total numbers and percentage values.

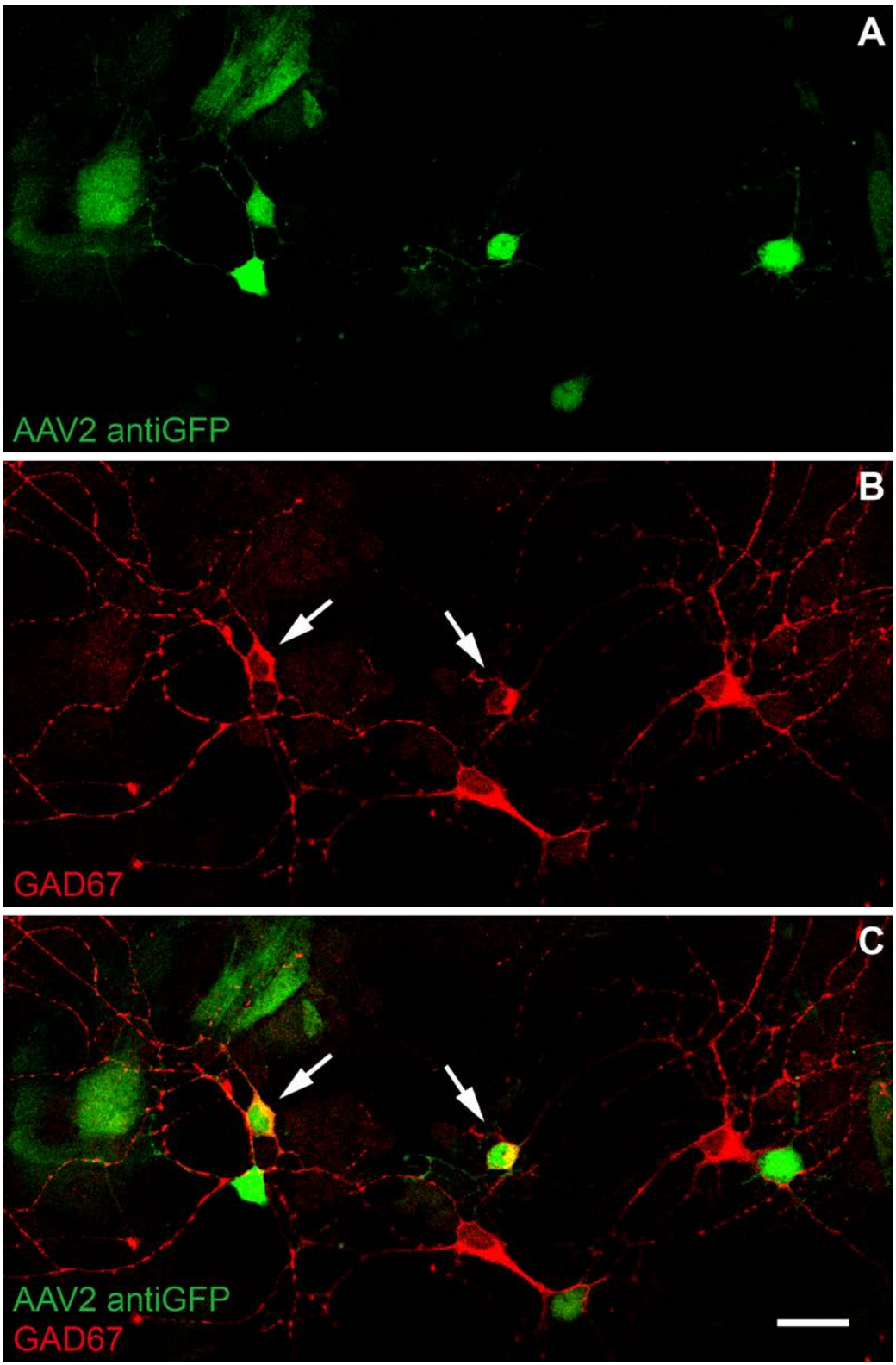

Figure 3.3.8: Identification of GABAergic amacrine cells in AAV2-GFP transduced cultures.

Dissociated retinal cultures transduced by AAV2-GFP were immunostained for GFP in green and for GAD67 in red. Arrows indicate infected cells immunoreactive for GAD67.
Scale bar = 20 µm.

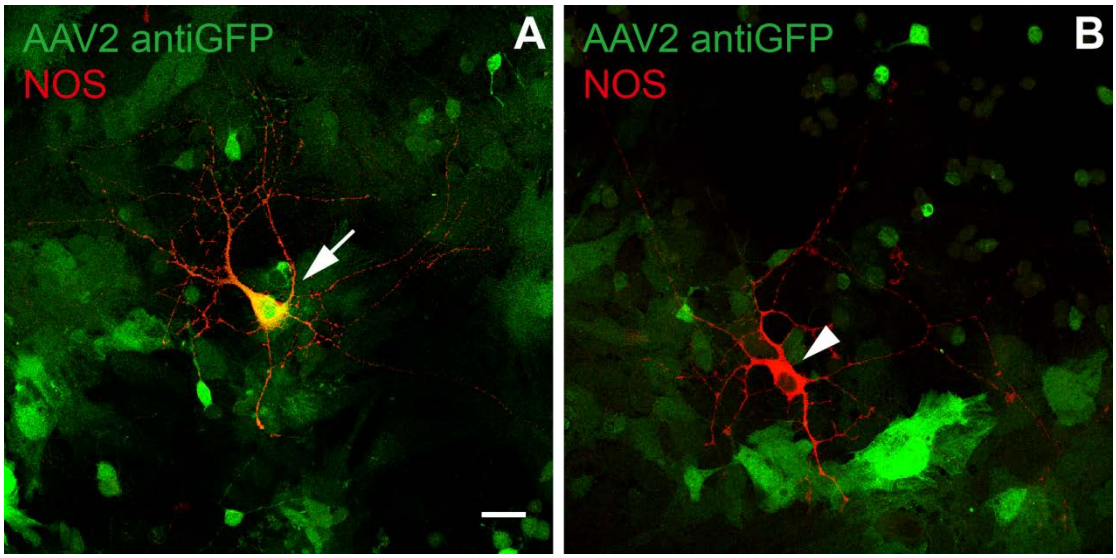

Figure 3.3.9: Identification of NOS amacrine cells in AAV2-GFP transduced cultures.

Dissociated retinal cultures transduced by AAV2-GFP were immunostained for GFP in green and for NOS in red. Arrow indicates an infected cell immunoreactive for NOS. Arrowhead indicates a NOS-positive cell that is negative for GFP.
Scale bar = 20 µm.

Generally speaking, AAV2 can be considered as the best choice for retinal transduction. It could infect all cell types of interest. The transduction rate reached around 100% for CaBP-immunoreactive cells and Syt2-immunoreactive cells, followed by about 80% for GlyT1- and GAD67-immunoreactive cells and nearly 50% for the NOS-immunoreactive cells. Although only 10% of the recoverin-immunoreactive cells were transduced by AAV2, this rate is the highest rate compared with the other serotypes. AAV6 was also able to infect all cell types of interest. However, the transduction efficiency was on average lower than for AAV2. While transduction efficiency was still above 90% for CaBP-immunoreactive and Syt2-immunoreactive cells, it considerably decreased for GlyT1-immunoreactive cells, GAD67-immunoreactive cells and NOS-immunoreactive cells. AAV1 infected horizontal cells well and showed some selectivity for glycinergic cells rather than GABAergic cells. AAV4 seemed to infect mainly recoverin-immunoreactive cells and few Syt2-immunoreactive cells. Both AAV8 and AAV9 did not target photoreceptors.

But AAV8 overall had a higher transduction efficiency than AAV9. Except for AAV2, the remaining serotypes all had zero or very low transduction efficiency for NOS-positive cells.

Table 3.3.1: Transduction efficiency of AAV serotypes in dissociated retinal cultures.

	AAV1		AAV2		AAV4		AAV6		AAV8		AAV9	
Recoverin	11/207	5%	16/156	10%	7/86	8%	8/121	6%	0/56	0%	0/135	0%
CaBP	34/35	97%	55/55	100%	0/56	0%	48/50	96%	47/58	81%	25/55	45%
Syt2	22/32	69%	45/46	98%	3/51	6%	59/63	94%	48/85	56%	31/65	48%
GlyT1	24/78	30%	53/66	80%	0/77	0%	31/70	44%	11/63	17%	9/88	10%
GAD67	0/72	0%	56/72	78%	0/65	0%	24/70	34%	25/70	36%	13/70	19%
NOS	0/30	0%-	14/29	48%	0/36	0%	3/38	8%	0/39	0%	2/43	5%

As a conclusion, AAV2 was able to not only infect many types of cells but also successfully transduce each cell type at a high rate. Thus, AAV2 was chosen to express Cygnet-2.1 in retinal neurons.

3.3.2 AAV transduction in organotypic retinal whole-mount cultures

Retinal whole-mount cultures are closer to the native tissue than dissociated cultures. Therefore, the transduction efficiency of AAVs was also characterized in whole-mount cultures. As the morphology of retinal cell types is well preserved in whole-mount cultures, the specificity of the transduction could be further verified.

AAVs encoding GFP were applied immediately after explanting the whole-mounts onto the membrane. In the first set of experiments with the cultures being in wells with culturing medium, AAVs were added directly on top of the cultures. After 8 days in culture, no GFP expression was detectable (data not shown). In the second set of experiments, whole-mount cultures were covered with a drop of AAV solution and were incubated for 15 ~ 20 minutes in a sterile environment at 37°C and 100% humidity. After that, cultures were transferred to wells containing culturing medium.

This procedure strongly increased the transduction efficiency. After about 4 days in culture, first evidence for GFP expression was detected. On the 8th day of cultivation, whole-mounts were fixed and sectioned vertically for further immunocytochemical investigations.

In general, the transduction efficiency in the whole-mount cultures was more heterogeneous than in dissociated cultures. Even within one whole-mount, GFP expression could be strong in one part, but much lower in other parts of the retina. Moreover, in stark contrast to the results obtained in dissociated retinal cultures, irrespective of the AAV serotype (AAV1, AAV2, AAV4, AAV6, AAV8, and AAV9) used, predominantly Müller cells were transduced. Figure 3.3.10 shows two examples of whole-mount cultures transduced by AAV2-GFP. Both in the folded culture (panel A) and flattened culture (panel B), cells expressing GFP were observed with the same morphology. Their somata (arrows) were always in the INL and only two thick processes protruded from the soma towards different directions: one (white arrowheads) towards the outer limiting membrane and another (yellow arrowheads) towards the inner limiting membrane. Often along these processes, some small spikes could be recognized. These cells own the very typical morphology of Müller cells. In the retina glutamine synthetase (GS) is exclusively expressed in Müller cells (Linser et al., 1984; Derouiche and Rauen, 1995). Counterstainings for GS-immunoreactivity (GS-IR, red) are shown in the overlay panels C & D. Most GFP-expressing cells appear in yellow due to co-staining with both antibodies. In the right-most cell in the folded culture (A) GS-IR is less clear. The antibody against GS exhibits low penetration. As the cell resides deep in the tissue, it is barely stained for GS. Nevertheless, according to its unique morphology, it can still be identified as Müller cell. Besides Müller cells, a very small number of photoreceptors and horizontal cells were also found that expressed GFP in both types of cultures (data not shown).

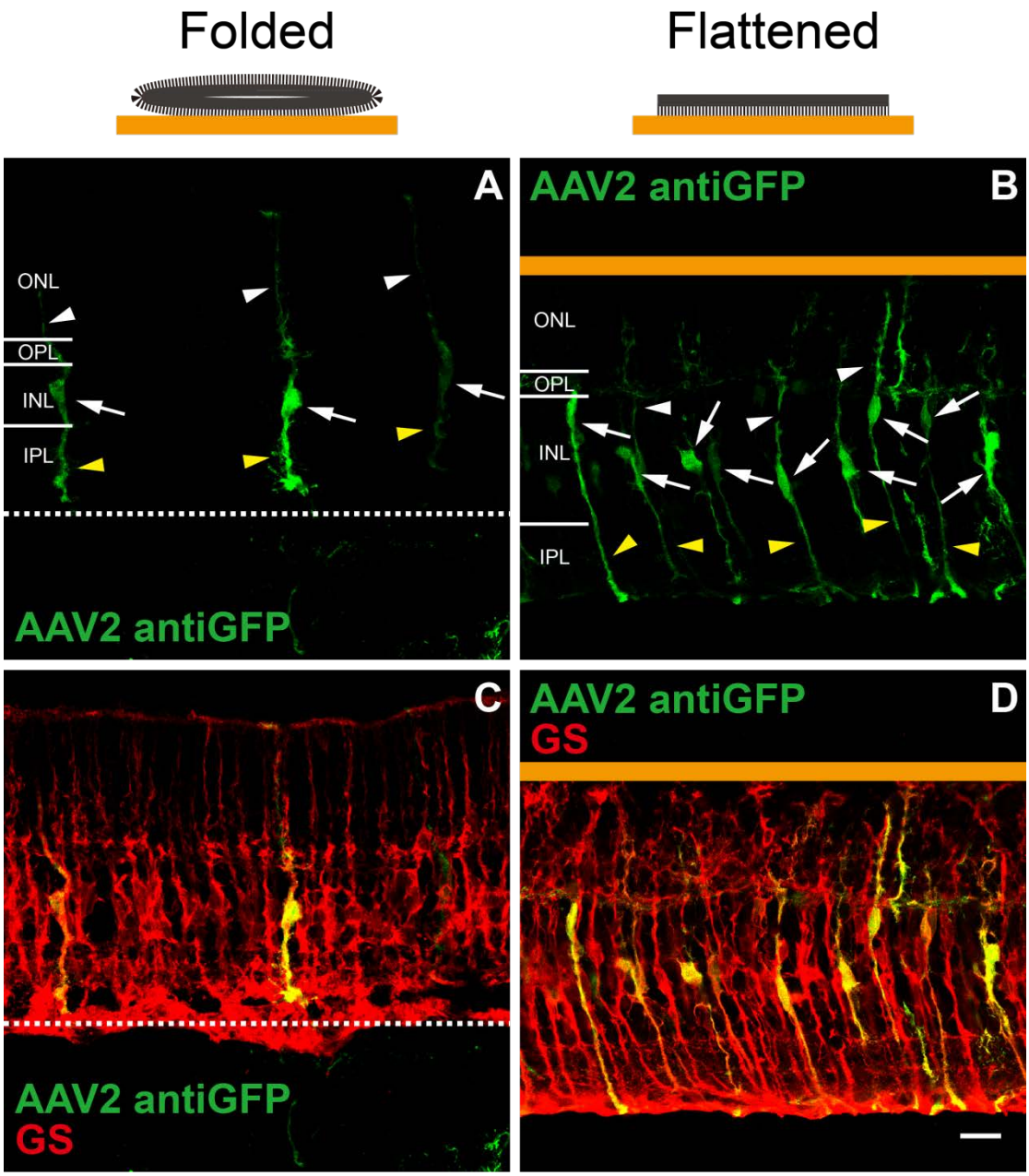

Figure 3.3.10: GFP expression in whole-mount retinal cultures upon AAV2-GFP transduction.

Vertical sections of whole-mount retinal cultures transduced by AAV2-GFP were immunostained for GFP in green and for GS in red. A & C are from a folded culture, B & D from a flattened culture. The dotted lines divide the upper and lower parts of the folded culture. The orange bars represent the culturing membrane in the flattened culture. Arrows indicate the somata of AAV2-GFP transduced Müller cells. White arrowheads indicate the outward projections and yellow arrowheads indicate the inward projections.

Scale bar = 20 µm.

Why is the transduction pattern of whole-mount cultures so different from that of dissociated cultures? In dissociated cultures, every cell is exposed to the medium and, thus, is accessible to the AAVs. In whole-mount cultures, most cells of interest are embedded within the tissue resulting in low accessibility. Müller cells extend their processes to the borders of the retina where they form large endfeet. Therefore, in both flattened and folded cultures Müller cells provide an accessible target for AAVs. This may explain why predominantly Müller cells were transduced in whole-mount cultures. However, the number of transduced Müller cells seemed higher in flattened cultures than in folded cultures.

Conclusion for AAV-mediated transduction *in vitro*

AAVs were found suitable to deliver foreign genes into retinal cells *in vitro*. Different AAV serotypes showed different specificity in the transduction of cell types in dissociated retinal cultures. AAV2 was able to infect many types of cells with high transduction efficiency. In whole-mount cultures the AAV serotypes tested (AAV1, AAV2, AAV4, AAV6, AAV8, and AAV9) did not show the same specificity as in dissociated retinal cultures but transduced predominantly Müller cells.

3.4 AAV-mediated transduction *in vivo*

3.4.1 Expression of GFP in the retina using AAV-mediated transduction *in vivo*

This section describes the results obtained when AAVs encoding GFP were delivered via ocular injection to infect retinal cells *in vivo*. Injections were performed on mice of the postnatal stage P5. Only one eye of each mouse was injected. The other eye served as control. After the eye had been exposed, a small opening was made and a thin needle was inserted into the eye. Once the needle reached the bottom of the eye ball, it was pulled back a little bit. A precise volume of 0.5 µl virus suspension was injected. As there is no clear vision through the optics of the eye at this developmental

stage, it could not be determined whether the injection was subretinal or intravitreal. But in this manner the viruses were injected as closest to the retina as possible. After 5 weeks or longer, injected mice were sacrificed and their retinae were isolated for immunohistochemical analysis. In this part, a total of 23 retinae were studied: 5 for AAV1-GFP, 4 for AAV2-GFP, 3 for AAV4-GFP, 3 for AAV6-GFP, 4 for AAV8-GFP, and 4 for AAV9-GFP.

Figure 3.4.1 displays an overview of the transduction efficiency of the different AAV serotypes *in vivo*. All microphotographs in this figure were captured by detecting the endogenous fluorescence of GFP. In general, all tested AAV serotypes were able to transduce retinal cells *in vivo*. Again, AAV2-GFP showed the highest transduction efficiency. However, in all transduced retinae at several sites discrete disturbances of the retinal layering were observed. These disturbed structures might be due to mechanical damage during the injection and occured independent of the AAV serotype used. Moreover, higher GFP expression was mostly found in such disturbed regions. Probably, the mechanical damage made these regions more accessible to the viruses. Nevertheless, in retinae transduced by AAV2-GFP, AAV8-GFP, and AAV9-GFP, GFP expression was also observed within well-preserved regions. In the following, the transduction pattern of each AAV serotype will be discussed in detail.

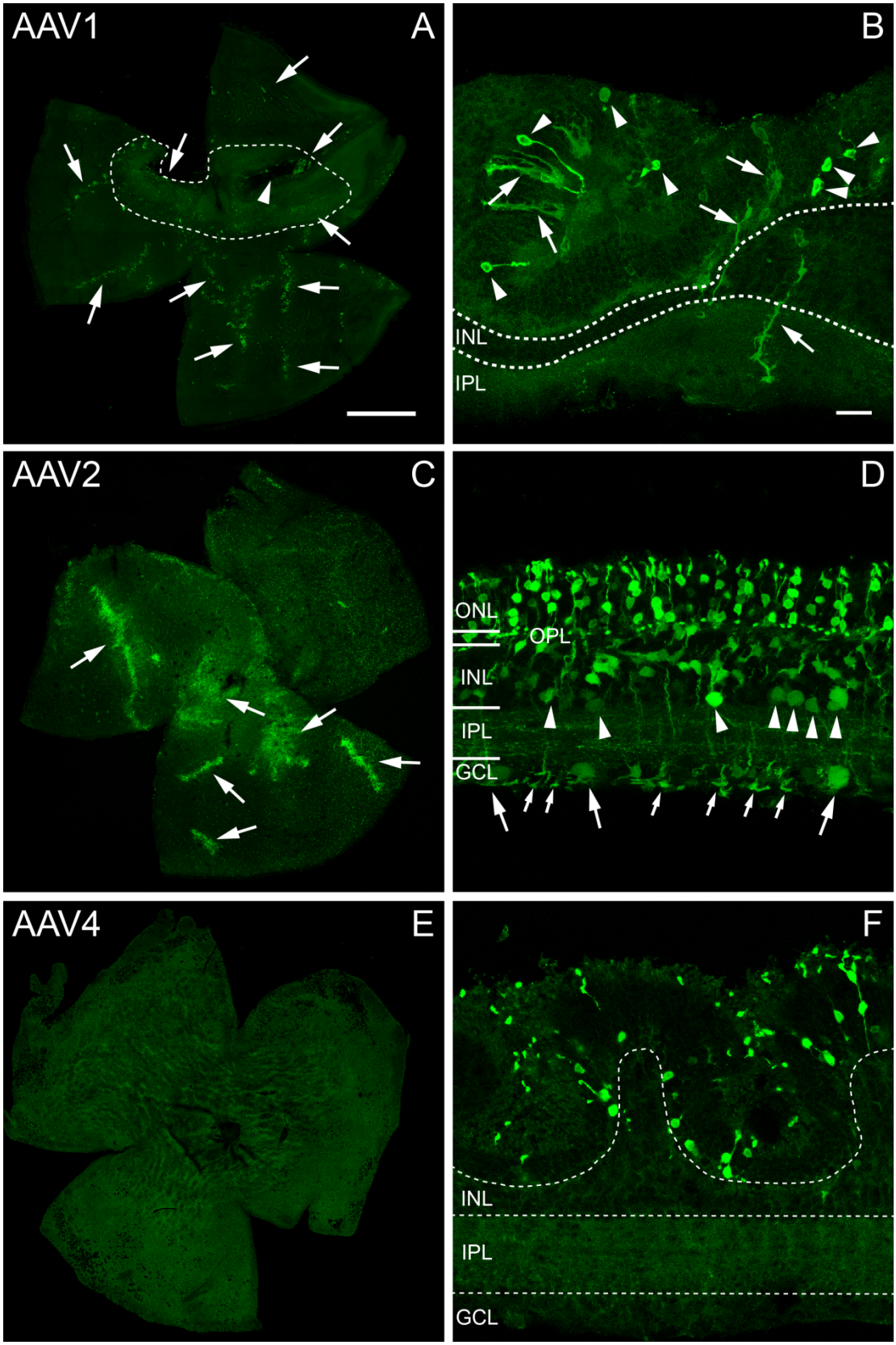

Figure 3.4.1: GFP expression in the retina upon AAV transduction in vivo.

Retinae were transduced in vivo by AAV1-GFP (A & B), AAV2-GFP (C & D), AAV4-GFP (E & F), AAV6-GFP (G & H), AAV8-GFP (I & J), and AAV9-GFP (K & L). Whole-mounted retinae are shown in A, C, E, G, I & K. Vertical sections are shown in B, D, F, H, J & L.

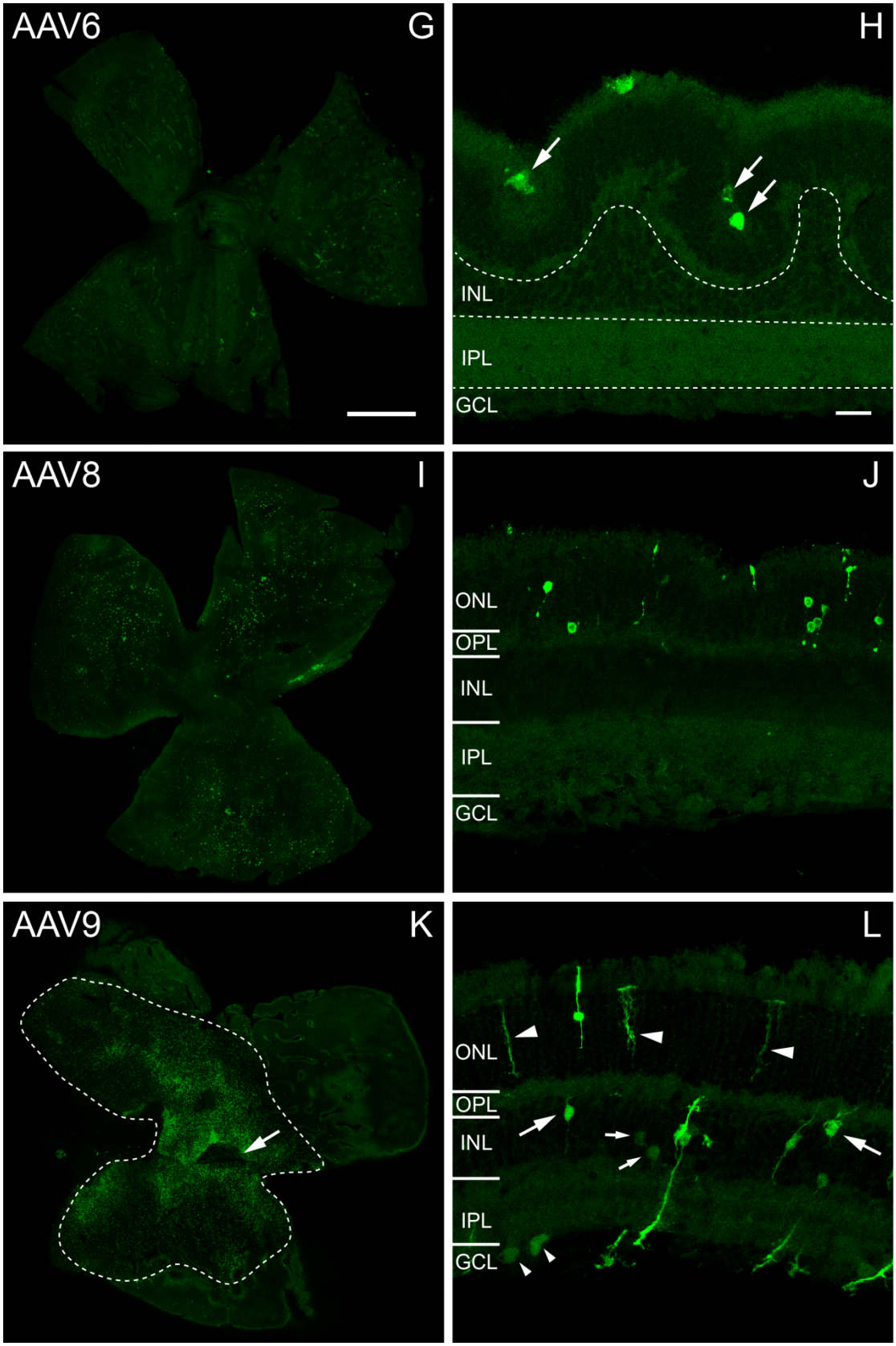

The green fluorescence represents endogenous GFP fluorescence. A, dotted line marks the region of high transduction efficiency; arrowhead indicates the injection site; arrows indicate sites of strong GFP expression. In B, dotted lines indicate retinal layering; arrowheads mark infected

photoreceptors; arrows indicate infected Müller cell processes. In C, arrows indicate strong GFP-expression. In D, arrowheads indicate infected amacrine cells in the INL; big arrows indicate infected neurons in the GCL; small arrows indicate infected Müller cell endfeet. In F, the dotted lines mark the retinal layering. In H, the dotted lines mark the retinal layering; arrows indicate infected cells, presumably RPE cells. In K, the dotted line marks the region of GFP expression; arrow indicates the injection hole. In L, big arrowheads indicate processes of infected Müller cells; big arrows indicate infected bipolar cells in the INL; small arrows indicate infected amacrine cells in the INL; small arrowheads indicate infected neurons in the GCL.
Scale bar = 1 mm in A, C, E, G, I & K.
Scale bar = 20 μm B, D, F, H, J & L.

AAV1-GFP transduction is shown in a retinal whole-mount preparation in Figure 3.4.1 A. Strong green fluorescence was observed at several discrete areas (arrows). A hole in the retina is marked by the arrowhead. It might be the result from the needle damaging the retina during the injection. Around the hole (marked by the dotted line), the number of GFP-positive cells was higher than in other regions, probably due to the short diffusion distance for viral particles from the injection site. Vertical sections of retinae transduced by AAV1-GFP, however, revealed that in regions with high GFP expression the retinal layering was strongly disturbed. An example is shown in B. The retina was folded and it was difficult to identify layers unequivocally. Most labeled cells display thick processes with small spikes (arrows), typical for Müller cells. Few infected small cells were found in the outer retina (arrowheads) - probably photoreceptors. In well-preserved regions, no GFP expression was observed or, occasionally, few photoreceptors displayed green fluorescence (data not shown).

Figure 3.4.1 C & D show retinae that were transduced by AAV2-GFP. GFP expression was high almost throughout the entire retina (C). At several sites (arrows) GFP expression level was particularly high. Similar to data shown in B, in these regions the retinal structure was damaged (data not shown). In the remaining parts of the tissue not only the retinal structure was better preserved, but also a decent number of cells expressing GFP was observed. The vertical section in D was obtained from a better preserved part of an AAV2-GFP infected retina. The retinal layering was intact. However, the thickness of the ONL was reduced compared to a normal retina,

indicating that a pronounced number of photoreceptors had degenerated. The inner retina did not exhibit signs of degeneration. In all layers, many cells were found to express GFP. Besides many photoreceptors in the ONL and several neurons (big arrows) in the GCL, also a substantial number of GFP-positive cells were found in the INL. The cells close to the IPL were easily identified as amacrine cells (arrowheads). The remaining positive cells in the INL were more difficult to identify. Big end feet in the GCL (small arrows) indicated that Müller cells had been infected. The question whether bipolar cells were transduced will be analyzed using counterstainings in the next chapter.

For AAV4-GFP the overall expression level of GFP was low (Figure 3.4.1 E). When analyzing vertical sections of AAV4-GFP transduced retinae, all cells expressing GFP were located in the outer part of the retina and were identified as photoreceptors due to their small somata. GFP expression was mostly observed in disordered regions. In the example shown in F, the entire outer part of the retina and the INL were folded like a wave. Although the IPL and the GCL were preserved, there was no GFP expression at all in the inner retina.

Figure 3.4.1 G shows a whole-mounted retina infected by AAV6-GFP. In dissociated retinal cultures, the transduction efficiency of AAV6-GFP was rather high. In contrast, *in vivo* the transduction efficiency was found extremely low in all injections. Spot-like weak green fluorescence was observed. When looking at the vertical section shown in H, the cells expressing GFP were located at the outer limiting border of the retina. Sometimes, GFP-positive cells (arrows) were embedded in the trough of the wave-like structures formed by the folded outer layers. Their large somata and the fact that no processes were observed could suggest that they were cells of the retinal pigment epithelium (RPE) sticking to the tissue when the retina was isolated from the eye cup. Unfortunately, within the proper retina no sign of GFP expression was detected.

In Figure 3.4.1 I, a number of cells were observed to express GFP in the

whole-mounted retina transduced by AAV8-GFP. However, the density of GFP-positive cells was lower than in retinae transduced by AAV1 and AAV2; and there was no region with particularly higher transduction efficiency. Photoreceptors were the main targets for AAV8. As is shown in Figure 3.4.1 J, in a well-preserved region GFP expression was found in photoreceptors in the ONL, similar to the AAV4-GFP transduced retina. In disturbed regions, nevertheless, very rarely Müller cells, amacrine cells, displaced amacrine cells and ganglion cells were also found to express GFP (data not shown).

AAV9 also showed high transduction efficiency in the mouse retina *in vivo.* The typical infection pattern is presented in one whole-mount (Figure 3.4.1 K). A great number of cells were found with strong GFP expression in a large area of the retina (marked by the dotted line). An arrow indicates a hole where the viruses were injected. The GFP expression was high near the hole and gradually dropped towards the periphery. When studying vertical sections of AAV9-GFP transduced retinae, very strong GFP expression was mostly found in damaged parts of each retina (data not shown), like in Figure 3.4.1 B & F. However, the well preserved parts also showed a good transduction pattern. One vertical section is shown in Figure 3.4.1 L. In the ONL, a very limited number of photoreceptors were infected. Some bipolar cells (big arrows) and amacrine cells (small arrows) in the INL and some displaced amacrine cells (small arrowheads) in the GCL were found to express GFP. Besides, Müller cells also expressed GFP. Their typical thick processes are indicated by big arrowheads.

Comparing the transduction efficiency of the different AAV serotypes *in vivo*, AAV2 was again the most promising serotype due to its high efficiency. In particular, many cells in the INL were targeted by AAV2. In the following part, AAV2-GFP infected neurons in the INL will be further analyzed to find out if they are also involved in the NO-cGMP pathway.

3.4.2 AAV2 targeted neurons in the INL involved in NO-cGMP pathway.

The key enzyme involved in the NO-cGMP pathway is the soluble guanylate cyclase (sGC). Expression of Cygnet-2.1 in these cells is of particular interest to study the NO-stimulated synthesis of cGMP. Ding and Weinberg studied the distribution of sGC in rat retina using a polyclonal antibody raised against the β1 subunit of sGC (Ding and Weinberg, 2007). Here, I employed this antibody to determine whether sGC-immunoreactive cells were targeted by AAV2.

Figure 3.4.2 shows a vertical section of an AAV2-GFP transduced mouse retina that was labelled for sGC in red. The green signal represents endogenous GFP fluorescence. The inner retina is shown at higher magnification in B, D, and F. In A, many cells in the ONL and a few cells in the INL were observed with good GFP expression. In the sGC-staining (C & D), also many cells in the INL were found immunoreactive. In the overlay (E & F), two sGC-positive cells (arrows) also showed green fluorescence. They were identified as bipolar cells due to the position and shape of their somata and their dendrites directed towards the OPL. Their axon terminal systems could not be resolved. Another green bipolar cell (arrowhead) with clear axon was negative for sGC-IR. Its axon ended in the innermost layer of the IPL, suggesting that this cell was a rod bipolar cell.

PKCα-staining was performed on other sections from the same retina to identify rod bipolar cells. Quite a number of rod bipolar cells were found to be infected by AAV2. One example is shown in Figure 3.4.3. Four GFP-expressing cells (arrowheads) appeared immunoreactive for PKCα. Another cell with GFP fluorescence (arrow in A) was negative for PKCα. Based on the form of the soma and a weak endfoot staining in the GCL, this cell is most likely a Müller cell. By analyzing sections from retinae transduced *in vivo* by AAV2 (N = 4), rod bipolar cells and Müller cells represented a large fraction of GFP-expressing cells in the INL.

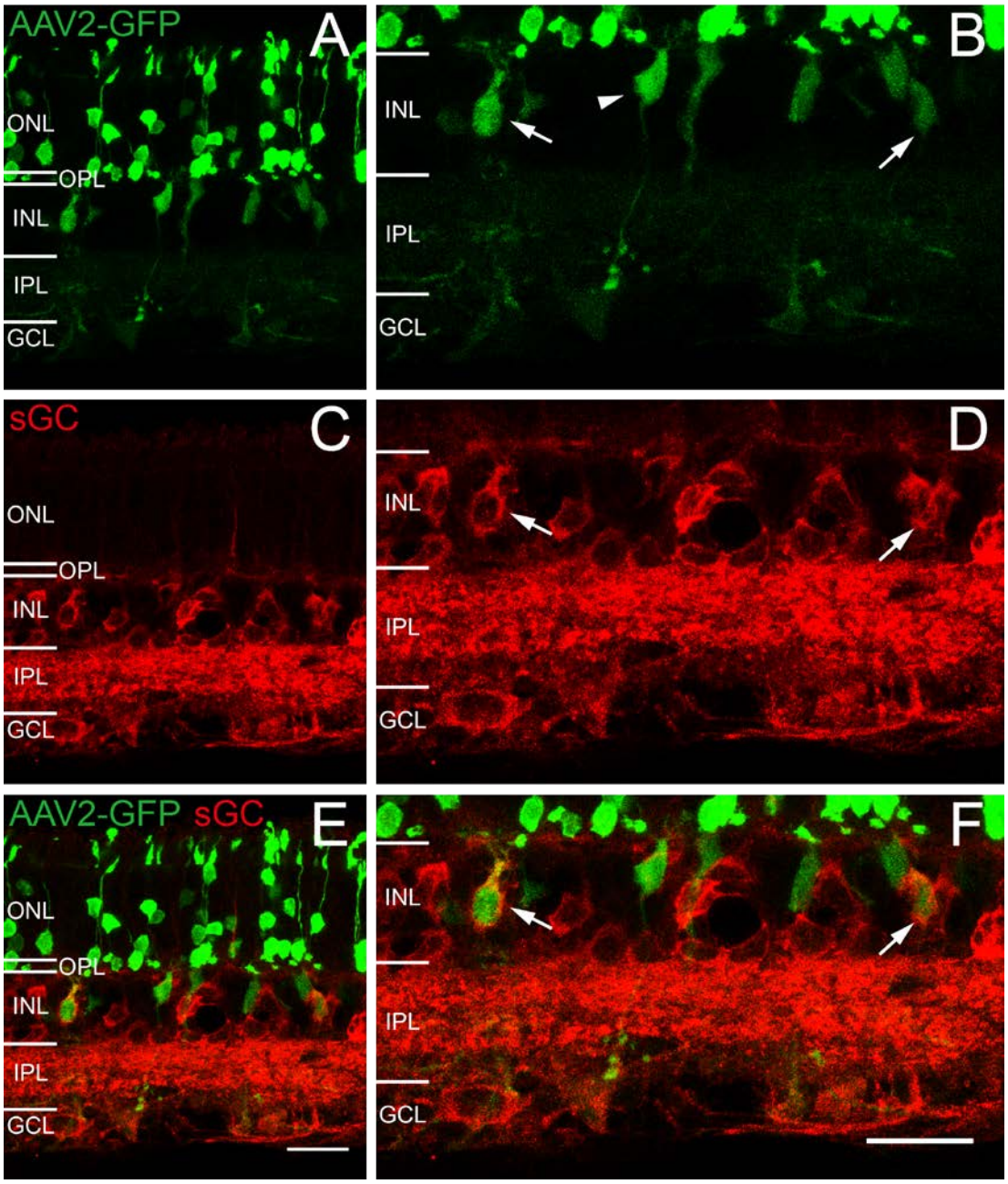

Figure 3.4.2: sGC-immunoreactive bipolar cells targeted by AAV2.

A vertical section of AAV2-GFP transduced retina was immunostained for sGC in red. Green label reflects endogenous GFP fluorescence. Higher magnification of the inner retina is shown in B, D & F. Arrows indicate two cells positive for GFP and sGC-IR. Arrowhead indicates a rod bipolar cell expressing GFP only.

Scale bar = 20 µm.

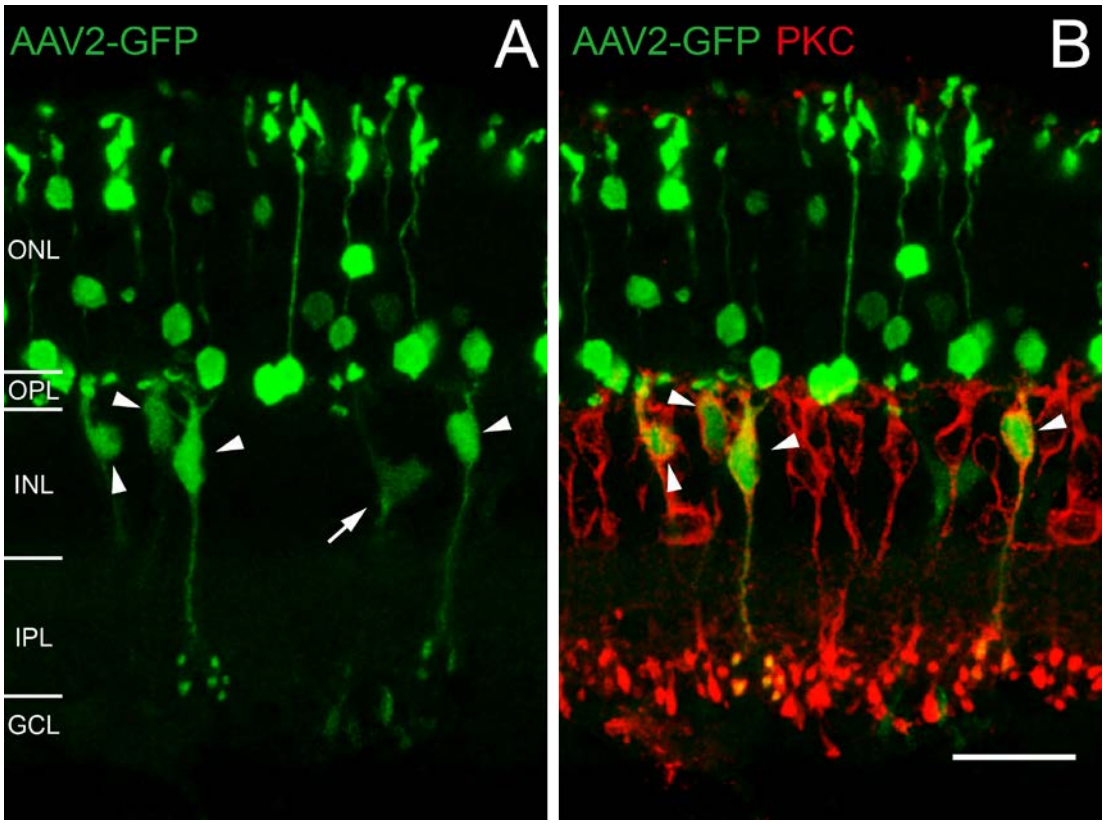

Figure 3.4.3: Rod bipolar cells infected by AAV2.
A vertical section of AAV2-GFP transduced retina was immunostained for PKCα in red. Green label represents endogenous GFP fluorescence. Arrowheads indicate several PKCα-positive rod bipolar cells expressing GFP. Arrow indicates one GFP-expressing Müller cell.
Scale bar = 20 μm.

It was not possible to systematically count and statistically classify all cell types in the inner retina that were infected by AAV2. Nevertheless, by using counterstainings with cell-type specific markers, I also found type 3a and type 5 bipolar cells that were infected by AAV2-GFP (data not shown). These two types of bipolar cells displayed cGMP-like IR upon stimulation with NO donors (Zhao, 2010).

Besides bipolar cells, sGC-immunoreactive amacrine cells were also found to become transduced by AAV2-GFP. Figure 3.4.4 A shows one sGC-positive amacrine cell (arrow) in the INL with GFP expression. In panel B, two displaced amacrine cells (arrows) in the GCL were found positive for both sGC and GFP.

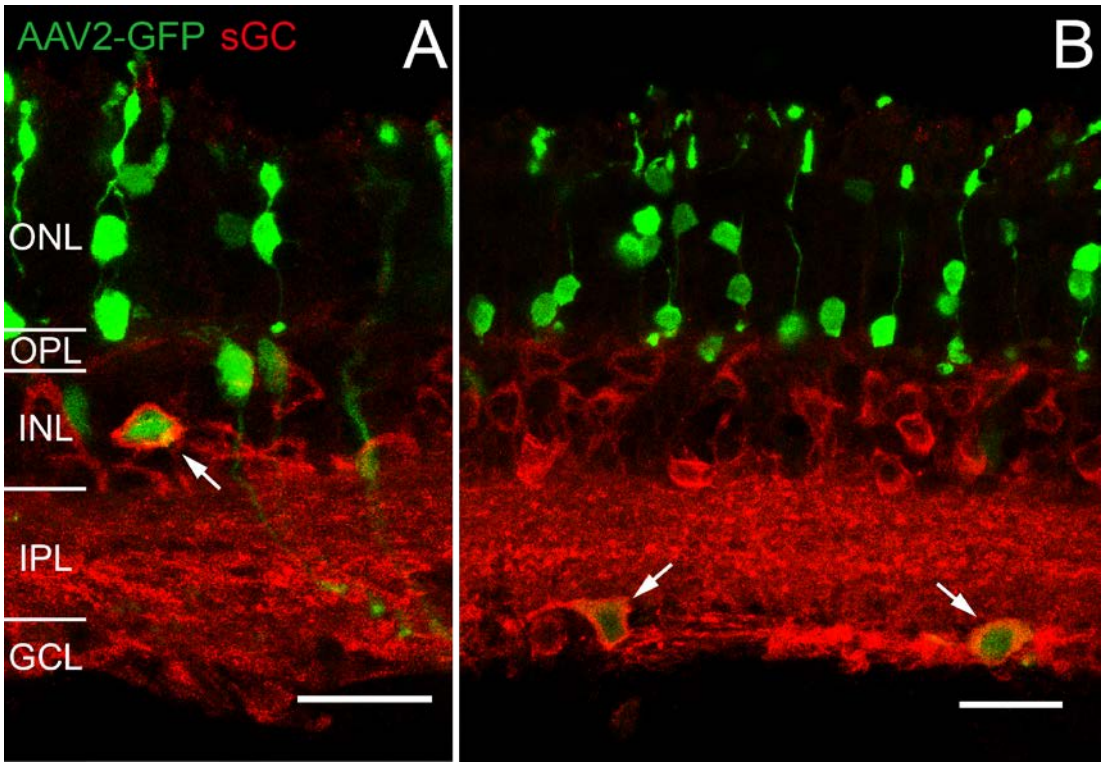

Figure 3.4.4: sGC-immunoreactive amacrine cells targeted by AAV2.
A vertical section of AAV2-GFP transduced retina was immunostained for GFP in green and sGC in red. Arrows indicate sGC-positive amacrine cells in A and sGC-positive displaced amacrine cells in B, which were infected by AAV2.
Scale bar = 20 µm.

Conclusion for AAV-mediated transduction *in vivo*

From all serotypes, AAV2-GFP displayed the highest transduction efficiency *in vivo* and targeted sGC-immunoreactive cells. Therefore, AAV2 was chosen as the vector to introduce the Cygnet-2.1 sensor into retinal neurons to investigate the NO-induced cGMP synthesis.

3.5 AAV2-mediated expression of Cygnet-2.1 in dissociated retinal cultures

3.5.1 Expression of the viral form of Cygnet-2.1 sensor

In order to produce AAVs encoding Cygnet-2.1, the original cDNA had to be modified and cloned into a viral vector. Prior to using this vector to generate viruses, the functionality of this Cygnet-2.1 variant expressed from the viral plasmid, termed vCygnet-2.1, had to be tested.

For this purpose, FlpTS GC-A cells were co-transfected with cDNAs encoding vCygnet-2.1 and PDE5a. Figure 3.5.1 A shows a screenshot from one of the imaging experiments, two transfected cells were recorded. Cygnet-2.1 sensors expressed from the viral plasmid were distributed in the cytosol, the same distribution pattern observed upon the expression from the original cDNA (Figure 3.1.3).

The functionality of the sensor was proven in the imaging experiments. In Figure 3.5.1 B, the signals of Cygnet-2.1 recorded from the two cells in Figure 3.5.1 A were plotted as the change in the ratio CFP/YFP ($\Delta R/R_0$) over time. Upon each of the three stimulations with ANP, a transient change was observed indicating a change in FRET efficiency. The maximum FRET change (14% ~ 19%) was similar to that recorded in previous experiments using the original cDNA (Chapter 3.1). As a conclusion, the sensors expressed from the modified DNA vCygnet-2.1 were fully functional.

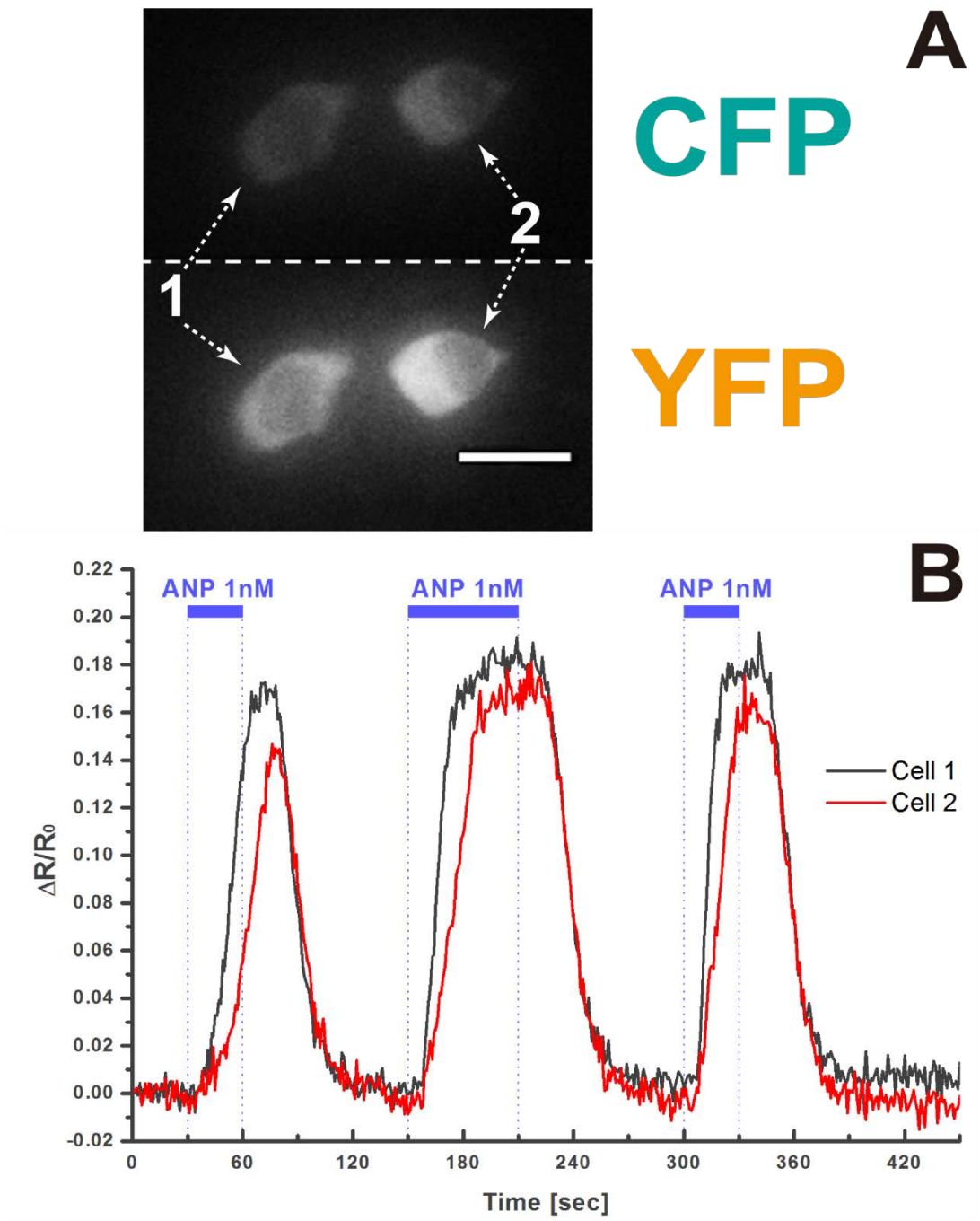

Figure 3.5.1: Functional sensors can be expressed from vCygnet-2.1 plasmid upon transfection.

A: Screenshot from an imaging experiment recording two FlpTS GC-A cells expressing sensors from the vCygnet-2.1 plasmid.

B: The FRET change of both cells was plotted over time. ANP (1nM) was applied during seconds 30 to 60, 150 to 210, and 300 to 330, respectively. In each case, both cells showed rapid FRET changes after both onset and offset of ANP, indicating transient elevation of the intracellular cGMP concentration upon application of ANP.

Scale bar = 20 µm.

3.5.2 cGMP-imaging of dissociated retinal cultures using Cygnet-2.1

Before I used Cygnet-2.1 in the dissociated retinal cell culture, I tested whether the synthesis of cGMP in retinal neurons could be stimulated by incubation with NO donors. An antibody against cGMP was used to detect cGMP-IR (Zhao, 2010). Cultures were incubated either with the NO donors SNP (1 mM) or SNAP (100 μM) in Ames' medium or with Ames' mdium alone for 10 minutes and fixed immediately. After fixation, cultures were immunostained for cGMP and sGC. Nuclei were stained with TO-PRO3. The immunocytochemical results are shown in Figure 3.5.2. The cells (arrows and arrowheads) that were immunoreactive for sGC comprised about 15% of the total population of cultured cells. After incubation with the NO donors SNP (A-C) and SNAP (D-F), cGMP-IR was found in nearly all sGC-positive cells (marked by arrows). Only few sGC-positive cells (arrowheads) were negative for cGMP-IR. Hence, cGMP-IR and sGC-IR matched very well. When cultures were incubated without NO donor (G-I), sGC-positive cells (arrowheads) showed no cGMP-IR. However, some small cells that were negative for sGC displayed cGMP-IR. Based on the soma size and appearance, these cells resembled photoreceptors. Photoreceptors express membrane bound pGCs that cannot be activated by NO. Double-stainings for cGMP and recoverin did not yield a perfect match between cGMP-IR and recoverin-IR (data not shown).

In summary, the immunocytochemical approach proved that the intracellular cGMP concentration in cultured sGC-positive retinal cells can be greatly increased upon NO stimulation.

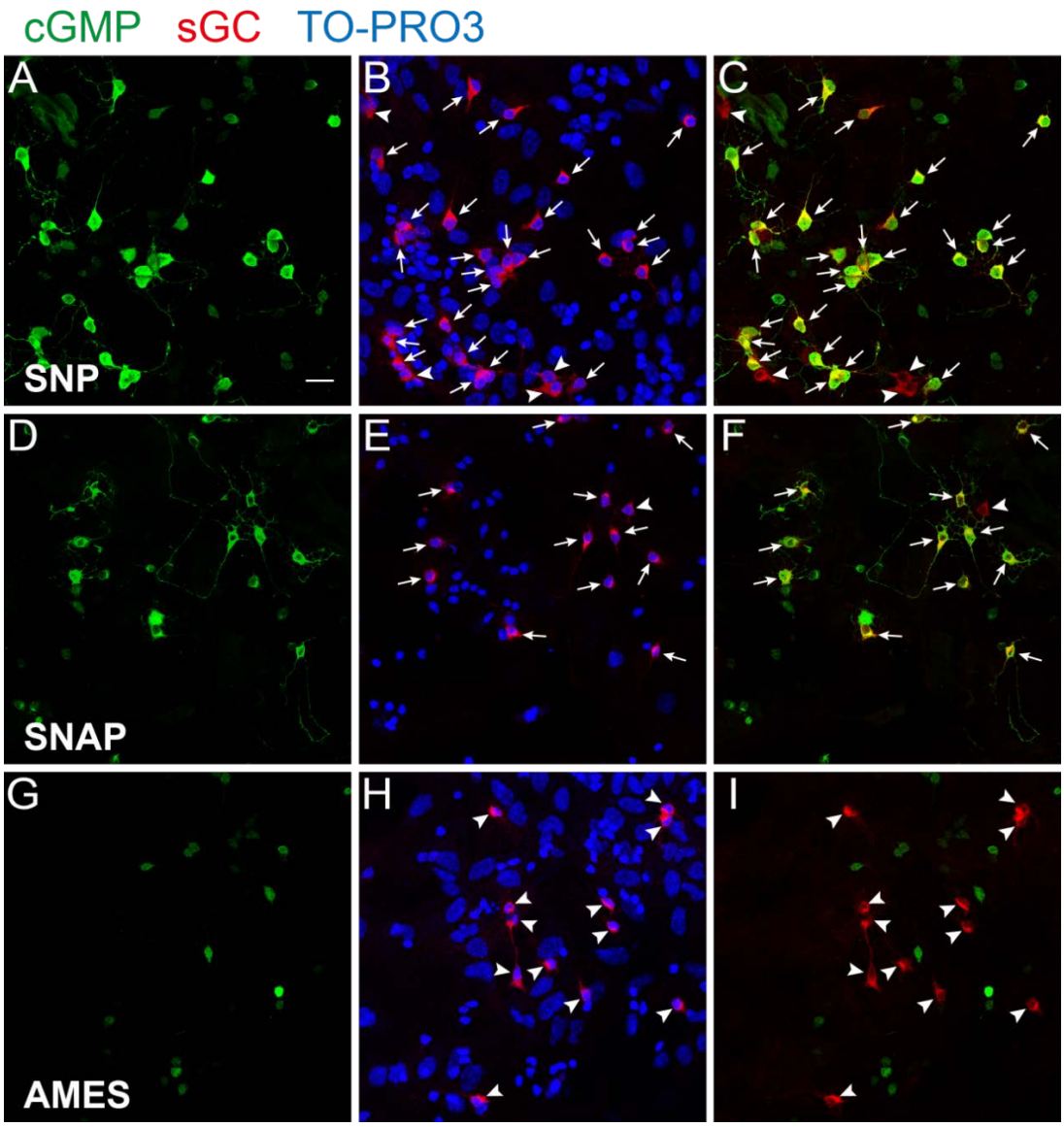

Figure 3.5.2: Stimulation with NO increased cGMP-IR in sGC-positive cells in dissociated retinal cultures.

A-C, Cultures incubated with 1 mM SNP; D-F, cultures incubated with 100 µM SNAP; G-I, cultures incubated with Ames' mdium. All arrows indicate sGC-positive cells with cGMP-IR. All arrowheads indicate sGC-positive cells without cGMP-IR.

Scale bar = 20 µm.

In the following experiments, dissociated retinal cultures were transfected with vCygnet-2.1 using lipofectamine on the 2nd day of cultivation. After 24 hours of expression, cells were used for cGMP-imaging. Unfortunately, the transfection efficiency was extremely low. Only 2 to 5 cells per coverslip were found to express Cygnet-2.1. By imaging many cultures (N>20), I found some cells (n=16) that

expressed the Cygnet-2.1 sensors and responded to the stimulation with exogenous NO.

Figure 3.5.3 A displays a recording from one cell. A transient FRET change was recorded during the initial application of 100 μM SNAP. The CFP/YFP ratio increased fast by about 18% upon the onset of stimulation and decreased slowly upon washout. During the second stimulation, the NO donor and the PDE inhibitor IBMX were applied together for 1 minute. A similar fast increase in the ratio was recorded. The maximal FRET change was approximately 18%, similar to the previous peak. The FRET change could not be further increased by IBMX, suggesting that either stimulation with 100 μM SNAP already induced the maximal cGMP elevation in the cell or that the elevated cGMP concentration saturated the sensor. After the offset of the NO donor, IBMX was superfused continuously for another 1 minute. During this time, the signal barely decreased, indicating that degradation of cGMP was prevented by IBMX. Upon washout, the signal slowly recovered to baseline, which implicated the clearance of cGMP. The imaging results for the first time revealed the real-time dynamics of cGMP in retinal neurons.

After the imaging, the coverslip was fixed and stained immunocytochemically. The double-staining (Figure 3.5.3 B-D) showed that the imaged cell was immunoreactive for sGC.

NO is a radical and changes of the sensor signal observed in the presence of NO might be due to unspecific changes in the sensor properties induced by direct interaction of the sensor with NO. To rule this out, control experiments were performed in HEK-293 cells that have no sGC. Changes in the sensor signal in the presence of an NO donor would argue for unspecific effects of NO on the sensor protein. To this end, HEK-293 cells were transfected with the same DNA used in dissociated retinal cultures. Upon the expression of Cygnet-2.1, cells were imaged and stimulated with the same concentration of NO donor as in the retinal experiment. No FRET change was observed during stimulation (data not shown). These controls

indicate that the Cygnet-2.1 signals recorded in the retinal neuron shown in Figure 3.5.3 were not due to an unspecific interaction of Cygnet-2.1 with NO but represented an increase in the internal cGMP concentration upon stimulation of sGC by NO.

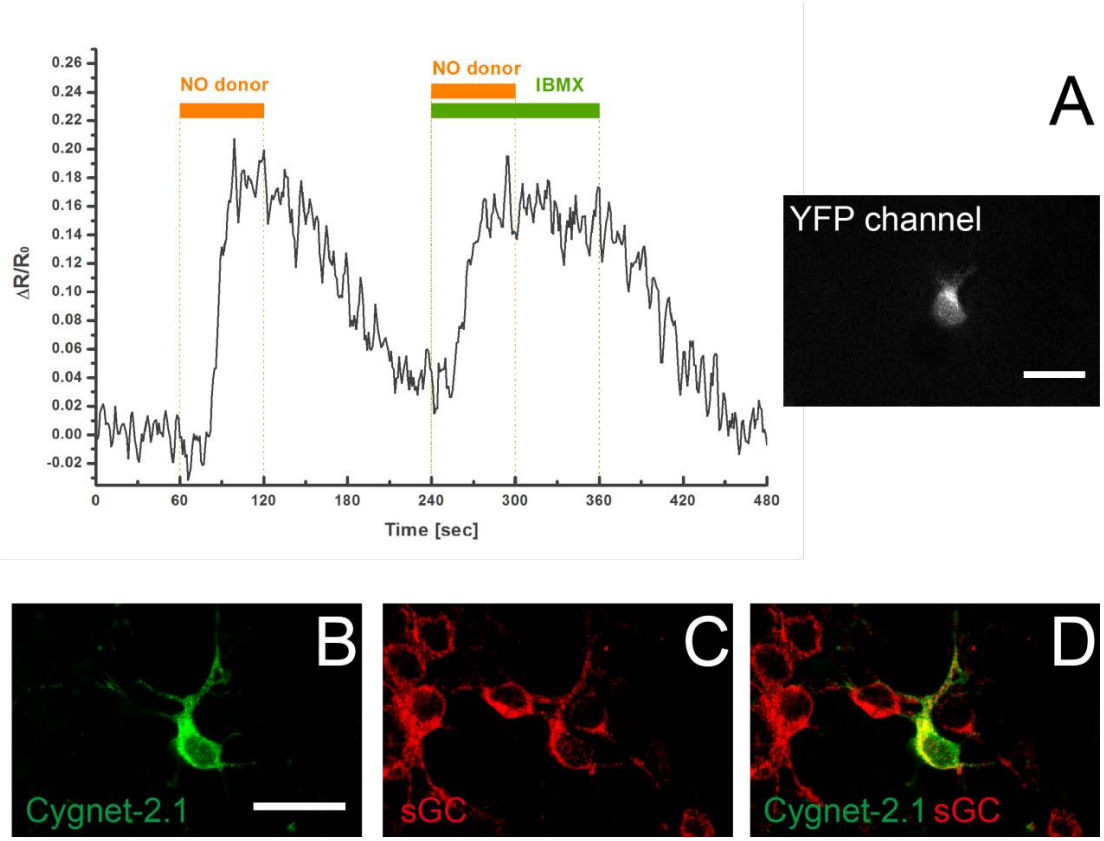

Figure 3.5.3: Real-time dynamics of intracellular cGMP monitored by transfected Cygnet-2.1 sensor in dissociated retinal culture.

A: The FRET change of a cultured retinal neuron transiently transfected with Cygnet-2.1 was plotted over time. The NO donor SNAP (100 µM) was applied twice from 60 to 120 seconds and from 240 to 300 seconds, respectively. The PDE inhibitor IBMX (100 µM) was applied during seconds 240 to 360. The cell showed two fast FRET changes during the application of NO and slow recovery upon wash out. During the second application, the amplitude of the signal was not further increased by the co-perfusion of IBMX, but the duration was prolonged by further IBMX application. The right image shows a screenshot of the YFP channel of the imaged cell.

B-D: The imaged cell in A was immunoreactive for sGC (red).

Scale bar = 20 µm.

3.5.3 Transduction with AAV2-Cygnet-2.1 leads to non-functional sensor

In the next set of experiments, AAV2 was used to express Cygnet-2.1 (AAV2-Cygnet-2.1) in retinal dissociated cultures. Following the protocol used for AAVs-GFP transduction, retinal dissociated cultures were incubated with AAV2-Cygnet-2.1 on the 2nd day of cultivation. After six days of expression, cultures were used for cGMP-imaging. All imaging conditions were identical to those used in previous imaging experiments (like Figure 3.5.3 in Chapter 3.5.2). Fluorescence of the sensor proteins could be detected. However, the fluorescence intensity was lower than in cells transfected with lipofectamine, while the number of transduced cells per coverslip (> 100 cells/coverslip) was higher that the number of transfected cells (2 ~ 5 cells/coverslip). A total of 76 recordings were performed on 25 independent cultures using the NO donor, SNAP. In none of the recorded cells a FRET change was observed upon stimulation with SNAP. Figure 3.5.4 A shows a recording of a AAV2-Cygnet-2.1 transduced cell. The signal was constant during the whole recording, irrespective of the stimulation with SNAP (100 μM). Another 6 recordings from 4 individual samples were performed with a different NO donor, SNP. Again, no responses to SNP were observed. Figure 3.5.4 B shows a recording with prolonged application of SNP (1 mM).

There are two possible explanations for the negative results: 1) AAV2-Cygnet-2.1 transduced cells in dissociated cultures did not contain sGC and, therefore, did not respond to NO; or 2) the sensors expressed upon transduction with AAV2-Cygnet-2.1 were not functional.

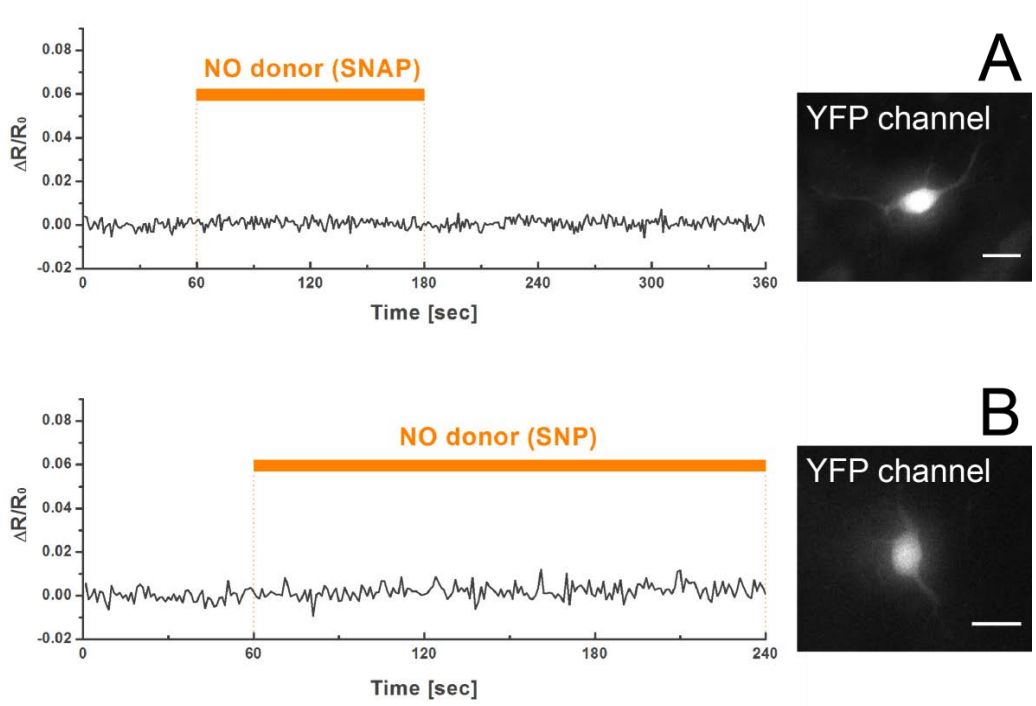

Figure 3.5.4: Cygnet-2.1 sensors seem non-functional in dissociated retinal cultures upon AAV2-Cygnet-2.1 transduction.

A: The sensor signal of a cultured retinal cell transduced with AAV2-Cygnet-2.1 was plotted over time. No signal change was recorded upon the stimulation with SNAP (100 µM).

B: The sensor signal of a cultured retinal cell transduced with AAV2-Cygnet-2.1 was plotted over time. No signal change was recorded upon the stimulation with SNP (1 mM).

Images in A and B show screenshots of the YFP channel for each cell.

Scale bar = 20 µm.

The first possibility could be tested by immunohistochemical detection of sGC in transduced neurons. Unfortunately, the number of cells showing fluorescence upon transduction with AAV2-Cygnet-2.1 was much higher than the number of fluorescent cells upon lipofectamine transfection. In addition, the fluorescence intensity in AAV2-Cygnet-2.1 transduced cells was much lower than that in the cells transfected with lipofectamine. Therefore, it was extremely difficult to identify the cells that had been imaged again after the immunocytochemistry. However, there are several clues supporting the assumption that the sensor is non-functional. First, in all cells that expressed functional Cygent-2.1, sensor fluorescence was restricted to the cytoplasm while the nucleus was always devoid of fluorescence (see e.g. Figure 3.5.3 A

screenshot and B-D). The same is true for other sensor proteins of similar composition, e.g. the cAMP sensor Epac (data not shown). Most likely, the full sensor protein is too large to pass the nuclear pores. In cells that had been transduced with AAV2-Cygnet-2.1, fluorescence was also detected in the nucleus. This may indicate that the sensor protein is not intact and that the smaller fluorescent fragments can enter the nucleus. In this case, it is important to study not only the ratio change (ΔR), but also the initial ratio of CFP/YFP (R_0). The average R_0 of cells expressing Cygnet-2.1 upon AAV2-Cygnet-2.1 transduction (n=25) was nearly 2 times higher than the average R_0 of cells transfected with Cygnet-2.1 using lipofectamine (n=31) (Figure 3.5.5). This unexpected high R_0 of AAV2-Cygnet-2.1 may indicate that CFP and YFP exist independent of each other in the cell because the sensor is degraded.

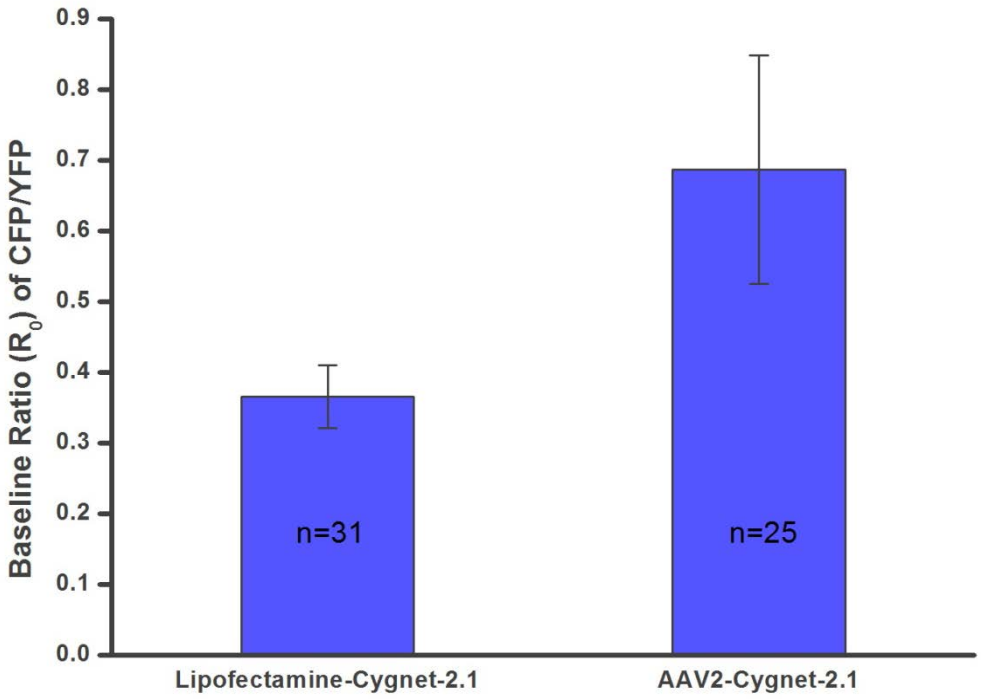

Figure 3.5.5: Baseline ratio of Cygnet-2.1 upon AAV2-Cygnet-2.1 transduction was higher than the ratio upon lipofectamine transfection.

Baseline ratio of Cygnet-2.1 sensors upon lipofectamine transfection was averaged from 31 individual recordings (left bar), while baseline ratio of the sensors after AAV2-Cygnet-2.1 transduction was averaged from 25 individual recordings (right bar). The R_0 after viral transduction was nearly two times higher than after lipofectamine transfection. $P=3.16\times10^{-10}$ by t-test.

Additional controls were performed in FlpTS GC-A cells, the cell line that had been used to characterize Cygnet-2.1 in initial experiments (compare Chapter 3.1). Cells were transduced with AAV2-Cygnet-2.1. After four days, fluorescence was observed in many cells and cells were used for imaging experiments. Within 4 individual recordings including 20 different cells, no FRET change was observed upon ANP stimulation. One of the recordings is shown in Figure 3.5.6. Five FlpTS GC-A cells were recorded in the field of view (screenshot). Between seconds 60 to 120, ANP (1 nM) was applied but no change in the fluorescent signal was recorded. Once again, fluorescence was found in both nucleus and cytosol quite different from the situation in lipofectamine transfected FlpTS GC-A cells (see Figure 3.1.2 and Figure 3.5.1 A), but similar to virally transduced dissociated retinal cultures (Figure 3.5.4 screenshots).

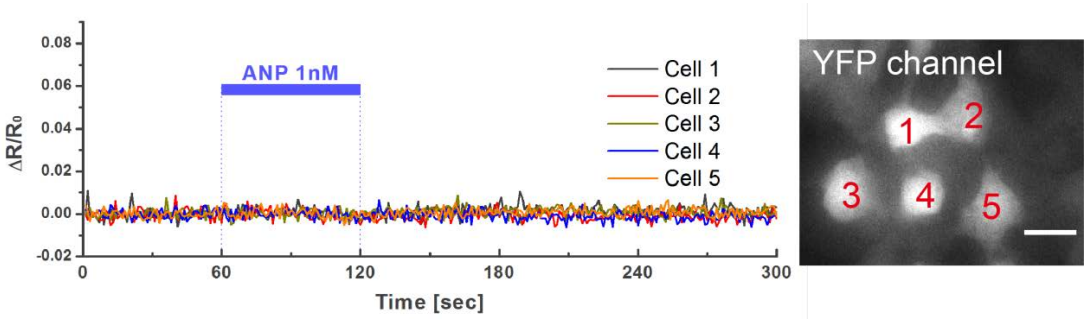

Figure 3.5.6: AAV2-Cygnet-2.1 transduction did not yield functional Cygnet-2.1 sensor in FlpTS GC-A cells.

The sensor signal of five FlpTS GC-A cells transduced with AAV2-Cygnet-2.1 was plotted over time. No signal change was recorded upon the application of ANP (1 nM) between 60 to 120 seconds.

Right image shows a screenshot of the YFP channel for these five cells.

Scale bar = 20 µm.

Conclusion for AAV-mediated expression of Cygnet-2.1

All results in this chapter strongly suggest that Cygnet-2.1 sensors expressed upon AAV-mediated transduction were not functional in the target cells.

4. DISCUSSION

The intracellular messenger cGMP is supposed to play a vital role in retinal signal processing and adaptation. The aim of the present study was to establish a method that allows to spatially and temporally monitor changes in the internal cGMP concentration in retinal cells using the genetically encoded sensor Cygnet-2.1. As a first step, the sensor had to be characterized using a cell model in which cGMP synthesis could be reliably and reproducibly triggered. I chose the FlpTS GC-A cell line. The cell line expresses the particulate guanylate cyclase A (pGC-A) which can be activated by the atrial natriuretic peptide ANP. Cygnet-2.1 reliably revealed the synthesis and degradation of intracellular cGMP upon stimulation with ANP (Chapter 3.1). As the next step, Cygnet-2.1 had to be expressed in retinal cells. To this end, retinal cultures were established (Chapter 3.2) and seven different AAV serotypes encoding GFP were screened for their transduction efficiency in this *in vitro* model. AAV2 was selected as the most promising vector based on its wide range of transduction patterns among the retinal cell types and the high transduction efficiency (Chapter 3.3). AAV-mediated transduction was also established *in vivo.* AAVs were delivered via ocular injection to newborn mice (Chapter 3.4). Again, AAV2 was determined as the most promising candidate for transduction of retinal neurons. Finally, Cygnet-2.1 sensors were expressed in dissociated retinal cultures by using lipofectamine transfection and AAV-mediated transduction. Using lipofectamine transfection, changes in Cygnet-2.1 fluorescence revealed a fast increase in the internal cGMP concentration upon NO stimulation in cultured retinal neurons that were immunoreactive for sGC. Upon AAV2-mediated transduction, no change in the Cygnet-2.1 fluorescence could be detected in retinal cells upon stimulation with NO donors or in the FlpTS GC-A cells upon stimulation with ANP. Most likely, AAV-mediated transduction did not yield functional Cygnet-2.1 sensors (Chapter 3.5). Nevertheless, the proof of principle experiments clearly demonstrated that it is possible to investigate cGMP metabolism in the retina under physiological conditions using Cygnet-2.1. Once functional Cygnet-2.1 can be expressed upon viral

transduction, this project can be carried on. In the following, I will discuss each of the above mentioned steps in an own chapter.

4.1 Sensitivity and selectivity of Cygnet-2.1

As a first step, Cygnet-2.1 had to be characterized using the FlpTS GC-A cell model in which cGMP synthesis could be triggered by ANP. Cygnet-2.1 reliably revealed the synthesis and degradation of intracellular cGMP upon stimulation with ANP (Chapter 3.1). Cygnet is the first genetically encoded FRET-based cGMP sensor (Honda et al., 2001). Honda and coworkers used N-or C-terminally truncated versions of the type I α isoform of protein kinase G (PKG-Iα) and fused it to the two fluorescent proteins CFP and YFP that can work as a FRET pair. One N-terminally truncated sensor version showed a decreased FRET efficiency upon cGMP binding and was called Cygnet-1 (cyclic GMP indicator using energy transfer). However, this first sensor still displayed kinase activity. To silence the kinase activity, a catalytically inactive mutant Cygnet-2 was generated, but, with relatively low sensitivity (K_D (cGMP) = 1.9 µM). Native PKG-Iα has a K_D for cGMP of approximately 100 nM (Ruth et al., 1991). In the advanced version Cygnet-2.1, YFP was substituted by a pH-insensitive YFP version and its sensitivity was greatly improved with an apparent K_D (cGMP) of 600 nM (Honda et al., 2005). The dynamic working range of Cygnet-2.1 was described to be from 11 nM to 15 µM with a maximal FRET change of 48%. All these data were obtained from titration experiments performed in cuvettes (Honda et al., 2001; Honda et al., 2005). Until now, a reliable quantification of Cygnet-2.1 has not been performed in living cells. The intracellular environment of living cells comprises many influences like pH, temperature, protein-protein interaction etc. which might affect the performance of the sensor. Therefore, in my thesis, the percentage of FRET change could not be correlated quantitatively to the internal cGMP concentration. Instead, changes in the CFP/YFP ratio (or the FRET changes) were only evaluated in a qualitative way: 1) if the ratio increased, it was assumed that the intracellular cGMP

concentration increased; 2) if the ratio decreased, it was assumed that the intracellular cGMP decreased; 3) if the ratio remained constant, it was concluded that the intracellular cGMP concentration did not change.

In FlpTS GC-A cells that served as model system, the maximum FRET change was in the range of 12% ~ 25% (Chapter 3.1). This is similar to results reported from cultured vascular smooth muscle cells (Honda et al., 2005). In these cells the brain natriuretic peptide (BNP) produced a 20% FRET change in Cygnet-2.1 upon stimulation of the pGC-A. Based on their calibration, the FRET change might indicate an increase of the intracellular cGMP concentration in FlpTS GC-A cells to 200 ~ 800 nM. When the FlpTS GC-A cells were transfected with the cGMP specific phosphodiesterase PDE5a, the maximum FRET change was reduced to 7% ~ 20% which might correspond to an increase of the cGMP concentration to 100 ~ 500 nM. As nearly all ratio curves showed plateau phases during stimulation, the lowered FRET change might indicate that PDE5a can efficiently lower the maximal cGMP concentration to about 50% ~ 60% of its value in the absence of PDE5a.

Ideally, a cGMP sensor would only react to cGMP. In cuvette experiments Cygnet-2.1 also responded to cAMP with a K_D (cAMP) of 300 µM. Hence, Cygnet-2.1 displays a 500 fold lower sensitivity for cAMP than for cGMP (Honda et al., 2005). Surprisingly, in my experiments Cygnet-2.1 yielded clear signals upon stimulation of FlpTS GC-A cells with noradrenaline that activates adrenergic receptors coupled to adenylate cyclase and cAMP synthesis (Figure 3.1.9, Chapter 3.1.4). As there is no evidence in the literature indicating that noradrenaline activates pGC, the most likely interpretation is that Cygnet-2.1 detected the rise in internal cAMP. As the signal was similar in amplitude to the signal induced by pGC-A activation, one would have to conclude that the internal cAMP concentration upon noradrenaline stimulation was roughly 500 fold higher than the cGMP concentration upon ANP stimulation. On the other side, the FRET-based sensor Epac1 has been generated for the detection of cAMP (Nikolaev et al., 2004). It seems that Epac1 can also react to cGMP. Epac1 has been reported to reveal changes in internal cGMP in Drosophila motoneurons

(Shakiryanova and Levitan, 2008). I also expressed Epac1 in FlpTS GC-A cells and recorded responses to stimulation with ANP (data not shown). Hence, both sensors do not only respond to changes in the concentration of their target cyclic nucleotide but also to changes of the "wrong" cyclic nucleotide. Therefore, the sensors should be used with the appropriate caution. For example in retinal cells, Cygnet-2.1 signals cannot always be unequivocally identified as changes in the internal cGMP concentration, especially if there is no clear relation to a stimulus. On the other hand, data are more easily to interpret if Cygnet-2.1 is used to monitor cGMP synthesis upon stimulation with NO donors acting on soluble guanylate cyclases. In this case, the most likely explanation for a Cygnet-2.1 signal is the increase in the internal cGMP concentration. Thus, in principle with the appropriate caution, Cygnet-2.1 should be useful to study the NO-cGMP pathway in the retina.

4.2 Development, degeneration and remodelling of retinal culture

In order to develop techniques to express Cygnet-2.1 in retinal cells, three types of retinal cultures were established as model systems. To express Cygnet-2.1, two different techniques were used: transfection using the lipofectamine method and transduction using AAVs. AAV-mediated transduction was studied using seven different serotypes of AAVs encoding GFP. During the thesis I focused on organotypic retinal whole-mount cultures and dissociated retinal cell cultures. In retinal whole-mount cultures, the intact retina could be cultured up to 16 days, while mostly maintaining the typical organization. Clear retinal layering could be observed throughout the culture. In dissociated retinal cell cultures, all main types of retinal neurons could be grown on coated coverslips and survived for more than 4 weeks. However, degeneration also occurred in all retinal cultures and limited the time frame of cultivation.

4.2.1 Organotypic retinal whole-mount culture

In this study, retinae of young mice at P8 were cultured in two ways: either “folded” or “flattened”. In both cases, the retinal layering could be preserved for 16 days. In addition, because at P8 the retina is not fully mature; the retinal explants still can develop during cultivation. As is shown in the recoverin-staining (Figure 3.2.1, Chapter 3.2), *in vivo* type 2 bipolar cells became recoverin-immunoreactive at P10. In both folded and flattened cultures of P8 retina, type 2 bipolar cells turned immunoreactive for recoverin after four days of cultivation. Hence, compared to the native tissue, the recoverin expression was delayed for two days, yet type 2 bipolar cells were still capable of developing *in vitro*. Nevertheless, cultivation certainly has effects on the tissues. Not only recoverin-IR in type 2 bipolar cells was delayed, but PKCα-IR in rod bipolar cells was delayed (Figure 3.2.2) as well. Whether this indicates lack of certain factors needed for development or time needed to recover from the isolation procedure cannot be decided.

However, in both types of whole-mount cultures, degeneration was always observed and was most pronounced in that part of the retina that had attached to the membrane.

In folded cultures, two layers of the retinal tissue were sandwiched and placed onto the membrane. As is shown in cell type specific immunostainings (Figure 3.2.1 - 3.2.4, Chapter 3.2), the lower part of the tissue that was attached to the membrane showed very fast degeneration. After 2 days *in vitro*, its originally well-organized structure was strongly disorganized while the upper tissue seemed to grow properly. Generally, the outer half of the upper tissue, including the ONL, the OPL and the outer margin of the INL, showed nearly well-preserved structures. But in the immunostainings for PKCα, calretinin, and NOS (Figure 3.2.2 - 3.2.4, Chapter 3.2), signs of degeneration were visible in the inner margin of the INL, the entire IPL and the GCL. Most obviously, the cells in the GCL had disappeared after about 2 days of cultivation (Figure 3.2.4, Chapter 3.2). As loss encompassed both soma and processes, strong structural disturbances in the IPL occured. Thus, in PKCα stainings (Figure 3.2.2,

Chapter 3.2), there were discrete gaps in the layer of the rod bipolar cell axon terminal systems.

In flattened cultures, the degeneration started from the photoreceptors, which were attached to the membrane. Under such circumstances, the ONL, the OPL, and the outer margin of the INL were most strongly affected by degeneration. Because of the continuous loss of photoreceptors, the ONL became thinner and thinner during cultivation (Figure 3.2.1, Chapter 3.2). Therefore, the postsynaptic neurons were also affected due to missing presynaptic partners. The entire OPL displayed a wave-like shape and some horizontal cell somata misplaced to the ONL were observed (Figure 3.2.3, Chapter 3.2). In addition, when the cultivation was in progress, a substantial number of rod bipolar cell somata moved towards the inner margin of the INL while more and more gaps were found in-between existing somata, indicating rod bipolar cell loss.

Other groups grew similar flattened whole-mount cultures of mouse retina obtained on embryonic day 15 ~ 17 for about 18 days (Tomita et al., 1996; Hatakeyama et al., 2001). Caffe and his co-workers were able to culture flattened mouse retina of P2 for 26 days using a very sophisticated serum-free medium (Caffe et al., 2001). It seems that the components of the medium play a big role in culturing young retina for a longer time. Nevertheless, the time frame for preserving retinal explants in my study was sufficient to perform the transduction and allow for gene expression.

4.2.2 Dissociated retinal cell culture

Cells dissociated from mouse retina could be cultured for more than 4 weeks in my study. Cells were prepared from animals of P2 to P4. When cells were obtained from mice older than P4, they could not be cultured for more than 2 days. For dissociated retinal cell cultures, laminin-coated coverslips and serum-containing medium were necessary. With the laminin coating, dissociated cells settled on the coverslips much faster, which greatly increased the survival rate. In addition, neurites were grown

earlier on laminin-coated coverslips than on coverslips without coating, in agreement with a previous report that laminin promotes neuritic regeneration of cultured neurons (Manthorpe et al., 1983). Based on my observation, a good survival rate of mouse retinal neurons is strongly related to cell-cell interactions. The earlier neurites grow out, the earlier neurons can interact with each other and, thus, the more cells can survive *in vitro*. Besides, the presence of glia cells was found to promote survival of cultured neurons. During very preliminary experiments, I attempted to grow glia free cultures by using serum free medium (serum-free DMEM or serum-free Neurobasal medium (Gibco)) in order to obtain pure neuronal cultures. In these cultures, neurons died rapidly within two to four days of cultivation while glia cells vanished. It was reported that rat retinal cells can be cultured in serum-free medium (Gomes and Cayouette, 2010). However, the same group pointed out that under these conditions cell survival is drastically decreased for mouse retinal cells. Most likely, the glia cells form a supporting cell layer on which neurons grow or they also secrete factors that are essential for mouse retinal neurons to survive.

Identification of cell types is an important issue in dissociated cultures. In this kind of culture the environment is totally different from that of native tissue. For example, Syt2-immunoreactive type 6 bipolar cells most notably changed to multipolar-like morphology (Figure 3.2.8, Chapter 3.2). Nevertheless, nearly all main cell types, except for ganglion cells could be identified based on cell type specific immunostaining and morphological parameters, i.e. soma size or neurite length. In addition, quite a number of cells were found to express sGC in the cultures and they showed cGMP-IR after the stimulation with NO donors (Figure 3.5.2, Chapter 3.5).

4.3 AAV-mediated transduction

To express foreign proteins like Cygnet-2.1, the cDNA encoding the protein has to be introduced into the target cells. In this thesis, two gene delivery approaches have been

used: lipofectamine-mediated transfection and AAV-mediated transduction. Both methods worked well in HEK-293 cells. However, it was much more difficult to introduce genes into retinal neurons. In this case, AAV-mediated transduction was more efficient than lipofectamine-induced transfection (data not shown). AAVs are also suited to transduce cells *in vivo*. Hence, AAVs are promising candidates for delivering gene cargos into cells both *in vitro* and *in vivo*.

4.3.1 AAV-mediated transduction *in vitro*

During my studies, seven different serotypes of AAVs were tested and they all successfully transduced retinal cells *in vitro*. Except for AAV5 that displayed an extremely low transduction efficiency, the remaining six serotypes of AAVs (AAV1, AAV2, AAV4, AAV6, AAV8, and AAV9) were further applied for characterization of AAV-mediated transduction both *in vitro* and *in vivo*, displaying serotype-dependent transduction patterns.

In dissociated retinal cultures, the number of viral particles per seeded cell could be easily adjusted. Moreover, in this kind of culture the access of the viruses to the cultured cells was optimal. The percentage of transduced cells in dissociated cultures was on average less than 10%. However, it should be kept in mind that the cultures comprised several cell types. As each AAV serotype may target certain cell types preferentially, the transduction efficiency should be determined for each cell type. Table 3.3.1 (Chapter 3.3.1) summarizes the transduction efficiency of different serotypes for identified cell types. AAV2 could infect all identified cell types and showed the highest efficiency. AAV6 also could infect all types listed in the table, but showed lower efficiency in each group than AAV2. The remaining AAV serotypes showed certain selectivity for different cell types. For example, AAV1 targeted glycinergic cells better than GABAergic or NOS-positive amacrine cells. Roughly 30% of the glycinergic cells were transfected. However, glycinergic cells comprise several subtypes in the mouse retina (Pourcho and Goebel, 1985; Menger et al., 1998; Radhakrishnan, 2009). It could be that each of the different glycinergic cell

populations is transduced with a similar efficiency of around 30%. On the other hand, certain glycinergic cell types might be transduced with higher efficiency while other cell types might not be transduced at all, yielding an average transduction rate of 30%. AAV4 seemed to mainly target photoreceptors (identified by recoverin-IR and soma size) with about 8% efficiency, which is close to the efficiency of AAV2, but did not target amacrine cells at all. If one would like to focus on photoreceptors and minimize expression of sensors or other optogenetic tools in other cell types, AAV4 might be a promising candidate. AAV8 and AAV9 were similar to each other, except that AAV8 had nearly two fold higher efficiency for CaBP-positive cells than AAV9. However, it should be noted that the immunomarkers listed in the table usually stain more than one cell type - except for CaBP that is predominantly found in horizontal cells and to a much lesser extent in certain amacrine cells. If it was desirable to determine transduction efficiency in the different retinal cell types in more detail, more counterstainings with a greater variety of cell-specific markers would be necessary.

In whole-mount cultures transduced by AAVs, GFP expression was predominantly found in Müller cells. For most retinal cell types, accessibility is strongly reduced in the whole-mounted retina. Müller cells on the other hand span the entire retina and extend large endfeet to the retinal borders, making them more accessible. Very similar results for AAV1, 2, and 5 were reported in whole-mount retinal explants from P7 mice (Pang et al., 2008). In addition, AAV2 was the most efficient serotype in their studies, which agrees with my findings. In general, the authors reported higher transduction efficiency than was observed in my study. This might be related to the longer incubation time of the explants with the viruses (30 minutes in their studies, 15 minutes in mine). In my studies, however, the incubation time was limited to 15 minutes as explants were nearly dried out after 15 minutes of incubation with virus in the absence of medium.

4.3.2 AAV-mediated transduction *in vivo*

Surprisingly, transduction *in vivo* yielded infection patterns that differed from those

observed *in vitro*. Generally, the transduction efficiency was lower *in vivo* than in dissociated cultures. This is most probably an effect of the reduced accessibility of retinal cells in the intact retina. Often, at sites with higher GFP expression the retinal structures were found to be disturbed. Most likely, the retina was damaged during the injection which enhanced the accessibility for the viruses. AAV2 was found to efficiently transduce many cells in the middle layers of the retina even at sites where the retina was intact. Some of AAV2-infected cells (including cone bipolar cells and amacrine cells) in the INL were also sGC-immunoreactive, a prerequisite for the investigation of cGMP metabolism controlled by NO with Cygnet-2.1.

As judged from vertical sections of retinae transduced *in vivo* in my study, AAV2 infected photoreceptors, bipolar cells, amacrine cells, ganglion cells, and Müller cells. The transduction patterns were not fully identical to those of previous studies by other groups (Table 4.1). There are three parameters that mainly differ between the studies: animal age, promoter for vectors and position of injection (intravitreal or subretinal).

Table 4.1: Transduction pattern of AAV2 in native mouse retina.

Mouse	Promoter	Position	Transduction Pattern	References
P7	CBA*	intravitreal	ganglion cells, Müller cells	(Pang et al., 2008)
		subretinal	photoreceptors	
Adult	CMV	intravitreal	amacrine cells, ganglion cells, Müller cells	(Auricchio et al., 2001)
		subretinal	photoreceptors	
P0	CAG**	subretinal	horizontal cells, amacrine cells, ganglion cells	(Watanabe et al., 2013)
Adult	CAG	subretinal	photoreceptors, horizontal cells, ganglion cells	(Charbel Issa et al., 2013)
P5	CMV	intravitreal / subretinal	photoreceptors, bipolar cells, amacrine cells, ganglion cells, Müller cells	(my data)

* CBA: chicken β-actin promoter

** CAG: CMV-actin-globin hybrid promoter

During my ocular injections, I found it difficult to determine the exact position of the needle as the optics of the eye is blurry in young animals. From earlier reports (Auricchio et al., 2001; Pang et al., 2008), subretinal injection yielded photoreceptor transduction while intravitreal injection lead to transduction of inner retinal cells. In the other two papers (Charbel Issa et al., 2013; Watanabe et al., 2013), this difference was not observed. This would mean that even with subretinal administration, the viruses could cross the entire thickness of the retina and infect cells in all layers. Although the injection position was not exactly determined in my experiments, using AAV2 I found transduction throughout the entire thickness of the retina.

Promoters may also influence the transduction pattern. Actually, there is not a promoter that can target all types of retinal neurons. On the other hand, during most applications, not all cell types need to be targeted. Theoretically, using a cell type specific promoter can restrict the transgene expression to the desired cells. As an extension of this project in the future, one could try to exclusively transduce sGC-immunoreactive cells with AAV2 expressing Cygnet-2.1 under the control of an sGC promoter.

In this thesis, for several reasons *in vivo* transduction was established in newborn mice. In such young mice, the retinal limiting membranes are supposed to be less well developed and, therefore, hinder virus diffusion to a lesser extent than in adult retina. In addition, performing transduction in young mice can save time for expression. Once the mice become adult, their retinae can be used for imaging experiments as sensor expression is complete. Apart from AAV mediated transduction, electroporation is another method to deliver cDNA encoding optogenetic sensors to cells. In this case, cDNA is applied in form of plasmids. Since electroporation works more efficient for mitotic cells than postmitotic cells, DNA injection and electroporation must be performed in newborn mice (Venkatesh et al., 2013). However, there seem to be unexpected disadvantages when performing ocular injections in young animals. In my studies retinal folds and disturbed layering were consistently found after the injection. The mechanical damage was most probably

caused during the injection process. Young mice have very soft retinae that can be easily affected by pressure changes in the small eye ball or by accidental contact with the injection needle. Adult mice have larger eyes that might be less sensitive to mechanical damage. Moreover, adult mouse eyes provide clear vision through the pupil. With the help of appropriate optical tools, it is possible to locate the exact position of the injection needle: subretinal or intravitreal. Numerous publications have shown that it is possible to transduce neurons in the adult mouse retina (Auricchio et al., 2001; Yang et al., 2002; Lei et al., 2009; Park et al., 2009; Giove et al., 2010; Lei et al., 2010; Charbel Issa et al., 2013; Kay et al., 2013; Birke et al., 2014; Trapani et al., 2014). Therefore, in future studies it should be considered to perform ocular injection in adult mouse, rather in young animals.

Vertical sections of transduced retinae revealed a certain degree of tropism for each AAV serotype. AAV1 targeted photoreceptors and Müller cells with low efficiency (Figure 3.4.1, Chapter 3.4.1). Very similar results were reported in adult mouse retina using AAV1 and the same CMV promoter (Auricchio et al., 2001). When AAV1 was used with the CBA promoter, transduction showed even lower efficiency and was restricted to Müller cells (Pang et al., 2008). In contrast, AAV1 in conjunction with the CAG promoter showed very high transduction efficiency in photoreceptors, horizontal cells, and Müller cells after subretinal administration in P0 mice (Watanabe et al., 2013). For AAV4, GFP expression was found nearly only in photoreceptors in my data (Figure 3.4.1, Chapter 3.4.1). No report on AAV4 transduction in the retina was found in the literature. When AAV6 was used with the CMV promoter in the adult mouse retina (Yang et al., 2002) or with the CAG promoter in rat retina (Klimczak et al., 2009), no retinal neurons were transduced, but retinal pigment epithelium cells, which fits to my data (Figure 3.4.1, Chapter 3.4.1). The stark difference in the expression patterns observed with AAV6 *in vitro* and *in vivo* cannot be explained. Nevertheless, it seems that AAV6 is not suitable for transducing retinal cells *in vivo*. The transduction efficiency of AAV8 seems to be low (Park et al., 2009). Again, using the CAG promoter instead of the CMV promoter could increase the

transduction efficiency (Watanabe et al., 2013). AAV9 in conjunction with the CMV promoter strongly infected photoreceptors and Müller cells following subretinal injection (Lei et al., 2009). Again in Watanabe's studies, AAV9 using the CAG promoter could target more cell types: photoreceptors, horizontal cells, amacrine cells and ganglion cell, but no Müller cells (Watanabe et al., 2013). In summary, the use of the CAG promoter should be considered in future studies, as it might yield better expression.

4.4 Cygnet-2.1 expression upon AAV-mediated transduction

Using antibodies against cGMP, I could show that the intracellular cGMP concentration in cultured sGC-positive retinal cells can be greatly increased by NO stimulation (Figure 3.4.2., Chapter 3.4.2). Cygnet-2.1 sensors were successfully expressed in dissociated retinal cultures using lipofectamine transfection. Upon stimulation with an NO donor transfected retinal cells showed clear changes in the CFP/YFP ratio, indicating an increase in the internal cGMP concentration (Figure 3.4.3, Chapter 3.4.2). Both results agree well and prove that dissociated retinal cell cultures can be used as an *in vitro* retina model to study the NO-cGMP pathway.

Thereafter, AAVs were used to introduce Cygnet-2.1 into cultured retinal cells. Upon transduction, more than 100 cells/coverslip showed fluorescence (compared to 2 - 5 cells/coverslip in the cultures that were transfected using lipofectamine). Hence, transduction efficiency was much higher than transfection efficiency. Surprisingly and most unfortunately however, it seems as if Cygnet-2.1 was not functional upon AAV-mediated transduction. This holds true for expression in retinal neurons in which cGMP synthesis was stimulated with NO (Figure 3.4.4, Chapter 3.4.3) and for FlpTS GC-A cells that were stimulated with ANP (Figure 3.4.6, Chapter 3.4.3).

Why is Cygnet-2.1 not functional when expressed using AAVs? In order to generate AAVs, Cygnet-2.1 had to be cloned into an appropriate plasmid. Using this plasmid

for lipofectamine transfection yielded functional sensors. Hence, the problem does not lie in the DNA sequence but seems to originate in the packaging of DNA into AAVs or in the expression of sensor protein from the packed and virally transduced (but not from the transfected) DNA in the infected cell.

Most probably, the DNA encoding Cygnet-2.1 was not correctly packed into the viral capsid. Native AAVs contain a single-stranded DNA that is about 4.7 kilobases long. In the viruses used in this thesis, the transgene was incorporated in a self-complementary form to increase the speed of expression. Thus, the effective length of the DNA was shortened to 50% (about 2350 bp). The CMV promoter (630 bp) plus Cygnet-2.1 (3200 bp) occupy 3830 bp. Probably, this caused problems in packaging the DNA into the viral capsid. How this results in nonfunctional sensors, is not entirely clear. One might assume that the DNA strand is fragmented during packaging. On the other hand, both CFP and YFP fluorescence could be detected upon transduction. As YFP is located at the C-terminus of the sensor, YFP fluorescence can theoretically only be expected if the total cDNA – from the promoter to the 3' end - has been transcribed. At present it can only be speculated how the DNA might be affected during the packing process to yield non-functional sensors.

A similar situation was observed in the case of the FRET-based cAMP sensor Epac1 in our lab. The Epac1 protein is of similar size as Cygnet-2.1. Again, Epac1 was not functional if expressed via AAV mediated transduction. Preliminary experiments suggest that using the DNA in the single-stranded rather than in the self-complementary form may yield functional Epac1 upon AAV mediated transduction (Nadine Gruteser, ICS-4, personal communication). If these results can be confirmed, it is suggested to also express Cygnet-2.1 using the single-stranded rather than the self-complimentary form.

4.5 Outlook

In this thesis, the genetically encoded cGMP sensor Cygnet-2.1 has been characterized in the cell model FlpTS GC-A. Retinal cultures were established as *in vitro* retina models. The metabolism of the second messenger cGMP was spatiotemporally monitored in retinal cultures, which principally proves the feasibility of using Cygnet-2.1 to study the NO-cGMP pathway in the mouse retina. Moreover, AAV-mediated transduction was established *in vitro* in retinal cultures as well as *in vivo* using ocular injections. Unfortunately, upon AAV-mediated Cygnet-2.1 expression no responses to cGMP synthesis could be detected. However, the problem might be solved by using single-stranded rather than self-complementary DNA. Alternatively, cDNA coding for Cygnet-2.1 might be introduced into retinal cells using the electroporation method (Matsuda and Cepko, 2004, 2007; Lagali et al., 2008). Once functional Cygnet-2.1 sensors can be expressed in retinal neurons *in vivo*, the investigation of cGMP metabolism by NO modulation could be conducted in a straightforward way.

In addition, the techniques that were established in this thesis like ocular injection, *in vitro* retinal models and AAV approaches can be used for many other applications. For example, in the retina cAMP metabolism and its modulation remains mysterious as well. Thus, the cAMP sensor Epac1 could be employed to study cAMP metabolism using these established platforms. Taken together, the present study has established several methods that are very useful in many aspects of retinal research.

5. REFERENCES

Abramoff, M. D., Magalhaes, P. J. and Ram, S. J. (2004). "Image processing with ImageJ." Biophotonics International **11**(7): 36-42.

Agbandje-McKenna, M. and Kleinschmidt, J. (2011). "AAV capsid structure and cell interactions." Methods Mol Biol **807**: 47-92.

Atchison, R. W., Casto, B. C. and Hammon, W. M. (1965). "Adenovirus-associated defective virus particles." Science **149**(3685): 754-756.

Atchison, R. W., Casto, B. C. and Hammon, W. M. (1966). "Electron microscopy of adenovirus-associated virus (AAV) in cell cultures." Virology **29**(2): 353-357.

Auricchio, A., Kobinger, G., Anand, V., Hildinger, M., O'Connor, E., Maguire, A. M., Wilson, J. M. and Bennett, J. (2001). "Exchange of surface proteins impacts on viral vector cellular specificity and transduction characteristics: the retina as a model." Hum Mol Genet **10**(26): 3075-3081.

Baldridge, W. H. and Fischer, A. J. (2001). "Nitric oxide donor stimulated increase of cyclic GMP in the goldfish retina." Vis Neurosci **18**(6): 849-856.

Beavo, J. A. and Brunton, L. L. (2002). "Cyclic nucleotide research -- still expanding after half a century." Nat Rev Mol Cell Biol **3**(9): 710-718.

Beavo, J. A. and Reifsnyder, D. H. (1990). "Primary sequence of cyclic nucleotide phosphodiesterase isozymes and the design of selective inhibitors." Trends Pharmacol Sci **11**(4): 150-155.

Berns, K. I., Kotin, R. M. and Labow, M. A. (1988). "Regulation of adeno-associated virus DNA replication." Biochim Biophys Acta **951**(2-3): 425-429.

Birke, M. T., Lipo, E., Adhi, M., Birke, K. and Kumar-Singh, R. (2014). "AAV-mediated expression of human PRELP inhibits complement activation,

choroidal neovascularization and deposition of membrane attack complex in mice." Gene Ther **21**(5): 507-513.

Blom, J., Giove, T., Deshpande, M. and Eldred, W. D. (2012). "Characterization of nitric oxide signaling pathways in the mouse retina." J Comp Neurol **520**(18): 4204-4217.

Blom, J. J., Blute, T. A. and Eldred, W. D. (2009). "Functional localization of the nitric oxide/cGMP pathway in the salamander retina." Vis Neurosci **26**(3): 275-286.

Blute, T. A., Velasco, P. and Eldred, W. D. (1998). "Functional localization of soluble guanylate cyclase in turtle retina: modulation of cGMP by nitric oxide donors." Vis Neurosci **15**(3): 485-498.

Boycott, B. B. and Wässle, H. (1991). "Morphological Classification of Bipolar Cells of the Primate Retina." Eur J Neurosci **3**(11): 1069-1088.

Brister, J. R. and Muzyczka, N. (2000). "Mechanism of Rep-mediated adeno-associated virus origin nicking." J Virol **74**(17): 7762-7771.

Caffe, A. R., Ahuja, P., Holmqvist, B., Azadi, S., Forsell, J., Holmqvist, I., Soderpalm, A. K. and van Veen, T. (2001). "Mouse retina explants after long-term culture in serum free medium." J Chem Neuroanat **22**(4): 263-273.

Charbel Issa, P., De Silva, S. R., Lipinski, D. M., Singh, M. S., Mouravlev, A., You, Q., Barnard, A. R., Hankins, M. W., During, M. J. and Maclaren, R. E. (2013). "Assessment of tropism and effectiveness of new primate-derived hybrid recombinant AAV serotypes in the mouse and primate retina." PLoS One **8**(4): e60361.

Chirmule, N., Propert, K., Magosin, S., Qian, Y., Qian, R. and Wilson, J. (1999). "Immune responses to adenovirus and adeno-associated virus in humans." Gene Ther **6**(9): 1574-1583.

Curcio, C. A., Sloan, K. R., Kalina, R. E. and Hendrickson, A. E. (1990). "Human

photoreceptor topography." J Comp Neurol **292**(4): 497-523.

Derouiche, A. and Rauen, T. (1995). "Coincidence of L-glutamate/L-aspartate transporter (GLAST) and glutamine synthetase (GS) immunoreactions in retinal glia: evidence for coupling of GLAST and GS in transmitter clearance." J Neurosci Res **42**(1): 131-143.

Ding, J. D. and Weinberg, R. J. (2007). "Distribution of soluble guanylyl cyclase in rat retina." J Comp Neurol **502**(1): 734-745.

Dizhoor, A. M., Ray, S., Kumar, S., Niemi, G., Spencer, M., Brolley, D., Walsh, K. A., Philipov, P. P., Hurley, J. B. and Stryer, L. (1991). "Recoverin: a calcium sensitive activator of retinal rod guanylate cyclase." Science **251**(4996): 915-918.

Förster, T. (1948). "Zwischenmolekulare Energiewanderung und Fluoreszenz." Annalen der Physik **437**(1-2): 55-75.

Feil, R. and Kemp-Harper, B. (2006). "cGMP signalling: from bench to bedside. Conference on cGMP generators, effectors and therapeutic implications." EMBO Rep **7**(2): 149-153.

Fox, M. A. and Sanes, J. R. (2007). "Synaptotagmin I and II are present in distinct subsets of central synapses." J Comp Neurol **503**(2): 280-296.

Ghosh, K. K., Bujan, S., Haverkamp, S., Feigenspan, A. and Wässle, H. (2004). "Types of bipolar cells in the mouse retina." J Comp Neurol **469**(1): 70-82.

Giove, T. J., Sena-Esteves, M. and Eldred, W. D. (2010). "Transduction of the inner mouse retina using AAVrh8 and AAVrh10 via intravitreal injection." Exp Eye Res **91**(5): 652-659.

Goldstein, I. M., Ostwald, P. and Roth, S. (1996). "Nitric oxide: a review of its role in retinal function and disease." Vision Res **36**(18): 2979-2994.

Gomes, F. A. F. and Cayouette, M. (2010). Retinal Cell and Tissue Culture. Protocols for Neural Cell Culture. L. C. Doering, Humana Press**:** 175-191.

Gotzes, S., de Vente, J. and Müller, F. (1998). "Nitric oxide modulates cGMP levels in neurons of the inner and outer retina in opposite ways." Vis Neurosci **15**(5): 945-955.

Graham, F. L., Smiley, J., Russell, W. C. and Nairn, R. (1977). "Characteristics of a human cell line transformed by DNA from human adenovirus type 5." J Gen Virol **36**(1): 59-74.

Greferath, U., Grunert, U. and Wässle, H. (1990). "Rod bipolar cells in the mammalian retina show protein kinase C-like immunoreactivity." J Comp Neurol **301**(3): 433-442.

Hatakeyama, J., Tomita, K., Inoue, T. and Kageyama, R. (2001). "Roles of homeobox and bHLH genes in specification of a retinal cell type." Development **128**(8): 1313-1322.

Haverkamp, S., Ghosh, K. K., Hirano, A. A. and Wässle, H. (2003). "Immunocytochemical description of five bipolar cell types of the mouse retina." J Comp Neurol **455**(4): 463-476.

Haverkamp, S. and Wässle, H. (2000). "Immunocytochemical analysis of the mouse retina." J Comp Neurol **424**(1): 1-23.

Hofmann, F., Feil, R., Kleppisch, T. and Schlossmann, J. (2006). "Function of cGMP-dependent protein kinases as revealed by gene deletion." Physiol Rev **86**(1): 1-23.

Hoggan, M. D., Blacklow, N. R. and Rowe, W. P. (1966). "Studies of small DNA viruses found in various adenovirus preparations: physical, biological, and immunological characteristics." Proc Natl Acad Sci U S A **55**(6): 1467-1474.

Honda, A., Adams, S. R., Sawyer, C. L., Lev-Ram, V., Tsien, R. Y. and Dostmann, W.

R. (2001). "Spatiotemporal dynamics of guanosine 3',5'-cyclic monophosphate revealed by a genetically encoded, fluorescent indicator." Proc Natl Acad Sci U S A **98**(5): 2437-2442.

Honda, A., Sawyer, C. L., Cawley, S. M. and Dostmann, W. R. (2005). "Cygnets: *in vivo* characterization of novel cGMP indicators and *in vivo* imaging of intracellular cGMP." Methods Mol Biol **307**: 27-43.

Jacobs, J. W., Vlasuk, G. P. and Rosenblatt, M. (1987). "Atrial natriuretic factor receptors." Endocrinol Metab Clin North Am **16**(1): 63-77.

Jameson, K. A., Highnote, S. M. and Wasserman, L. M. (2001). "Richer color experience in observers with multiple photopigment opsin genes." Psychon Bull Rev **8**(2): 244-261.

Jeon, C. J., Strettoi, E. and Masland, R. H. (1998). "The major cell populations of the mouse retina." J Neurosci **18**(21): 8936-8946.

Johansson, K., Bruun, A., deVente, J. and Ehinger, B. (2000). "Immunohistochemical analysis of the developing inner plexiform layer in postnatal rat retina." Invest Ophthalmol Vis Sci **41**(1): 305-313.

Kandel, E., Schwartz, J. and Jessell, T. (2000). Principles of Neural Science, Fourth Edition New York, McGraw-Hill Medical.

Kaupp, U. B., Niidome, T., Tanabe, T., Terada, S., Bonigk, W., Stuhmer, W., Cook, N. J., Kangawa, K., Matsuo, H., Hirose, T. and et al. (1989). "Primary structure and functional expression from complementary DNA of the rod photoreceptor cyclic GMP-gated channel." Nature **342**(6251): 762-766.

Kawamura, S. (1993). "Rhodopsin phosphorylation as a mechanism of cyclic GMP phosphodiesterase regulation by S-modulin." Nature **362**(6423): 855-857.

Kay, C. N., Ryals, R. C., Aslanidi, G. V., Min, S. H., Ruan, Q., Sun, J., Dyka, F. M.,

Kasuga, D., Ayala, A. E., Van Vliet, K., Agbandje-McKenna, M., Hauswirth, W. W., Boye, S. L. and Boye, S. E. (2013). "Targeting photoreceptors via intravitreal delivery using novel, capsid-mutated AAV vectors." PLoS One **8**(4): e62097.

Kim, I. B., Lee, E. J., Kim, K. Y., Ju, W. K., Oh, S. J., Joo, C. K. and Chun, M. H. (1999). "Immunocytochemical localization of nitric oxide synthase in the mammalian retina." Neurosci Lett **267**(3): 193-196.

Klimczak, R. R., Koerber, J. T., Dalkara, D., Flannery, J. G. and Schaffer, D. V. (2009). "A novel adeno-associated viral variant for efficient and selective intravitreal transduction of rat Muller cells." PLoS One **4**(10): e7467.

Krupinski, J., Lehman, T. C., Frankenfield, C. D., Zwaagstra, J. C. and Watson, P. A. (1992). "Molecular diversity in the adenylylcyclase family. Evidence for eight forms of the enzyme and cloning of type VI." J Biol Chem **267**(34): 24858-24862.

Labrecque, J., Mc Nicoll, N., Marquis, M. and De Lean, A. (1999). "A disulfide-bridged mutant of natriuretic peptide receptor-A displays constitutive activity. Role of receptor dimerization in signal transduction." J Biol Chem **274**(14): 9752-9759.

Lagali, P. S., Balya, D., Awatramani, G. B., Munch, T. A., Kim, D. S., Busskamp, V., Cepko, C. L. and Roska, B. (2008). "Light-activated channels targeted to ON bipolar cells restore visual function in retinal degeneration." Nat Neurosci **11**(6): 667-675.

Lei, B., Zhang, K., Yue, Y., Ghosh, A. and Duan, D. (2009). "Adeno-associated virus serotype-9 efficiently transduces the retinal outer plexiform layer." Mol Vis **15**: 1374-1382.

Lei, B., Zhang, K., Yue, Y., Ghosh, A. and Duan, D. (2010). "Adeno-associated virus serotype-9 mediated retinal outer plexiform layer transduction is mainly through the photoreceptors." Adv Exp Med Biol **664**: 671-678.

Lin, B. and Masland, R. H. (2006). "Populations of wide-field amacrine cells in the mouse retina." J Comp Neurol **499**(5): 797-809.

Linser, P. J., Sorrentino, M. and Moscona, A. A. (1984). "Cellular compartmentalization of carbonic anhydrase-C and glutamine synthetase in developing and mature mouse neural retina." Brain Res **315**(1): 65-71.

Lusby, E., Fife, K. H. and Berns, K. I. (1980). "Nucleotide sequence of the inverted terminal repetition in adeno-associated virus DNA." J Virol **34**(2): 402-409.

Müller, F. and Kaupp, U. B. (1998). "Signal transduction in photoreceptor cells." Naturwissenschaften **85**(2): 49-61.

MacNeil, M. A. and Masland, R. H. (1998). "Extreme diversity among amacrine cells: implications for function." Neuron **20**(5): 971-982.

Maelicke, A. (1990). "The cGMP-gated channel of the rod photoreceptor--a new type of channel structure?" Trends Biochem Sci **15**(2): 39-40.

Manthorpe, M., Engvall, E., Ruoslahti, E., Longo, F. M., Davis, G. E. and Varon, S. (1983). "Laminin promotes neuritic regeneration from cultured peripheral and central neurons." J Cell Biol **97**(6): 1882-1890.

Marc, R. E. (1988). "The role of glycine in the mammalian retina." Progress in Retinal Research **8**(0): 67-107.

Masland, R. H. (2001). "The fundamental plan of the retina." Nat Neurosci **4**(9): 877-886.

Matsuda, T. and Cepko, C. L. (2004). "Electroporation and RNA interference in the rodent retina *in vivo* and *in vitro*." Proc Natl Acad Sci U S A **101**(1): 16-22.

Matsuda, T. and Cepko, C. L. (2007). "Controlled expression of transgenes introduced by *in vivo* electroporation." Proc Natl Acad Sci U S A **104**(3): 1027-1032.

McCarty, D. M., Monahan, P. E. and Samulski, R. J. (2001). "Self-complementary recombinant adeno-associated virus (scAAV) vectors promote efficient transduction independently of DNA synthesis." Gene Ther **8**(16): 1248-1254.

Menger, N., Pow, D. V. and Wässle, H. (1998). "Glycinergic amacrine cells of the rat retina." J Comp Neurol **401**(1): 34-46.

Michelfelder, S. and Trepel, M. (2009). "Adeno-associated viral vectors and their redirection to cell-type specific receptors." Adv Genet **67**: 29-60.

Milam, A. H., Dacey, D. M. and Dizhoor, A. M. (1993). "Recoverin immunoreactivity in mammalian cone bipolar cells." Vis Neurosci **10**(1): 1-12.

Monahan, P. E. and Samulski, R. J. (2000). "Adeno-associated virus vectors for gene therapy: more pros than cons?" Mol Med Today **6**(11): 433-440.

Morgans, C. W., Zhang, J., Jeffrey, B. G., Nelson, S. M., Burke, N. S., Duvoisin, R. M. and Brown, R. L. (2009). "TRPM1 is required for the depolarizing light response in retinal ON-bipolar cells." Proc Natl Acad Sci U S A **106**(45): 19174-19178.

Nawy, S. and Jahr, C. E. (1990). "Suppression by glutamate of cGMP-activated conductance in retinal bipolar cells." Nature **346**(6281): 269-271.

Nawy, S. and Jahr, C. E. (1991). "cGMP-gated conductance in retinal bipolar cells is suppressed by the photoreceptor transmitter." Neuron **7**(4): 677-683.

Negishi, K., Kato, S. and Teranishi, T. (1988). "Dopamine cells and rod bipolar cells contain protein kinase C-like immunoreactivity in some vertebrate retinas." Neurosci Lett **94**(3): 247-252.

Nguyen-Legros, J., Versaux-Botteri, C. and Savy, C. (1997). "Dopaminergic and GABAergic retinal cell populations in mammals." Microsc Res Tech **36**(1): 26-42.

Niino, Y., Hotta, K. and Oka, K. (2009). "Simultaneous live cell imaging using dual

FRET sensors with a single excitation light." PLoS One **4**(6): e6036.

Nikolaev, V. O., Bunemann, M., Hein, L., Hannawacker, A. and Lohse, M. J. (2004). "Novel single chain cAMP sensors for receptor-induced signal propagation." J Biol Chem **279**(36): 37215-37218.

Nikolaev, V. O., Gambaryan, S. and Lohse, M. J. (2006). "Fluorescent sensors for rapid monitoring of intracellular cGMP." Nat Methods **3**(1): 23-25.

Osterberg, G. (1935). "Topography of the layer of rods and cones in the human retina." Acta Ophthalmol Suppl. **13**(6): 1-102.

Pandey, K. (1997). Physiology of the Natriuretic Peptides. Natriuretic Peptides in Health and Disease. W. Samson and E. Levin, Humana Press. **5:** 171-191.

Pang, J. J., Lauramore, A., Deng, W. T., Li, Q., Doyle, T. J., Chiodo, V., Li, J. and Hauswirth, W. W. (2008). "Comparative analysis of *in vivo* and *in vitro* AAV vector transduction in the neonatal mouse retina: effects of serotype and site of administration." Vision Res **48**(3): 377-385.

Park, T. K., Wu, Z., Kjellstrom, S., Zeng, Y., Bush, R. A., Sieving, P. A. and Colosi, P. (2009). "Intravitreal delivery of AAV8 retinoschisin results in cell type-specific gene expression and retinal rescue in the Rs1-KO mouse." Gene Ther **16**(7): 916-926.

Peichl, L. and Gonzalez-Soriano, J. (1994). "Morphological types of horizontal cell in rodent retinae: a comparison of rat, mouse, gerbil, and guinea pig." Vis Neurosci **11**(3): 501-517.

Ponnazhagan, S., Mukherjee, P., Yoder, M. C., Wang, X. S., Zhou, S. Z., Kaplan, J., Wadsworth, S. and Srivastava, A. (1997). "Adeno-associated virus 2-mediated gene transfer *in vivo*: organ-tropism and expression of transduced sequences in mice." Gene **190**(1): 203-210.

Pourcho, R. G. (1996). "Neurotransmitters in the retina." Curr Eye Res **15**(7):

797-803.

Pourcho, R. G. and Goebel, D. J. (1985). "A combined Golgi and autoradiographic study of (3H)glycine-accumulating amacrine cells in the cat retina." J Comp Neurol **233**(4): 473-480.

Pow, D. V. and Hendrickson, A. E. (1999). "Distribution of the glycine transporter glyt-1 in mammalian and nonmammalian retinae." Vis Neurosci **16**(2): 231-239.

Purves, D., Augustine, G., Fitzpatrick, D., Katz, L., LaMantia, A., McNamara, J. and Williams, S. (2001). Neuroscience, 2nd edition. Sunderland (MA), US, Sinauer Associates.

Röhrenbeck, J., Wässle, H. and Heizmann, C. W. (1987). "Immunocytochemical labelling of horizontal cells in mammalian retina using antibodies against calcium-binding proteins." Neurosci Lett **77**(3): 255-260.

Radhakrishnan, P. K. (2009). "Expression pattern of hyperpolarization-activated and cyclic nucleotide-gated channels in amacrine cells of the mouse retina". Master of Science, Aachen University of Applied Sciences.

Russwurm, M., Mullershausen, F., Friebe, A., Jager, R., Russwurm, C. and Koesling, D. (2007). "Design of fluorescence resonance energy transfer (FRET)-based cGMP indicators: a systematic approach." Biochem J **407**(1): 69-77.

Ruth, P., Landgraf, W., Keilbach, A., May, B., Egleme, C. and Hofmann, F. (1991). "The activation of expressed cGMP-dependent protein kinase isozymes I alpha and I beta is determined by the different amino-termini." Eur J Biochem **202**(3): 1339-1344.

Schneider, C. A., Rasband, W. S. and Eliceiri, K. W. (2012). "NIH Image to ImageJ: 25 years of image analysis." Nat Methods **9**(7): 671-675.

Scott, J. D. (1991). "Cyclic nucleotide-dependent protein kinases." Pharmacol Ther **50**(1): 123-145.

Shakiryanova, D. and Levitan, E. S. (2008). "Prolonged presynaptic posttetanic cyclic GMP signaling in Drosophila motoneurons." Proc Natl Acad Sci U S A **105**(36): 13610-13613.

Slaughter, M. M. and Miller, R. F. (1981). "2-amino-4-phosphonobutyric acid: a new pharmacological tool for retina research." Science **211**(4478): 182-185.

Tomita, K., Nakanishi, S., Guillemot, F. and Kageyama, R. (1996). "Mash1 promotes neuronal differentiation in the retina." Genes Cells **1**(8): 765-774.

Trapani, I., Colella, P., Sommella, A., Iodice, C., Cesi, G., de Simone, S., Marrocco, E., Rossi, S., Giunti, M., Palfi, A., Farrar, G. J., Polishchuk, R. and Auricchio, A. (2014). "Effective delivery of large genes to the retina by dual AAV vectors." EMBO Mol Med **6**(2): 194-211.

Vaney, D. I. (1990). "Chapter 2 The mosaic of amacrine cells in the mammalian retina." Progress in Retinal Research **9**(0): 49-100.

Venkatesh, A., Ma, S., Langellotto, F., Gao, G. and Punzo, C. (2013). "Retinal gene delivery by rAAV and DNA electroporation." Curr Protoc Microbiol **Chapter 14**: Unit 14D.14.

Wässle, H. and Boycott, B. B. (1991). "Functional architecture of the mammalian retina." Physiol Rev **71**(2): 447-480.

Wässle, H., Puller, C., Müller, F. and Haverkamp, S. (2009). "Cone contacts, mosaics, and territories of bipolar cells in the mouse retina." J Neurosci **29**(1): 106-117.

Watanabe, S., Sanuki, R., Ueno, S., Koyasu, T., Hasegawa, T. and Furukawa, T. (2013). "Tropisms of AAV for subretinal delivery to the neonatal mouse retina and its application for *in vivo* rescue of developmental photoreceptor disorders." PLoS One **8**(1): e54146.

Wilson, E. M. and Chinkers, M. (1995). "Identification of sequences mediating

guanylyl cyclase dimerization." Biochemistry **34**(14): 4696-4701.

Yamashita, M. and Wässle, H. (1991). "Responses of rod bipolar cells isolated from the rat retina to the glutamate agonist 2-amino-4-phosphonobutyric acid (APB)." J Neurosci **11**(8): 2372-2382.

Yang, G. S., Schmidt, M., Yan, Z., Lindbloom, J. D., Harding, T. C., Donahue, B. A., Engelhardt, J. F., Kotin, R. and Davidson, B. L. (2002). "Virus-Mediated Transduction of Murine Retina with Adeno-Associated Virus: Effects of Viral Capsid and Genome Size." Journal of Virology **76**(15): 7651-7660.

Yang, R. B. and Garbers, D. L. (1997). "Two eye guanylyl cyclases are expressed in the same photoreceptor cells and form homomers in preference to heteromers." J Biol Chem **272**(21): 13738-13742.

Zhao, Z. (2010). "cGMP metabolism and its modulation by nitric oxide in the mouse inner retina". Master of Science, Aachen University of Applied Sciences.

Zhou, X. and Muzyczka, N. (1998). "*In vitro* packaging of adeno-associated virus DNA." J Virol **72**(4): 3241-3247.

ACKNOWLEDGMENT

Foremost, I would like to express my deep sense of gratitude to Prof. Frank Müller (Forschungszentrum Jülich / RWTH Aachen University) for the continuous support of my doctoral study and research, guiding me to walk through the difficulties in scientific researches and scientific writing. I could not have imagined achieving this doctoral thesis without his patience, encouragement, enthusiasm, and immense knowledge.

I would like to thank Prof. Marc Spehr (RWTH Aachen University) for being the second supervisor and for spending valuable time on evaluating this thesis.

Besides, I own my sincere thanks to all the ICS-4 members in Forschungszentrum Jülich for constant support at all levels of my research project. I really appreciate Prof. Arnd Baumann and his group for supporting my cell cultures and producing plasmids and viruses for me, as well as many helpful discussions. My special thanks go to Christoph Aretzweiler for giving all technical assistance in immunochemistry. And I also would like to thank Dr. Johnny Hendriks for maintaining and developing the imaging system and helping with data analysis. In addition, I am so grateful to Dr. Sonia Biswas and (Dr.) Anna Sieben for encouraging me during my hard time, and also for all the fun we had during the last four years. It is my pleasure to work with both of you.

At last but not least, I would like to give my deepest thanks to my family: my parents and my wife. It is you who unconditionally love me, support me and encourage me through my entire life.

CURRICULUM VITAE

Personal information:

Name: Zhijian Zhao

Birth: 31.10.1982 in Shanghai, P.R.China

Address: Baierstr. 13, 52428 Jülich, Germany

E-mail: z.zhao@fz-juelich.de, zzj1031@gmail.com

Education and academic degree:

2010.08 – till date	Ph.D. thesis in Neurobiology Institute of Cellular Biophysics in Forschungszentrum Jülich, Germany with the doctoral degree awarded by RWTH Aachen University, Germany
2007.03 – 2010.07	M.Sc. in Biomedical Engineering Aachen University of Applied Sciences, Germany
2001.09 – 2005.06	B.Sc. in Pharmaceutical Preparation Nanjing University of Technology, P.R.China
1998.09 – 2001.07	Shanghai Datong High School, P.R.China

Work Experience:

2005.08 – 2007.01 Shanghai New Asiatic Pharmaceuticals Co., Ltd. (P.R.China)

Director of Manufacturing Line
Quality Assurance Clerk
Quality Control Analyst

Language Skills:

Chinese: mother tongue
English: fluent in speaking and writing
German: beginner

Talks:

European Retina Meeting 2011, Amsterdam, Netherlands.

Zhijian Zhao, Frank Müller: "Modulation of cGMP Synthesis in the Mouse Retina by Endogenously Released and by Exogenously applied Nitric Oxide"

European Retina Meeting 2013, Alicante, Spain.

Zhijian Zhao, Anna Sieben, Frank Müller: "Optogenetic approaches to detect cyclic nucleotides in the retina"

Congress posters:

22nd Neurobiology Doctoral Student Workshop (Neuro-DoWo) 2011, Bonn, Germany.

Zhijian Zhao, Laura Levike Kahle, Frank Müller: "Cyclic Nucleotide Detection via Genetically Encoded Sensors"

European Retina Meeting 2011, Amsterdam, Netherlands.

Zhijian Zhao, Frank Müller: "Modulation of cGMP synthesis in the mouse retina by endogenously released and by exogenously applied nitric oxide"

10th Göttingen Meeting of the German Neuroscience Society 2013, Göttingen, Germany

Zhijian Zhao, Frank Müller: "Detection of cGMP in mouse retinal neurons using immunohistochemistry and live cell imaging based on genetically encoded sensors"

8th PRO RETINA Research-Colloquium 2013, Potsdam, Germany

Zhijian Zhao, Anna Sieben, Frank Müller: "Optogenetic approaches to detect cyclic nucleotides in cultured cells and in the intact retina"

European Retina Meeting 2013, Alicante, Spain.

Zhijian Zhao, Anna Sieben, Frank Müller: "Optogenetic approaches to detect cyclic nucleotides in the retina"